Modelling shoreline development in a wave dominated delta

Validation of ShorelineS model using case study of Rhône delta, France

TU Delft

Dieuwe Boelens

Abstract

The vector based, freeform shoreline development model ShorelineS can efficiently simulate the development of a shoreline through the use of relatively simple bulk longshore transport formulas. This allows it to be multiple orders of magnitude more efficient compared to complex two-dimensional horizontal process-based models. The model does make some assumptions in order to be this efficient. One of these assumptions is the constant profile angle along the shoreline. This means the model does not account for bathymetry. The version of the ShorelineS model used is from 03/08/2023.

This study analyses the applicability of ShorelineS for simulation of a shoreline with a river mouth. To this extent a synthetic case of a shoreline with a river mouth is set up to analyse the model behaviour of ShorelineS in a simplified environment. The effect of many input parameters on the shoreline development is analysed. These parameters include wave parameters, channel parameters, transport parameters, model parameters, and relative sea level rise. The applicability is further tested in a more complex environment with a real-world case. For this, a hindcast is set up. The location of the hindcast is the shoreline of the Rhône delta. This is a wave dominated, sandy coast with a negligible tidal range. Data on the shoreline, the wave climate, the sediment budget, and the shoreline profile were required to get a successful hindcast.

The implementation of a river mouth in ShorelineS is done through specifying the river flow path as well as to what extent the channel should be kept. The sediment discharge is then approximated by a nourishment in the flow path that is pushed out to the shore. This approach was found to work well in a simplified environment through analysis of results from the synthetic case. The different simulations resulted in the expected model behaviour and the simulations were stable.

The results of the hindcast are mostly positive. The hindcast gets a good skill score and the simulations are mostly stable. The biggest differences between the simulated shoreline and the actual shoreline of the Rhône delta can be explained by the existence of relict sediment lobes along the shoreline. These lobes are the result of the combination of progradation and avulsion in the Rhône delta. They make the shoreline profile variable and provide time limited sediment sources.

ShorelineS cannot account for these naturally occurring lobes because of the assumption of the constant profile angle along the shoreline. Combining this with the fact that ShorelineS is incapable of simulating processes related to river dynamics such as avulsion and the forming of mouth bars limits the applicability of ShorelineS in environments governed by natural processes, such as the Rhône delta.

However, there is enough applicability for ShorelineS outside of these environments. When the shoreline is not governed by natural processes but is instead regulated by humans, a canal for instance, the results of the ShorelineS simulations will only get better. The big difference in time and cost efficiency compared to other models makes ShorelineS uniquely suited for applicability where the demand for accuracy of the simulation is lower. For instance, in data limited environments or on a global scale.

Table of Contents

1. Introduction

The global sea level is rising due to global warming (IPCC, 2023). Because of this, coastal areas are at risk. Coastal areas are relatively densely populated. This is because the coast offers great societal, economical, and agricultural value. Almost 42% of the entire population on Earth lives within 100 km of the coast (Ciscar et al, 2018). Evidently, with coastal areas being of such importance while also being the first place where the rise in sea level will be problematic, understanding the development of coastal zones is of the utmost importance in order to properly prepare and plan for the future.

Currently, a common way to predict shoreline development due to a (relative) rise in sea level is passive inundation. This means taking the current topography and simply raising the sea level, thereby moving the shoreline inwards to where the new sea level meets the topography (Anderson et al, 2018). However, this approach does not take into account the natural processes that are involved in coastal dynamics.

There are intricate physical processes and many different conditions that affect the movement of the shoreline over time such as the wave climate and the bathymetry. Rivers are also an important factor when considering shoreline development since they can provide a sediment influx to the shore. Not only is the shoreline altered by these natural processes, but the topography along shore itself will also change. This further influences the development of the shoreline over time as the sea level rises.

Understanding and predicting the development of the shoreline taking this into account will be an exciting challenge, but also a necessity in order to be prepared for a rise in relative sea level. It is therefore of great importance to develop the most efficient tools to help understand and predict shoreline development. This can be done with numerical modelling. Shoreline development models simulate the position of shorelines through time as a result of wave driven sediment transport.

One such model is ShorelineS. An interesting shoreline development model that trades of some of the complexity of other shoreline development models for efficiency. By allowing for some simplifications, such as a constant shoreline profile and no cross-shore sediment transport, ShorelineS is able to reduce the computational power needed to simulate the development of a shoreline over time by several orders of magnitude (Roelvink et al, 2020). This makes ShorelineS more time efficient and cost effective.

Because of this efficiency, ShorelineS could potentially be applied in large scope projects with for instance global coverage. Provided, of course, that the simplifications in ShorelineS lead to results that are reliable. Or at least, results that have enough use to validate the use of a faster and more efficient model.

The simulation of shoreline development with ShorelineS has already been analysed in different conditions such as in the vicinity of groynes (Roelvink et al, 2020), around spits (Mudde, 2019), and around artificial sediment nourishments (Roelvink et al, 2020). ShorelineS has an implementation that can simulate a river mouth together with its sediment discharge. However, how accurately ShorelineS can simulate the development of a river mouth is not yet known.

That is why the research question that this study aims to answer is:

What is the applicability of the ShorelineS shoreline model to accurately simulate the development of a shoreline with a river mouth?

To help answer this question the following sub questions are asked:

- Can the model successfully simulate shoreline development of a shoreline with a river mouth in a simplified environment?
- What is the applicability of the ShorelineS model to accurately simulate the development of a shoreline with a river mouth in a wave dominated delta?

An important step in determining the accuracy of the model is the validation of the simulations. This can be done through a hindcast. The Rhône delta in the south of France is the real-world case that will be used for the hindcast. This location was chosen for the hindcast as it is a wave dominated delta with a sandy shoreline and a tidal range that is negligible for the purposes of this study. This makes it suitable for the use of the ShorelineS model.

2. Literature review

2.1. Environmental setting

The Rhône river originates from the Rhône glacier in the Swiss Alps at an approximate altitude of 2200 metres. From here it flows through Lake Geneva, through parts of France, and is joined by many tributaries. As the river reaches the city of Arles it splits into its two main distributaries: the Grand-Rhône to the east and the Petit-Rhône to the west, which both empty into the Mediterranean Sea and form the Rhône delta (Figure 1).

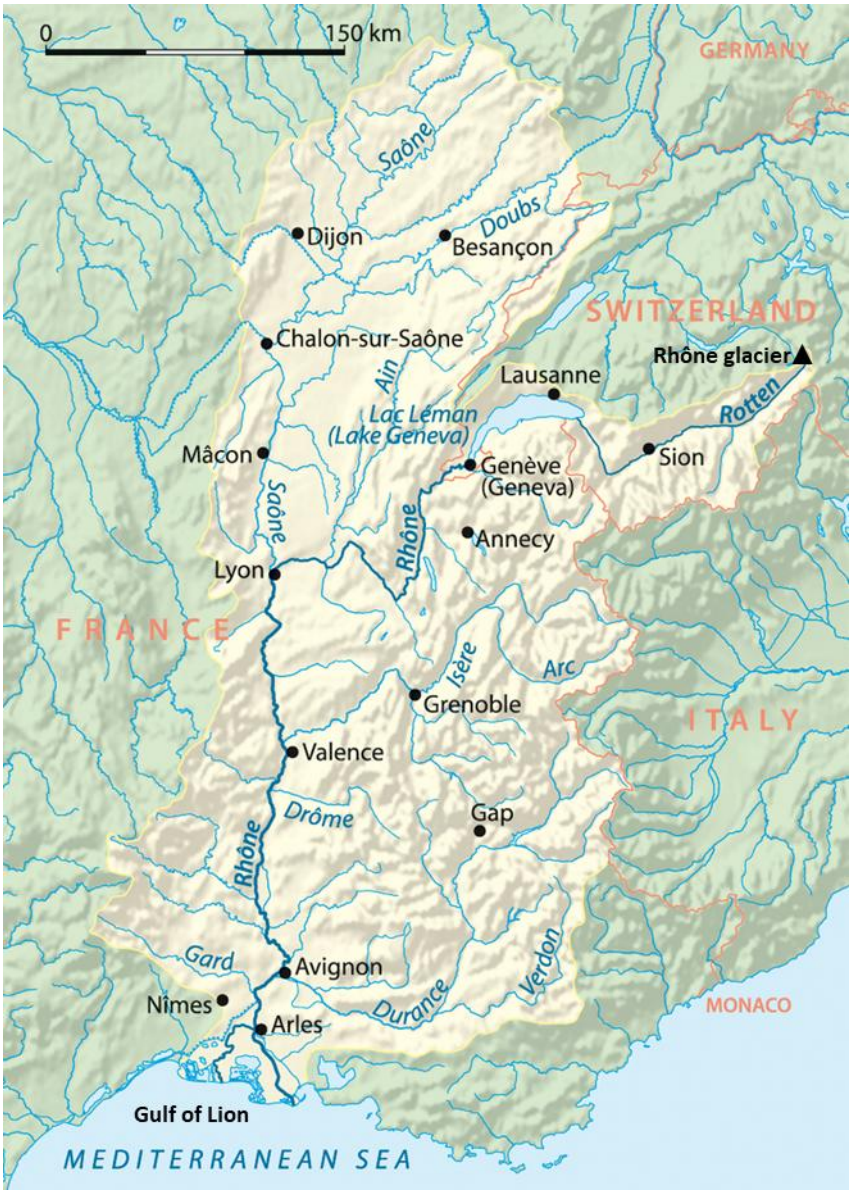

Figure 1: Drainage basin of the Rhône (adapted from NordNordWest, 2008, Wikimedia Commons).

The Rhône delta contains a region known as the Camargue. It is a natural region that consists of wetlands that are bordered by the Grand-Rhône and the Petit-Rhône on either side, and by the Gulf of Lion in the south. The Camargue has a triangular shape of approximately 150,000 hectares that has been a nature reserve since 1970. The coast extends over 95 kilometres and is entirely sandy. In the North of the Camargue is a fluvio-lacustrine zone dominated by fresh water. This area is used for agriculture. In the South is a lagoonal zone that is shaped by sea incursions. There are large salt marshes in this zone that are exploited for the production of sea salt by natural means. These zones

and the transition between them provide extremely variable ecological conditions in the Camargue, so it is no wonder that the flora and fauna are unique and diverse. For instance, the region is visited yearly by 150,000 birds, including flamingos, and is home to a unique horse race, as well as many different mosquitoes. In the case of a rapid change to this coastal zone, for instance due to relative sea level rise, this unique habitat could be lost (Fouchier, 2015).

The average annual liquid discharge of the Rhône is 1710 m^3/s. This was determined at Arles, which is approximately 40 km upstream from the coast. There is a strong inter-annual variation in the discharge of the Rhône. Ranging from over 5000 m^3/s at the high regime (usually winter and spring) to 650 m^3/s at the low regime (usually summer and fall). The distribution of the discharge between the Rhône's two distributaries is 10% for the Petit-Rhône and 90% for the Grand-Rhône (Maillet et al, 2006). Because of the sediment load carried by the two distributaries of the Rhône, sediment is deposited at the mouths of the Grand-Rhône and Petit-Rhône. Over time, when more sediment is deposited than is being eroded, the Rhône delta progrades.

2.2. Site description

Since 4000 BP the location of the Rhône channel has changed many times (Figure 2). The successive displacement of the river mouths has led to sediment deposits at the mouths that have partially stayed there even when the location of the active channel has changed. The resulting sediment deposits are known as relict sediment lobes. These relict sediment lobes are slowly being eroded since the river no longer discharges sediment at their mouth. Because of this they can be considered as time-limited sediment sources for the longshore sediment transport (Sabatier et al, 2006).

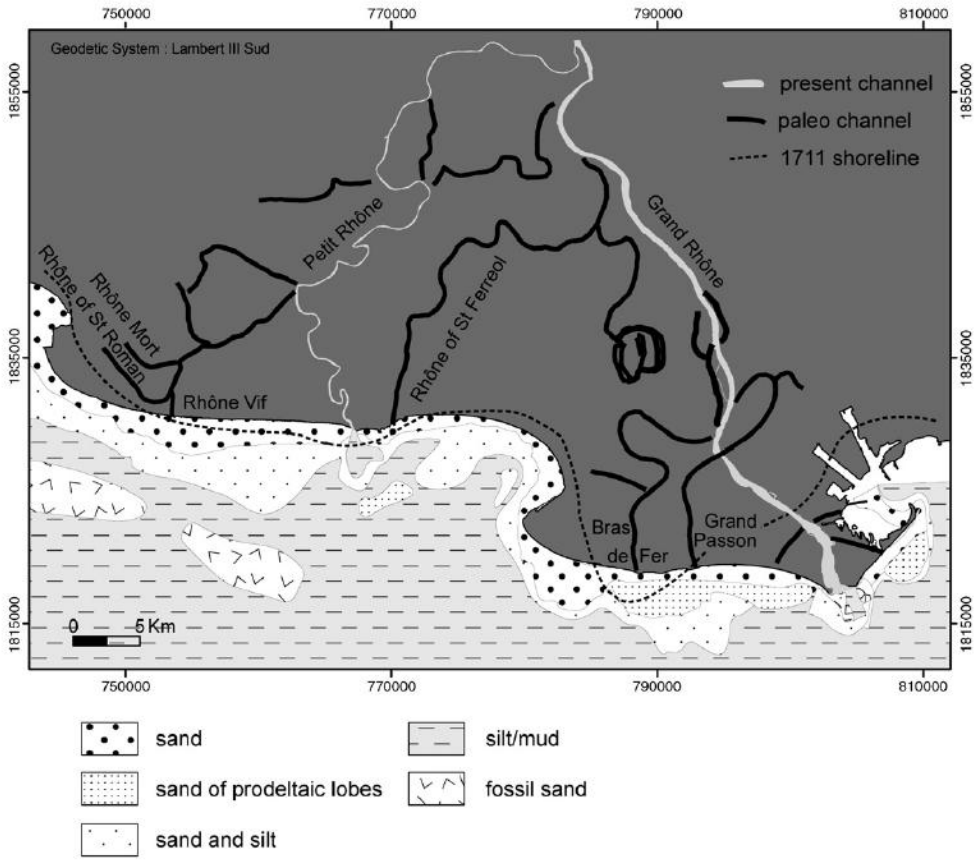

Figure 2: Shifts in the channels of the Rhône and its distributaries since 4000BP. The location of the Grand-Rhône channel has remained the same since 1711. The relict sediment lobes are indicated as prodeltaic lobes (Sabatier et al, 2006).

Since the prominent flood in 1711 the course of the Rhône changed from the Bras de Fer channel to the Grand Rhône. Since then, the location and the number of mouths of the Grand Rhône have changed. Since the moving of the main channel in 1711 the Grand Rhône had three distinct mouths (Figure 3). From West to East these are the Piémanson, The Roustan, and the Pégoulier mouth. In 1855 both the Piémanson and the Roustan mouth were closed off with dykes. In 1892 the Roustan mouth was re-opened. This led to the gradual filling in of the Pégoulier mouth (Sabatier et al, 2006). The diversion of sediment discharge from the Pégoulier mouth to the Roustan mouth resulted in erosion of the Pégoulier mouth. The eroded sediment was redistributed along the shore to the east, resulting in the formation of the La Gracieuse spit.

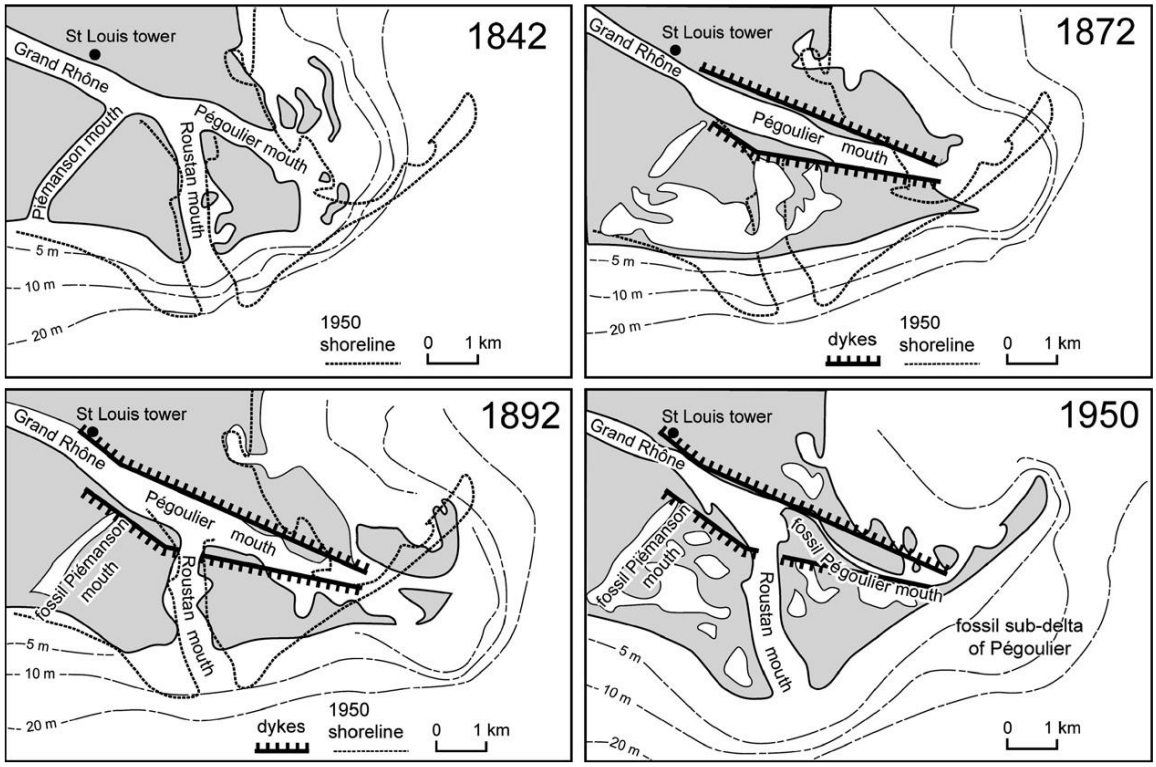

Figure 3: The evolution of the mouth of the Grand-Rhône from 1842 to 1950 (Sabatier et al, 2006).

The shoreline of the Rhône delta as it is today (Figure 4) will be described in detail as parts of this shoreline will be referenced many times throughout this study. The main features of the shoreline of the Rhône delta are the mouths of the two distributaries of the Rhône, the Petit-Rhône and the Grand-Rhône, in addition to three spits. From west to east these are the Espiguette spit, the Beauduc spit and the La Gracieuse spit.

Following the shoreline from west to east, the Espiguette spit is followed by the littoral of the Petite Camargue. To the east is the mouth of the Petit-Rhône which is directly next to the town Saintes-Maries-de-la-Mer. To the east of this town is the beach of Beauduc, situated in the Gulf of Beauduc, which is sheltered by the spit of Beauduc. With a width of about 4 km, the spit of Beauduc is very wide. It was formed from the eroded mouth of the Bras de Fer channel after the avulsion of the Rhône in 1711. Further to the east is the shore of Faraman. In the middle of this shore is Grau de la Dent, the point where the mouth of the Bras de Fer channel used to be. To the east is the Piémanson beach which lies to the west of the mouth of the Grand-Rhône. On the eastern bank is the Napoléon beach. This is where the old Pégoulier mouth used to be. To the east is the La Gracieuse spit. This spit extends into the gulf of Fos and shelters the town of Port-Saint-Louis-du-Rhône. The La Gracieuse spit forms the end of the shoreline of the Rhône delta.

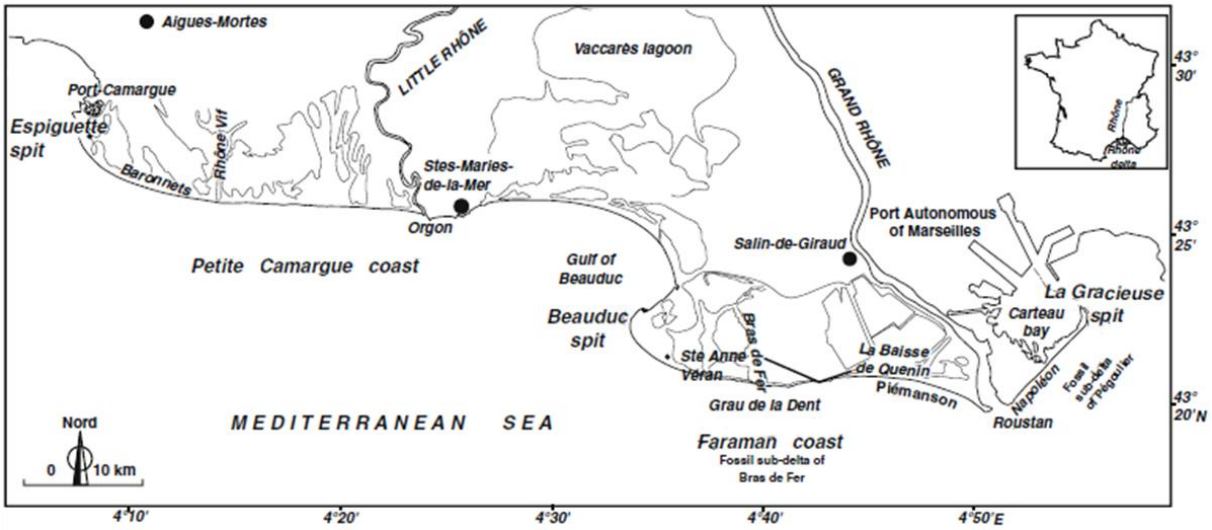

Figure 4: Map of the Rhône delta with mostly the same layout the delta has had since the second part of the 20th century (Adapted from Sabatier & Anthony, 2015).

A pattern can be discerned from the way the sediment is transported along the shoreline of the Rhône delta. Parts along the shoreline undergo accretion while other parts undergo erosion. Four distinct littoral drift cells can be recognised where erosion in one part of the cell causes accretion in another part of the cell (Figure 5). The coast of the Rhône delta can be considered as a closed box system since the Espiguette spit in the west and the La Gracieuse spit in the East act as sediment traps (Sabatier et al, 2006). The town of Saintes-Maries-de-la-Mer forms a barrier for longshore sediment transport. Therefore, the region between Saintes-Maries-de-la-Mer and the La Gracieuse spit can also be considered as a closed box system. This will be the region of interest for this study.

According to the littoral drift cell pattern (Figure 5) in the region of interest, the accretion zones are the Beauduc spit, the La Gracieuse spit, and the western bank of the mouth of the Grand-Rhône. The erosional zones include the shores of Faraman and Napoléon, where the Bras de Fer and Pégoulier relict sediment lobes are located (Sabatier & Suanez, 2003).

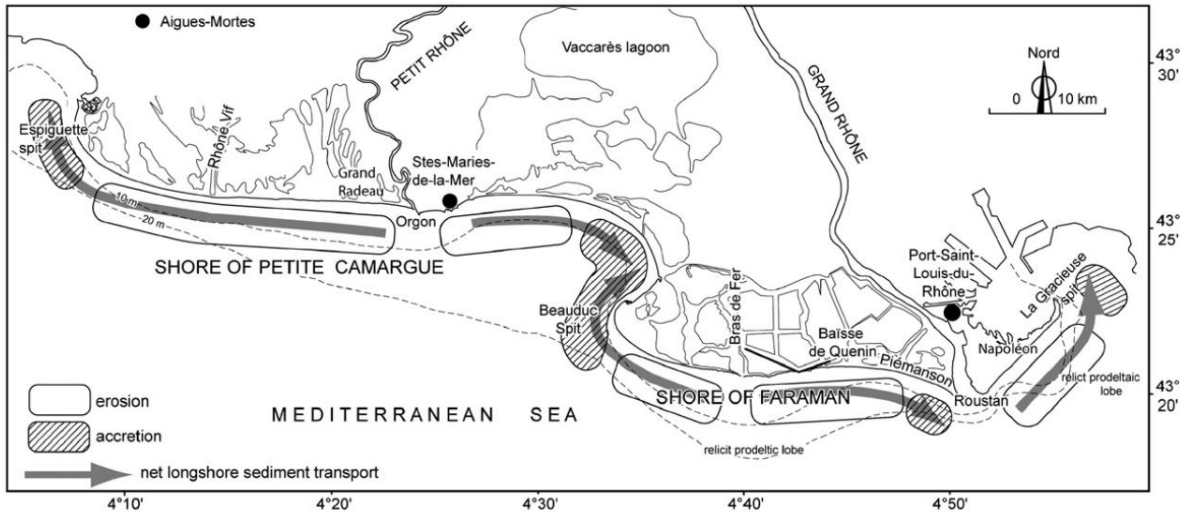

Figure 5: Map of the Rhône delta with the littoral drift cell pattern (Sabatier & Suanez, 2003).

The bathymetry near the shoreline of the Rhône delta shows a typical delta formation. The relict sediment lobes can also be seen when looking at the bathymetry in the gulf of Lion (Figure 6).

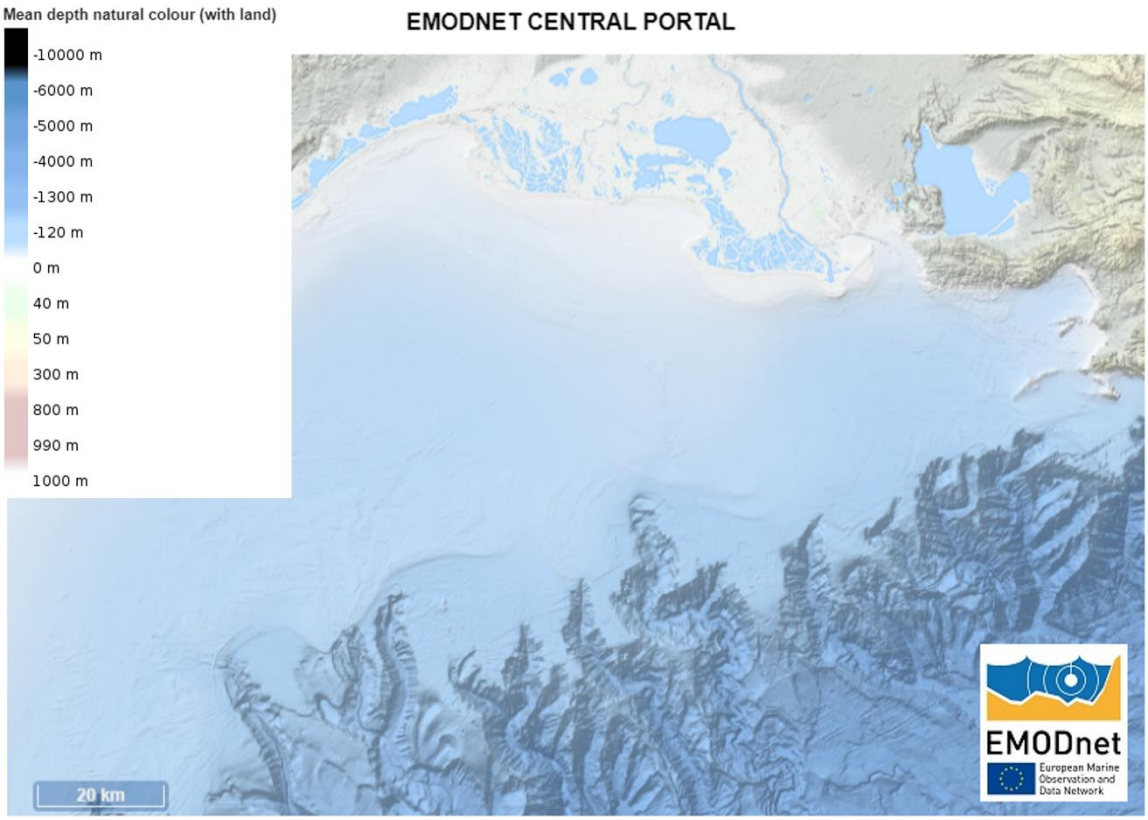

Figure 6: Bathymetry in the Gulf of Lion (EMODnet).

2.3. Wave climate

The wave climate in the Gulf of Lion is the statistical characterization of wave conditions such as wave height, wave period, and wave direction. The wave climate is predominantly the result of wind. The generation of waves by interaction with wind is dependent on the wind speed, the wind direction, the wind duration and the fetch (Reading, 2009). The fetch is the length of water over which the wind can blow unobstructed. The dominant winds that affect the Gulf of Lion are the dry and cold continental winds Tramontane and Mistral (Figure 7).

Figure 7: Dominant winds in the Gulf of Lion (adapted from Eric Gaba, 2008, Wikimedia Commons).

The Tramontane is a north-westerly wind channelled between the Pyrenees and the Massif Central. The Mistral is a northerly wind that is channelled between the Massif Central and the Alps, flowing down the Rhône valley (Langlais et al, 2009). These winds are associated with a short fetch and therefore produce waves in the Gulf of Lion with a low wave height, typically lower than 2 metres (de Madron et al, 2008), (Estournel et al, 2023). These winds blow the whole year long, 1 out of 3 days on average in the Camargue. They have characteristic speeds of about 15 metres per second (Millot, 1990).

The next most prevalent wind is the Marin, a warm and very humid south-easterly wind (Makaske & Augustinus, 1998). This wind is episodic, blowing mostly in autumn and winter. Although less frequent compared to the north-westerly winds, it can blow violently with storms reaching windspeeds of 25 metres per second. Since this wind blows over a long unobstructed stretch of water, or fetch, it can generate a lot higher waves compared to the northerly waves. The episodic nature of the Marin results in significant seasonal variability of wave height in the Mediterranean Sea (Figure 8).

The Marin is also known to cause heavy precipitation as the humid marine air comes in contact with the coastal relief, often resulting in river floods (de Madron et al, 2008). Because of these storm events, resulting in floods as well as strong longshore currents, these winds are of crucial importance to the coastal morphology (Millot, 1990). The analysis of historical hydrological data shows that storms from the southeast represent 70% of the storm events between 1979 to 2010 and that 20% of them were followed by a flood within a few days (Boudet et al, 2017). The frequency of major floods has been decreasing ever since the end of the little ice age (Sabatier & Suanez, 2003), (Milliman & Syvitski, 1992). However, recent changes to the climate due to global warming have reversed this trend (IPCC, 2023).

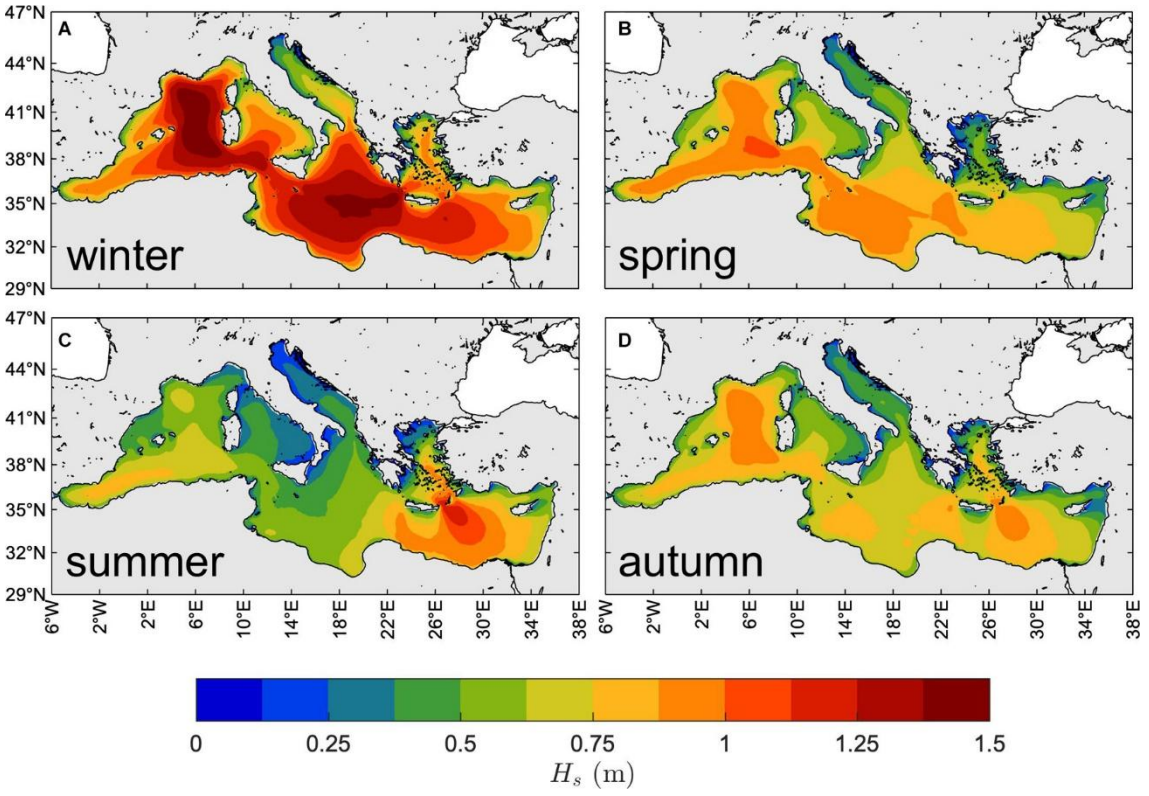

Figure 8: Yearly averaged seasonal 50th percentile of significant wave height for the Mediterranean Sea (1981-2018) (Barbariol et al, 2021).

2.4. Sea level

The sea level in the Gulf of Lion varies. On a relatively small timescale of a day the sea level changes because of the tides, but these just make the sea level oscillate around an equilibrium. On a bigger timescale of a year however, the sea level in the Gulf of Lion rises due to global warming (Suanez & Provansal, 1996).

The tidal cycle at the mouth of the Rhône is a semi-diurnal cycle with two high and low tides each day (Figure 9). Since the tides are linked to the lunar day, which is approximately 50 minutes longer than the solar day, the tidal cycle at the mouth of the Rhône is just over 24 hours. The Rhône delta has a negligible tidal range for the purposes in this study. On average the tidal range is about 20 centimetres with maximum values of 30 centimetres (Makaske & Augustinus, 1998).

Globally, the sea level rise was about 2 mm/yr between 1901 and 2018 (IPCC, 2023). The relative sea level rise in the Gulf of Lion was measured using a tide gauge at Grau de la Dent. Based on these measurements the relative sea level rise was determined to be 2.1 mm/yr during the 20th century, of which 1 mm/yr can be attributed to local subsidence (Suanez & Provansal, 1996). However, the sea level rise in the Gulf of Lion has not been constant throughout this period and has even fallen at one point. Therefore, the relative sea level rise is not representative of the entire period (Sabatier et al, 2009).

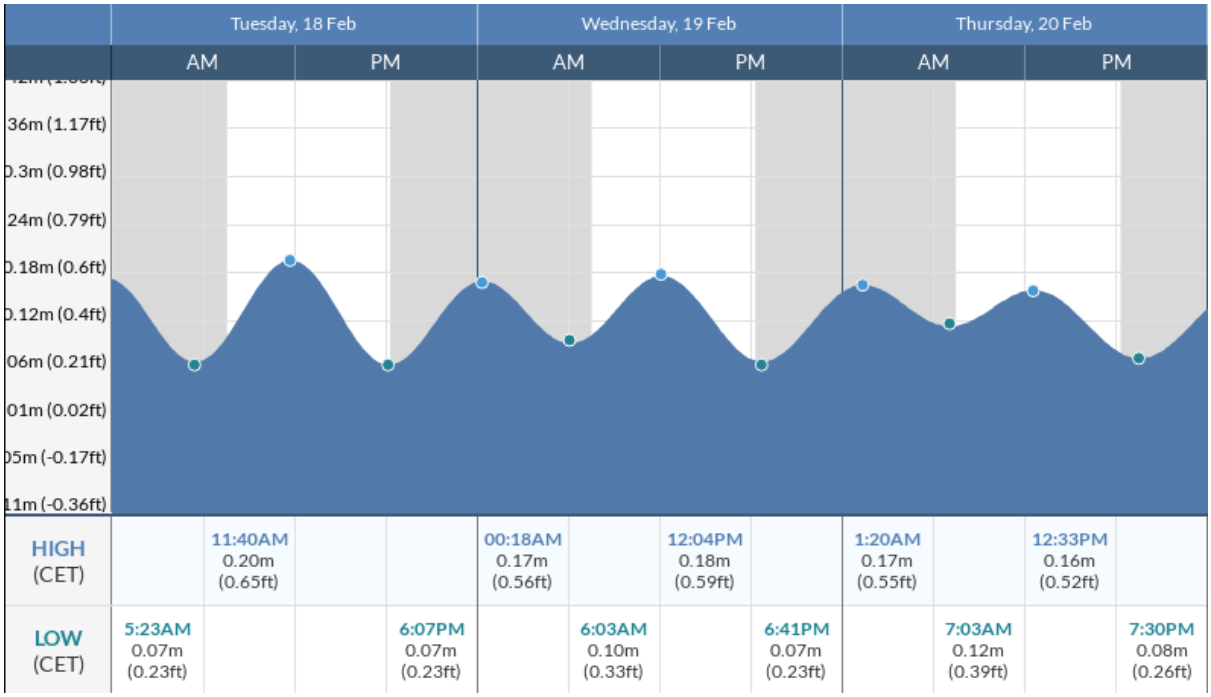

Figure 9: Tidal forecast at Port-Saint-Louis-du-Rhône showing the semi-diurnal cycle (tide-forecast.com).

The rise in relative sea level cannot realistically be stopped. However, it is still possible to prevent a further acceleration of rise in relative sea level. The IPCC (2023) has developed five shared socio-economic pathways (SSP) that illustrate different scenarios with different associated amounts of greenhouse gas emissions and associated possible climate responses. The most hopeful of these scenarios is SSP1, which represents a reduction of CO_2 emissions to net zero by the year 2050. This scenario has an associated relative sea level rise of about 5.5 mm/yr for the remainder of this century. The direst of these scenarios is SSP5, which represents a doubling of CO_2 emissions by the year 2050. This scenario has an associated relative sea level rise of about 11 mm/yr for the

remainder of this century (IPCC, 2023). These two scenarios will be used to test the effect of relative sea level rise on the development of the shoreline of the Rhône delta.

2.5. Shoreline profile

The interaction between the sediment and the waves results in a shoreline profile. The part of the shoreline profile that represents the zone with the most sediment movement is the shoreface. It extends from the fair-weather wave base to the mean low water. It can be further divided into the lower and upper shoreface. The lower shoreface is where, under fair-weather conditions, cross-shore processes such as shoaling prevail. The upper shoreface is where longshore processes prevail and where the waves break at the breaking line (Reading, 2009) (Sabatier et al, 2006). The lower and upper shoreface are separated by the depth of closure (Rozynski, 2024).

The zone where the sand distribution along the profile can change due to natural processes in either stormy or calm weather is called the active coastal zone. It extends from the depth of closure to the top of the beach berm (Figure 10). The associated height is known as the active profile height. The active coastal zone is the part of the shoreline profile that will be considered for the region of interest in this study.

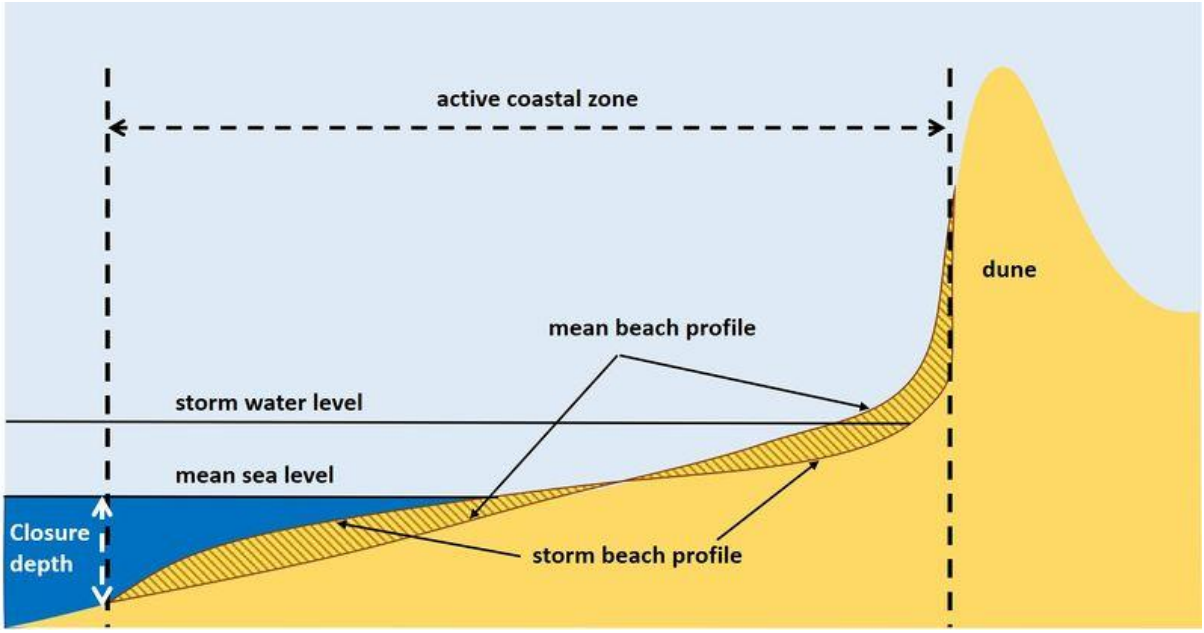

Figure 10: Shoreline profile showing the potential difference in sand distribution along the active coastal zone (Dronkers, 2025).

2.6. Sediment transport

The shoreline of a sandy coast consists of siliciclastic sediment. This sediment is deposited by rivers and redistributed along the coast by waves. Although siliciclastic sediment can contain both larger and smaller particles, this study focuses on the transport of sand. According to the Wentworth scale, sand consists of particles with a diameter between 0.0625 and 2 millimetres. According to extensive grain size analysis by Masselink et al (1992) that was carried out in the area between the Beauduc spit and the mouth of the Rhône, the mean grain size of the sand particles in the region of interest ranges from 0.18 to 0.33 millimetre.

The sediment discharged by the river can be divided into suspended sediment transport (SST) and bedload sediment transport (BST). The coarser sand particles are transported as bedload while the finer particles are transported in suspension. The percentage of sand that is transported as

suspended and bedload sediment transport depends on the river's flow conditions. The percentage of sand in suspension will be higher with more rapid flow. This is why floods can contribute an amount of sediment that is orders of magnitude higher than the mean (Pont et al, 2002).

When the sediment discharged by the river arrives at the mouth the flow decelerates. The coarser sediment usually gets deposited on the delta front in the form of a mouth bar while the finer sediment gets deposited further from the mouth (Reading, 2009). The sediment can then be transported along the shoreline. This sediment transport can be subdivided into a longshore transport component and a cross-shore transport component. The cross-shore component moves perpendicular to the shoreline by the combined action of wind, waves, tides, and the shore perpendicular currents that are formed as a result of these (Seymour, 2005). The longshore component concerns the movement of sediment along the shore. It is predominantly a function of the wave climate as the energy of nearshore waves is the most significant factor governing shoreline development (Reading, 2009).

2.7. ShorelineS

ShorelineS is a vector based, freeform shoreline model that can simulate shoreline development by using relatively simple sediment transport formulas which makes it cost efficient. Compared to detailed two-dimensional horizontal morphological models, ShorelineS is able to simulate a complex real-world case like the sand engine in a matter of minutes instead of months (Roelvink et al, 2020). ShorelineS aims to fill the void between affordable models that cannot capture the complexity of shoreline development and expensive models that can. The numeric computing environment in which ShorelineS is used is MATLAB. The version of ShorelineS discussed in this study is the version from 03/08/2023.

The fundamental formula used for the updating of the coastal section based on sediment transport is based on the conservation of sediment.

$$\frac{\partial n}{\partial t} = -\frac{1}{D_c}\frac{\partial Q_s}{\partial s} - \frac{RSLR}{\tan\beta} + \frac{1}{D_c}\sum q_i \qquad (1)$$

where n is the cross-shore coordinate, s is the longshore coordinate, t is time, D_c is the active profile height, $\tan\beta$ is the average profile slope in the active coastal zone, $RSLR$ is the relative sea-level rise (m/yr), and q_i is the source/sink term (m3/m/yr) due to cross-shore transport, overwashing, nourishments, sand mining, and exchanges with rivers and tidal inlets. Qs is the longshore sediment transport rate (m3/yr).

2.7.1. Longshore sediment transport formulas

The longshore sediment transport rate can be estimated with bulk longshore transport formulas. These formulas are based on simplified representations of physical processes that are calibrated with empirical coefficients. This allows for an estimate of the longshore transport rate while requiring relatively little input parameters (Mil-Homens et al, 2013). This makes these formulas relatively efficient and therefore suitable for ShorelineS.

There are six bulk transport formulas currently implemented in ShorelineS (Table 1). These are the CERC formula (USACE, 1984), the adapted CERC formula by Ashton & Murray (2006), the simplified CERC formula (Roelvink et al, 2020), the Kamphuis formula (Kamphuis, 1991), the modified Kamphuis formula by Mil-Homens (2013), and the van Rijn formula (van Rijn, 2014).

The CERC formula is based on the principle that the longshore transport rate is proportional to the longshore wave power per unit length of beach. The CERC formula is calibrated with data from sandy

beaches. It does not take variations in grain size or bed slope into account. Because of this it can only be used for sandy coasts. It can be written as:

$$Q_s = 0.023\, g^{0.5}\, (\gamma_{br})^{-0.51}\, \left(H_{s,br}\right)^{2.5}\, \sin(2\theta_{br}) \tag{2}$$

Where Q_s is the volumetric longshore transport rate, $H_{s,br}$ is the significant wave height at the breaking line, θ_{br} is the wave angle at the breaking line, and γ_{br} is the breaking coefficient.

In an effort to make the CERC formally based on more globally constant variables, deepwater wave variables instead of wave variables at the breaking line, Ashton & Murray (2006) suggested an adaptation of the CERC formula that is based on deepwater wave conditions and that accounts for refraction and shoaling:

$$\mathrm{Q_s} \;=\; \mathrm{K_2\, H_{s,0}^{\frac{12}{5}}\, T^{\frac{1}{5}}\, \cos^{\frac{6}{5}}(\theta_0)\;\; \sin(\,\theta_0)} \tag{3}$$

Where $H_{s,0}$ is the offshore significant wave height, T is the deepwater wave period, θ_0 is the deepwater wave angle, and K_2 is a calibration coefficient according to:

$$K_2 = \left(\frac{\sqrt{g\gamma}}{2\pi}\right)^{\frac{1}{5}} K_1, \qquad K_1 \sim 0.4\, m^{1/2}/s \tag{4}$$

A simplified version of the CERC formula was implemented in ShorelineS by Roelvink et al (2020). It is mainly meant for illustrating the principles of the model behaviour. It is the exact same formula as the original CERC formula except it uses the offshore significant wave height and the deepwater wave angle.

$$Q_s = 0.023\, g^{0.5}\, (\gamma_{br})^{-0.51}\, \left(H_{s,0}\right)^{2.5}\, \sin(2\theta_0) \tag{5}$$

Another bulk longshore transport formula was presented by Kamphuis (1991). This formula is calibrated on an extensive data set and accounts for both the bed slope and the grain size. It can be written as:

$$Q_s = \frac{2.33}{(\rho_s - \rho_w)(1-p)} \left(T_p\right)^{1.5} (\tan\beta)^{0.75} (D_{50})^{-0.25} \left(H_{s,br}\right)^2 [\sin(2\theta_{br})]^{0.6} \tag{6}$$

Where p is the porosity, ρ_s is the sediment density, ρ_w is the fluid density, T_p is the peak wave period, $\tan\beta$ is the bed slope, and D_{50} is the median grain diameter.

The formula by Kamphuis (1991) was re-evaluated by Mil-Homens (2013). After recalibration of the coefficients based on the least squares optimisation of an extensive data set, this re-evaluated formula is:

$$Q_s = \frac{0.15}{(\rho_s - \rho_w)(1-p)} \left(T_p\right)^{0.89} (\tan\beta)^{0.86} (D_{50})^{-0.69} \left(H_{s,br}\right)^{2.75} [\sin(2\theta_{br})]^{0.5} \tag{7}$$

Lastly, van Rijn (2014) proposed a bulk longshore transport formula that could be used for the longshore transport of gravel and shingle in addition to sand. This formula was developed by analysing the effect of swell waves, grain size, and profile shape on longshore transport by using the process-based CROSMOR-model. This formula was tested against the previously described bulk longshore transport formulas and performed better (van Rijn, 2014). The formula can be written as:

$$Q_s = \frac{0.00018}{(1-p)}\, K_{\mathrm{swell}}\, g^{0.5} (\tan\beta)^{0.4} (D_{50})^{-0.6} \left(H_{s,br}\right)^{3.1} \sin(2\theta_{br}) \tag{8}$$

K_{swell} is the swell factor. It takes the percentage of swell waves into account according to:

$$K_{swell} = 0.015\, p_{swell} + (1 - 0.01\, p_{swell}) \quad (9)$$

Author	Notation in ShorelineS	Formula
USACE, 1984 (simplified)	CERC	(5)
Ashton & Murray, 2006	CERC2	(3)
USACE, 1984	CERC3	(2)
Kamphuis, 1991	KAMP	(6)
Mil-Homens et al, 2013	MILH	(7)
van Rijn, 2014	VR14	(8)

Table 1: Longshore transport formulas that are implemented in ShorelineS. Note that here CERC3 is the original CERC formula by USACE (1984) while CERC is a simplified version of CERC3.

2.7.2. Model input

ShorelineS takes input in the form of an initial shoreline location, the offshore wave climate (significant wave height, peak wave period, and mean wave direction), and any nourishments, (permeable) structures or channels. Besides these there are input parameters such as the average shoreline profile slope, the relative sea-level rise, and model parameters such as the initial grid size, the timestep, and boundary conditions.

The shoreline is described as a string of grid points that are located on the mean sea level contour. It is possible to have multiple coast sections (that can be closed) in the model. For ShorelineS to correctly process the shoreline it should go from right to left.

The offshore wave climate can be given in three different forms. The first is in the form of constant wave height, wave period, and wave direction with the possibility to add a uniformly distributed spread to the wave direction. The second comes in the form of a predetermined set of wave conditions (measurements) where one combination is chosen at random for each timestep. The third option is a time series of wave conditions. This is similar to the previous option, but the predetermined set of wave conditions now also takes place at predetermined moments during the simulation. ShorelineS has the option to interpolate the wave data from multiple wave stations.

The local wave angle is determined from the offshore wave climate by transforming deepwater waves to near shore waves using Snell's law of refraction. These waves are in turn transformed to waves at the breaking line using the equations of van Rijn (2014). The relative sea level rise is implemented according to the Bruun rule (Bruun, 1962).

Nourishments, coastal structures such as groynes or revetments, and channels can all be introduced in the form of polygons. For nourishments, the polygons determine where the influx of sediment is going to be. Additional input as to how much sediment and the start and end times for the nourishment are also required. For coastal structures, the polygon specifies where the coastal structure needs to be implemented so that the sediment transport around the coastal structure can be handled correctly.

The implementation of a river channel in ShorelineS is done by specifying a flow path in the river channel using polygons. The desired width of the channel is also predefined. The sediment discharged by the river is approximated in the simulations by a nourishment in the river channel. ShorelineS checks at every timestep if the channel is still at the desired width and if that is not the case, sediment is moved through the channel towards the mouth. How well the channel width is maintained is controlled by a predefined adaptation factor. This is an efficient way to simulate a

shoreline with a channel that provides a sediment influx. However, it also means that no morphological processes of the river are simulated. This in turn means that natural features such as deltaic lobes and mouth bars will not be formed in the simulation.

Lateral boundary conditions can be specified for non-cyclic shorelines. These boundary conditions define the longshore transport at the boundary of the model. Four different types of lateral boundary conditions are possible. These are the Neumann boundary, the constant orientation boundary, the Dirichlet boundary, and the periodic boundary. The Neumann boundary sets the longshore transport at the boundary equal to the transport at the nearest grid point, implying a free in and outflow of sediment. The constant orientation boundary keeps the orientation of the shoreline at the boundary fixed throughout the simulation. The Dirichlet boundary sets the longshore transport at the boundary to a predetermined value. This can be a function of time or a scalar, representing a constant in and outflow of sediment. An impermeable wall at the boundary can be represented by setting this scalar to 0 (Mudde, 2019). The periodic boundary relates the transport rate at one boundary to the transport rate at another boundary.

2.7.3. Numerical implementation

All the input given to the model is gathered in a structure, S. After this the model operates according to the scheme in Figure 11. The first step the model goes through is the discretisation of the shoreline. The shoreline is divided into small segments that are connected at so called shoreline points. In the middle of each segment, halfway between two shoreline points, the longshore transport at that position is calculated using a staggered forward time-central space explicit scheme.

Figure 11: Flow diagram of ShorelineS model (Roelvink et al, 2020).

The model can add grid points when the length of the shoreline increases (for example at a growing spit) or remove grid points in case the length of the shoreline decreases (for example at an infilling bay). Smoothing of the grid can be applied to mitigate strong variations in grid size (Roelvink et al, 2020).

After the initialisation of the grid the time loop is initiated. ShorelineS allows for an adaptive timestep that ensures stability according to the following criterion.

$$\Delta t < \frac{D_c \Delta s^2}{4 Q_{max}} \tag{10}$$

The adaptive timestep is used because of the explicit scheme that is applied. For this study however, a fixed timestep had to be used due to technical problems with the adaptive timestep.

After the initialisation of the time loop the model runs through several different scripts that each govern a separate piece of the shoreline transformation (Figure 11). For each timestep this is repeated for all the different coast sections until the end of the simulation is reached.

To allow for the development of spits under an angle of incidence higher than the critical angle of incidence of 45°, a local upwind scheme is used instead of a central scheme when the angle of incidence passes the critical angle (As in Ashton et al (2001), but vector based). To properly simulate the developing of these spits the overwash process is also implemented in ShorelineS. This is done by checking the width of the barrier/spit against the critical width (Input parameter) at each timestep. If the width is narrower than the critical width, overwash takes place by moving the spit/barrier landward an amount related to the difference in width (Roelvink et al, 2020).

2.8. Coastal protection/Engineering works

Some efforts have been made to protect and preserve the coastal area of the Rhône delta. This is mostly the case for the area to the west of Saintes-Maries-de-la-Mer. Starting from 1975, this area has been equipped with 122 groynes and about 7 km of dykes. Despite this, the area still experiences erosion. This extensive human intervention in the shoreline development of the coast to the west of Saintes-Maries-de-la-Mer was part of the reason to exclude this part of the Rhône delta from the study.

When focussing on the region of interest there is also a number of coastal protection structures present. The Faraman shore is equipped with 32 groynes, a breakwater and dykes (Figure 12). These were constructed by the local salt mining company to protect the salt marshes to the north of the Faraman shore (Sabatier & Suanez, 2003). This completely closes the shore from the lagoons on the other side of the dunes (Suanez & Sabatier, 1999). An artificial dune ridge was created along the centre of the La Gracieuse spit (Figure 13) in 1992 to control the evolution of the spit and thereby keep the role of the spit as natural barrier for the ports in the gulf of Fos intact (Sabatier & Anthony, 2015), (Sabatier & Suanez, 2003). Furthermore, river avulsion is no longer possible due to dykes and other engineering works controlling the river channel (Sabatier et al, 2006).

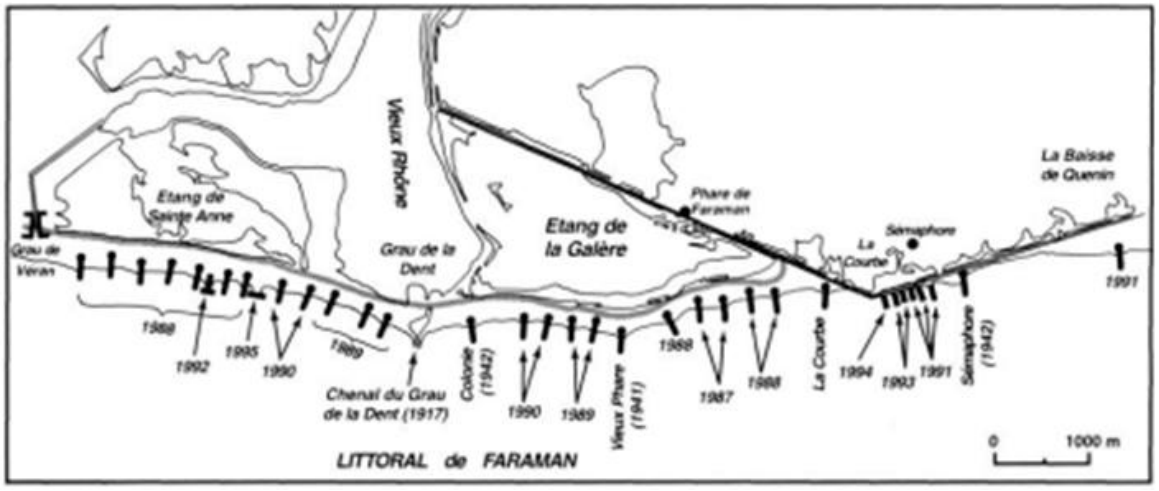

Figure 12: Coastal engineering structures present along the shoreline in the region of interest at the shore of Faraman (adapted from Suanez & Sabatier, 1999).

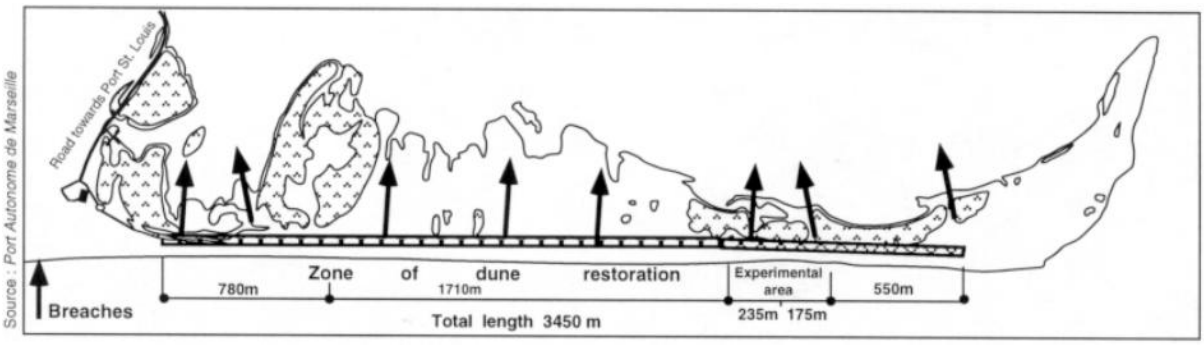

Figure 13: Dune management on the La Gracieuse spit (Port Autonome de Marseille).

The effect of the coastal protection works on the shoreline development in the region of interest is unclear, especially when considering the long-term effectiveness. It is unclear if the coastal protection works have led to less or more erosion. In the case of the latter, it would be the result of downdrift erosion from longshore transport blocking by groynes (Sabatier et al, 2009). The development of the shoreline in the region of interest in this study is considered under natural conditions, without any hard structures present. Therefore, the presence of these coastal protection works could have a negative impact on the results of this study depending on their impact on the development of the shoreline.

The impact of human intervention on the Rhône discharge sediment budget is very noticeable. The decline of land use for agriculture combined with reforestation improves the soil retention (Sabatier & Suanez, 2003), (Milliman & Syvitzki, 1992). This in turn lessens the amount of sediment that ends up in the river. A much bigger impact on the discharge of the Rhône is noticed from the construction of dams on the Rhône. Damming rivers causes a significant decrease in fluvial discharge and by extension sediment discharge. Here, the Rhône is no exception. Since the mid-20th century dams have been constructed along the river. This is one of the reasons why the sediment discharge of the Rhône has decreased by an order of magnitude over the past century (Milliman & Syvitski, 1992), (Pont et al, 2002). Currently, there are 24 hydroelectric dams on the Rhône alone (Provansal et al, 2014).

3. Data collection for Rhône hindcast

An important step in determining the accuracy of a shoreline development model is the validation of the model. This will be done through a hindcast of the Rhône delta. The availability of data on the Rhône delta limits the scope of the hindcast. The age of the youngest set of available data therefore dictates how far back in time the start date of the hindcast can be. To perform a successful hindcast using ShorelineS, detailed data are required on the historic shoreline positions, the wave climate at the time, and the sediment load of the river Rhône near its mouth. At the same time, parameters such as the median grain size of the sediment and the depth of closure are assumed to be constant over time and are therefore considered to be less limiting to the validation of the model.

3.1. Paleo-shoreline maps

References of the shoreline of the Rhône delta are needed for the hindcast and come in the form of cartographic representations of the shoreline of the Rhône delta at different periods in time. Historic maps and historic aerial imagery were considered that have the detail and resolution (< 50 x 50 m) that makes it possible to successfully distinguish and trace the shoreline (Table 2). The oldest source is the map shown in Figure 14. It dates back to 1827. Another map that dates back to 1856 is shown in Figure 15. Both maps come from the archives of the David Rumsey Historical Maps Collection.

Figure 14: Map of the “Bouches du Rhône” from the “Atlas encyclopedique contenant les cartes et les planches relatives a la geographie physique”, 1827. Resolution is 20 x 20 m (David Rumsey Historical Map Collection).

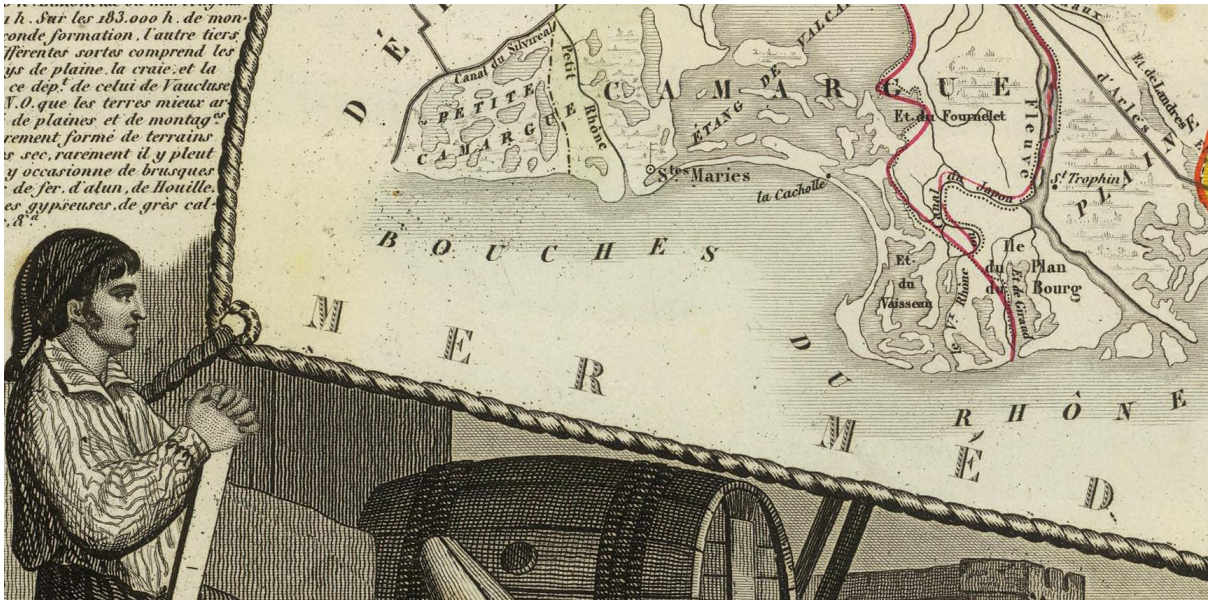

Figure 15: Map of the "Dept de Bes du Rhône" from the "Atlas National Illustre des 86 Departments et des Possessions De La France", 1856. Resolution is 47 x 47 m (David Rumsey Historical Map Collection).

The oldest aerial imagery that was considered as a reliable source for a shoreline position comes from a mission on 26-05-1960 that had the purpose to more accurately map the south of France. Figure 16 shows two photos from a series of 680 photos that were taken during this mission. They show the La Gracieuse spit to the east of the mouth of the Rhône, and the mouth of the Rhône itself respectively.

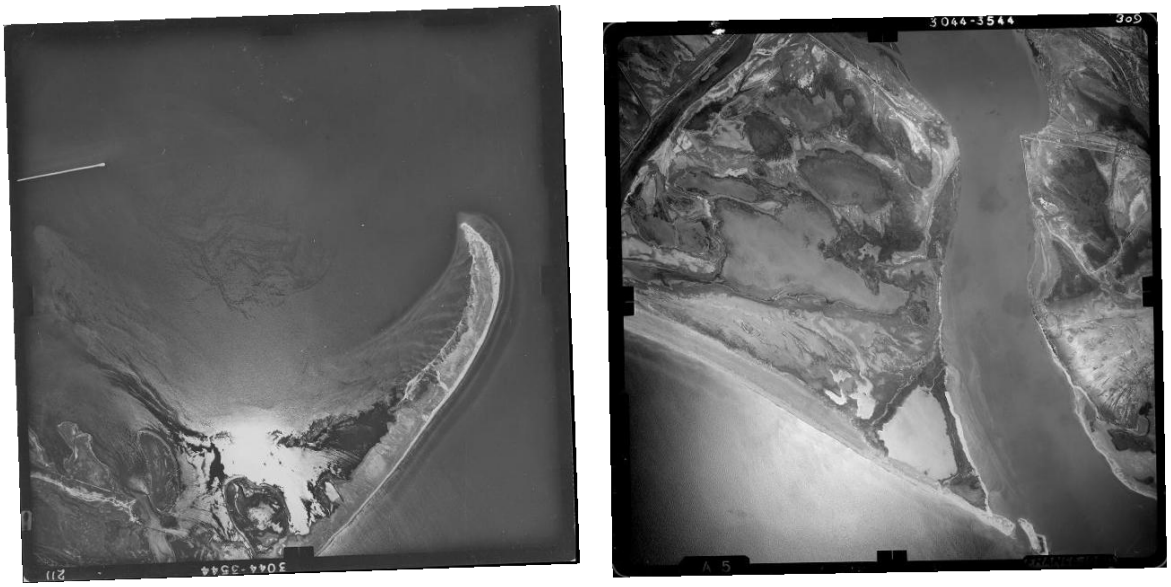

Figure 16: Two photos taken from a plane on a mission to map the south of France, 26-05-1960. Resolution is 10 x 10 m (Remonter le temps - IGN).

Unfortunately, it was not possible to find reliable shoreline position data in the period between 1960 and 1985. Because of this there is a big gap in the coverage of the shoreline positions. The next available shoreline position data is based on satellite imagery. The resolution of the satellite imagery

from 1985 is 30 x 30 m. For the years 2003, 2008 (Figure 17), 2011, 2014, 2017, and 2021 aerial imagery is used with a much higher resolution (Table 2).

Figure 17: Aerial imagery of the Rhône delta from 12/31/2008. Resolution is 50 x 50 cm (Remonter le temps - IGN).

Source	Year	Resolution (m)
David Rumsey Historical Map Collection	1827	20 x 20
David Rumsey Historical Map Collection	1856	47 x 47
Remonter le temps - IGN	1960	10 x 10
Landsat	1985	30 x 30
Remonter le temps - IGN	2003	0.5 x 0.5
Remonter le temps - IGN	2008	0.5 x 0.5
Remonter le temps - IGN	2011	0.5 x 0.5
Remonter le temps - IGN	2014	0.2 x 0.2
Remonter le temps - IGN	2017	0.2 x 0.2
Remonter le temps - IGN	2021	0.2 x 0.2

Table 2: Sources for all considered cartographic representations of the shoreline of the Rhône delta with their respective resolutions.

3.2. Wave climate

The longshore sediment transport is predominantly a function of the wave climate as the energy of nearshore waves is the most significant factor governing shoreline development (Reading, 2009). Under what angle the waves hit the coast, how high the waves are, and how long or how often they flow in certain directions greatly impacts the longshore transport. The wave climate consists of the wave height, the wave period, and the wave direction.

The wave climate data for the Rhône delta that will be used in this study is provided by ERA5 (Hersbach et al, 2018). ERA5 is the fifth-generation reanalysis of the global climate by the European Centre for Medium-Range Weather Forecasts (ECMWF). Among many atmospheric data, the ERA5 dataset provides a very large amount of global wave data. The data from ERA5 covers the period from 1940 to the present and is continuously being extended. Most of the data from ERA5 is available hourly and has a horizontal resolution of 0.28°. However, the wave data is produced on a reduced latitude/longitude grid with a resolution of 0.36°. The ERA5 wave data comes from ocean-wave observations made with satellite altimeters. However, these observations were only available since August 1991. The data from before 1991 is based on the atmospheric data since the ocean-

wave products are determined by the near-surface atmospheric forcing (Bell et al, 2021). This atmospheric data was already available since 1940. All the wave parameters used in this study account for both wind waves and swell (Hersbach et al, 2018).

The wave height input in the hindcast is taken as the significant height of combined wind and swell waves. It is defined as the average height of the highest third of wind-generated waves and swell and represents the difference in height between the wave crest and the wave trough (ECMWF, significant height of combined wind waves and swell, 2018). The wave period input is taken as the peak wave period. The peak wave period represents the period with the most energetic waves (ECMWF, peak wave period, 2018). Lastly, the wave direction input is taken as the mean direction of surface waves. The units are degree true (ECMWF, mean wave direction, 2018).

The data provided by ERA5 comes from a location 16 kilometres offshore from the Rhône coast, at 43.2 latitude and 4.7 longitude (Figure 18). The water depth at this point is 80 metres.

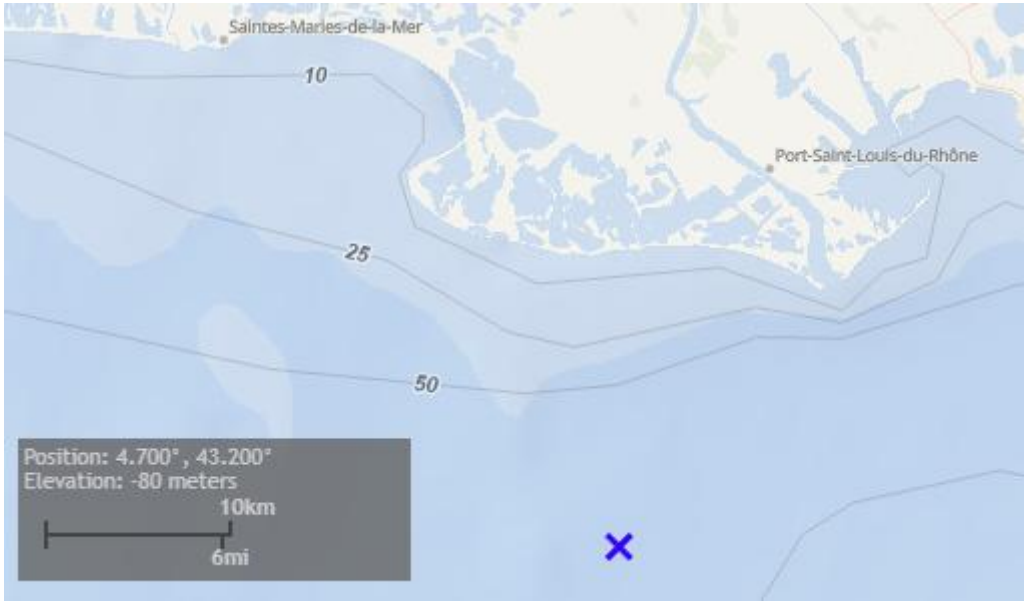

Figure 18: Location of offshore wave data with associated depth (NOAA Bathymetric data viewer)

3.3. Sediment budget

The sediment budget is the total of all the sediment sources and sinks. This study considers the sediment budget of the active coastal zone, as this is the region where the sand distribution along the profile can change. This study considers the portion of the sediment budget that consists of sand, as the distribution of sand along the shoreline is the focus in this study. Previous studies have shown that aeolian sediment transport and sediment transport due to overwash have a negligible effect on the sediment budget and are therefore not considered (Sabatier et al, 2006), (Sabatier & Anthony, 2015).

The shoreline of the Rhône delta between Saintes-Marie-de-la-Mer and the La Gracieuse spit can be considered as a closed box system because of the sediment traps on either end. Therefore, no sediment is assumed to be lost at the boundaries of the region of interest. The only sediment loss therefore comes from cross shore transport. This is assumed to be negligible compared to the longshore transport (Roelvink et al, 2020). Sources of sediment can be nourishments along the coast, of which there are none, and naturally deposited sediment from rivers, such as the Rhône.

There are two ways of determining the sediment volume that is deposited by the Rhône in the region of interest. The first way is by determining the sediment volume that is discharged by the river at the river mouth. This can be done with assumptions on relations to the total discharge of the river, by assumptions on what portion of this discharged sediment is sand, and by assumptions on the amount of discharged sand that ends up in the region of interest defined as the active coastal zone of the shoreline between Saintes-Maries-de-la-Mer and the La Gracieuse spit.

The second way of determining the sediment volume deposited by the Rhône is by performing volume calculations. This is done by analysing the sediment volume that is actively added to or subtracted from the shoreline between two timepoints. This approach also requires many assumptions to be made. Mainly, the assumption that the difference in sediment volume across the shoreline can be attributed to the sediment discharged by the Rhône. The results from this approach were deemed unreliable but can be found in appendix A. The first method is used instead.

The suspended sediment transport (SST) of the Rhône has been estimated by previous studies to be about 30 Mt/yr for the 19th and early 20th centuries. However, the sediment input from the Rhône has since decreased due to a reduction in floods since the end of the little ice age, due to agricultural decline and reforestation, and due to the construction of hydroelectric dams since 1950. The construction of dams especially decreases the bedload sediment transport (BST) of the river (Sabatier & Suanez, 2003), (Milliman & Syvitzki, 1992). Between 1980 and 2000, the SST is estimated at 9.6 Mt/yr (Sabatier & Suanez, 2003). Using the sediment porosity of 0.4 and the sediment grain density of 2.65 t/m^3, the weight can be converted to volume, resulting in 6.0 Mm^3/yr SST.

The BST of the Rhône has been estimated by previous studies, but with large variations. Provansal et al (2014) estimated the BST at about 10-15 Mm^3/yr at the beginning of the 20th century and at 0.4-1.4 Mm^3/yr in 2014. Maillet et al (2006) estimated the BST at 0.2-0.5 Mm^3/yr prior to the construction of dams in 1950 and at 2.5-5.0 * 10^4 m^3/yr in 2006. What can be concluded is that after the construction of dams, the BST has decreased massively. This massive reduction has a large impact on the total amount of sand discharged by the Rhône. A mean BST of 0.2 Mm^3/yr is taken for the calculation of the sediment budget for the Rhône.

The distribution of the discharge between the Rhône's two distributaries is 10% for the Petit-Rhône and 90% for the Grand-Rhône (Maillet et al, 2006). This does not necessarily translate one to one to a distribution for the sediment discharge between the two distributaries (Sabatier et al, 2006), but in this study that assumption is made to arrive at a sediment budget for the Rhône. The sand fraction of the SST was estimated at 6% in 2017 (Piégay et al, 2022). Combining the sand fraction of the SST with the mean BST results in a total sand volume of 0.51 Mm^3/yr that is discharged by the Grand-Rhône and ends up in the active coastal zone of the region of interest.

4. Data preparation for Rhône hindcast

For the hindcast to be as accurate as possible, which means the simulated shoreline matches the real shoreline as well as possible, it is important to have the data that matches the real-world case as close as possible as input for the model. In order to get to this point, a few extra steps had to be taken that modify or otherwise use the data described in chapter 3. These steps will be discussed for the interpreted shorelines, the wave data, the bathymetry, and the sediment budget.

4.1. Extracted shorelines

References of the position of the shoreline of the Rhône delta at the time of the hindcast are necessary not only as a starting point for the simulations, but also at other moments throughout the simulations to allow for the comparison of the results of the simulations to the real-world case. These references come in the form of cartographic representations of the shoreline of the Rhône delta at different moments in time that cover the span of the simulation. It is important that the shoreline can correctly be placed on a grid together with other orientation or location dependent input. Because of this the shoreline should consist of a shapefile with accurate coordinates. This can be obtained from a georeferenced map of the coast.

The oldest source for the historic shoreline of the Rhône delta that was considered because of its high resolution dates back to 1827 and shows the Rhône delta looking quite different compared to what it currently looks like. Notably, the grand Rhône still has its three mouths as described earlier in the site description section. Figure 19 shows the interpreted shoreline of the region of interest in this study highlighted in red.

Figure 20 shows the second oldest (1856) source considered, also with the interpreted shoreline for the region of interest highlighted. This map shows that the three mouths of the Rhône are still intact. Even though, according to Sabatier et al (2006), the Piémanson and Roustan mouth should have been closed off in the year 1855. This is likely because the construction of the dykes took place after the time this part of the map was drawn up but before finalisation and publication of the entire map.

Figure 19: Part of the map of the "Bouches du Rhône" that is relevant for this study with the interpreted shoreline highlighted in red (1827). Resolution is 20 x 20 m (adapted from David Rumsey Historical Map Collection).

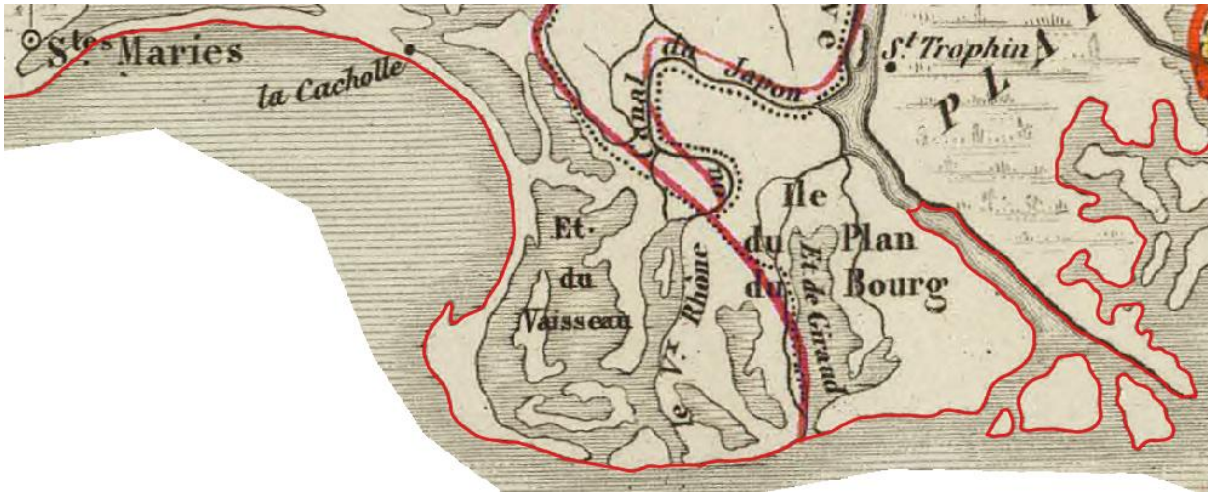

Figure 20: Part of the map of the "Dept de Bes du Rhône" that is relevant for this study with the interpreted shoreline highlighted in red (1856). Resolution is 47 x 47 m (adapted from David Rumsey Historical Map Collection).

The georeferencing process is a process where an image is coupled to a spatial reference system. This is done by taking landmarks with known coordinates in the image and then transforming the image in such a way that these points line up in the best way possible. There are multiple techniques for transforming the image. These include the affine transformation, other polynomial transformations, and the Thin Plate Spline (TPS) transformation.

In dated maps like the 1827 and 1856 maps it is hard to pinpoint places where one can be confident that the same feature exists in the same spot and therefore would give the exact coordinates. With few of these points the difference in the projection of the map between different transformation techniques is significant (Figure 21). Therefore, these maps were considered not suitable as sources for accurate shorelines for the years 1827 and 1856.

Figure 21: The georeferenced "Bouches du Rhône" map from 1827 overlaid on the current map of the Rhône delta. On the left the affine transformation is used while on the right the TPS transformation is used. The distance between the same point (the western bank of the mouth of the Grand-Rhône) on the 1827 and current map has been indicated for both types of transformations (Old Maps Online).

The oldest reference shoreline that has a high enough resolution (10 x 10 m) that allows for the tracing of the shoreline comes in the form of aerial imagery from a mission on 26-05-1960. The resulting map and interpreted shoreline are shown in Figure 22. At this time, the Roustan mouth is the only one of the three mouths that is still open. This is concurrent with Sabatier et al, 2006.

The interpreted shoreline extends approximately 3.5 kilometres into the Grand-Rhône channel, along its riverbanks, and is then cut off. This is done to get a smooth transition to a straight canal,

which is how the river channel will be approximated beyond 3.5 kilometres inland in later stages. This is done because the channel needs to be part of the shoreline for ShorelineS to be able to handle it. The flow path in the channel needs to extend from the northern boundary to the southern boundary. Because of this, the channel effectively cuts the shoreline into two parts. Since ShorelineS cannot account for river dynamics associated with the curvature of the channel, the curved part of the channel is replaced by a straight channel to avoid possible unforeseen complications to the simulation due to the curvature of the channel. This is the case for all interpreted shorelines described in this section.

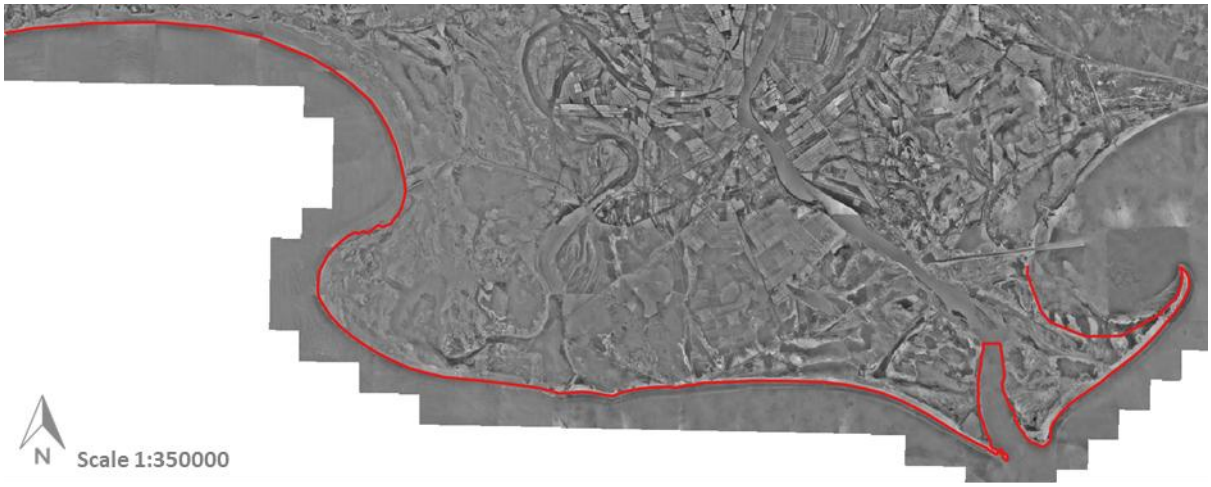

Figure 22: Map of the Rhône delta constructed from aerial imagery with the shoreline highlighted in red, 1960. Resolution is 10 x 10 m (Remonter le temps - IGN).

The next used reference shorelines are extracted from satellite imagery and aerial imagery. Figure 23 shows the satellite imagery from 1985 with the respective interpreted shoreline highlighted. All of the aerial imagery with their respective interpreted shorelines can be found in appendix H. Figure 24 shows a combined image of all the shorelines from 1960 to 2021 to more clearly show the difference between the interpreted shorelines at the different moments in time.

Figure 23: Satellite imagery of the Rhône delta with the shoreline highlighted. 1985 (Google Earth).

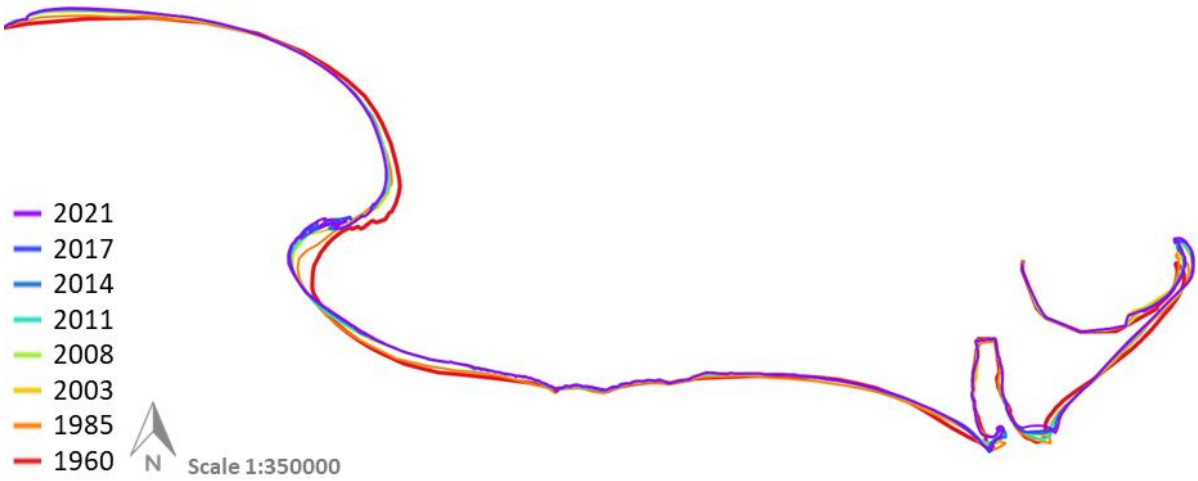

Figure 24: Overlay of the interpreted shorelines from 1960, 1985, 2003, 2008, 2011, 2014, 2017, and 2021.

All the shorelines on the maps shown in this chapter were carefully traced in the geographical information system software QGIS. The resulting interpreted shorelines were then all set to the same map projection that is used throughout the simulation, which is UTM zone 31N. Then, the interpreted shorelines were exported as shapefiles and converted to text files that contain all the x and y coordinates of the interpreted shoreline with the help of a MATLAB script. These text files can be used as input for ShorelineS and for the model comparison.

4.2. Wave data

The wave climate is the most important input parameter for the longshore transport of sediment. It consists of the significant wave height, the peak wave period, and the mean wave direction. To simulate longshore transport of sediment it is important to have wave data that accurately represents the conditions during the hindcast throughout the simulation.

The wave data taken from the ERA5 dataset consists of 21854 datapoints. A set of daily significant wave height, peak wave period, and mean wave direction from the beginning of the simulation in 01-01-1960 all the way to the end of the simulation in 01-01-2020. The wave data is taken at 00:00 UTC each day.

Figure 25 a, b, and c show the distribution of $H_{s,0}$, T_p, and the mean wave direction within the dataset. The histograms are normalised for probability. $H_{s,0}$ has a mean of 1.15 metres and a maximum height of 7.01 metres. T_p has a mean of 5.2 seconds. The mean wave direction shows an obvious peak at 300 degrees. Aside from this peak, a high percentage of the wave data have a wave direction between 100 and 200 degrees.

The wave direction found in this dataset can be compared to the dominant winds in the area. As stated in the background section, the dominant winds in the gulf of Lion are the north-westerly Tramontane and the northerly Mistral. The peak around 300 degrees coincides with these winds. On the other hand, the south-easterly Marin coincides with the percentage of the wave data that has a wave direction between 100 and 200 degrees.

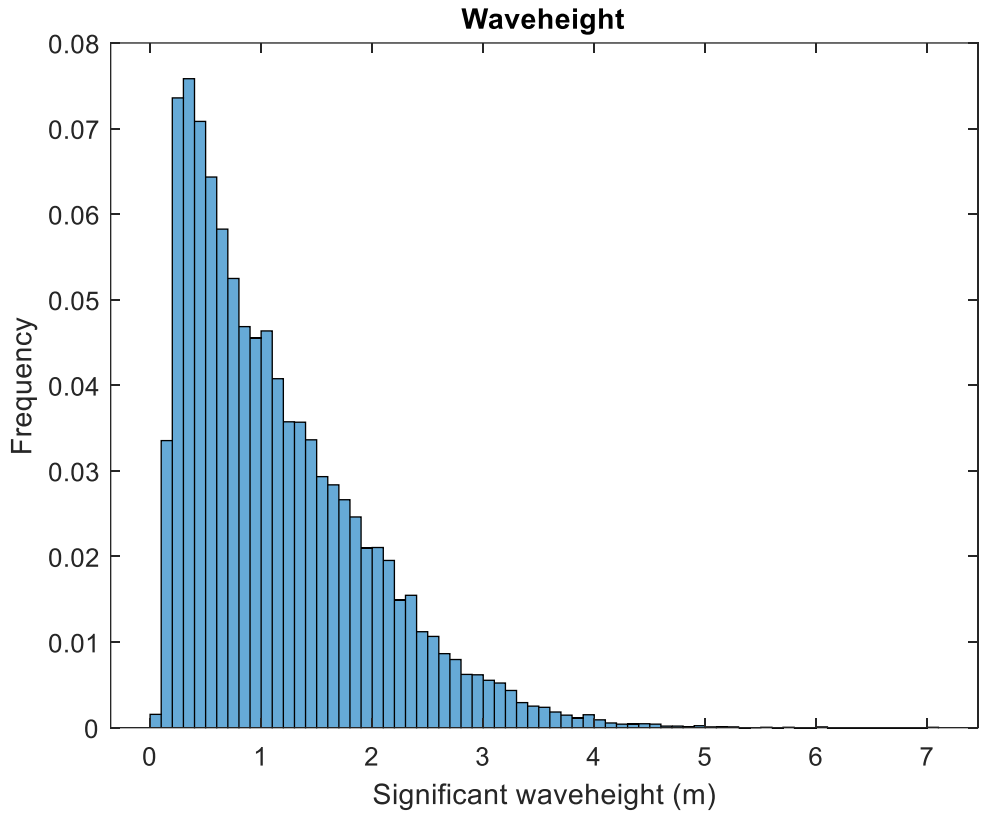
Waveheight
Frequency
0.08
0.07
0.06
0.05
0.04
0.03
0.02
0.01
0
0
1
2
3
4
5
6
7
Significant waveheight (m)

a.

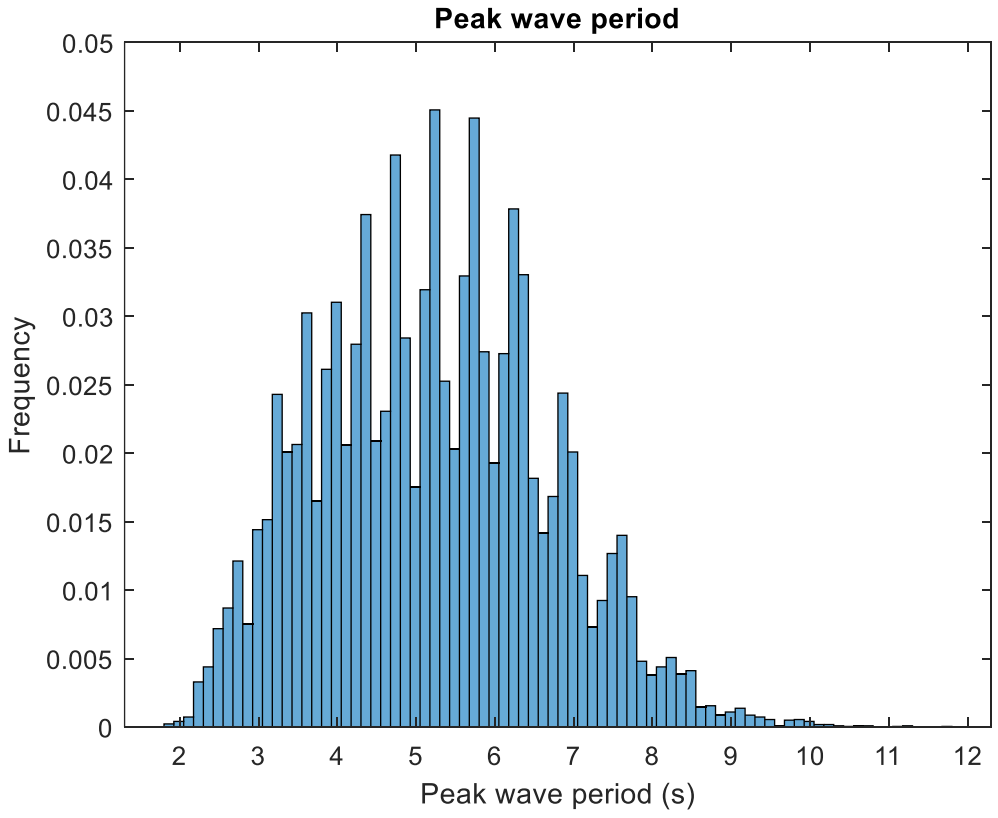
Peak wave period
Frequency
0.05
0.045
0.04
0.035
0.03
0.025
0.02
0.015
0.01
0.005
0
2
3
4
5
6
7
8
9
10
11
12
Peak wave period (s)

b.

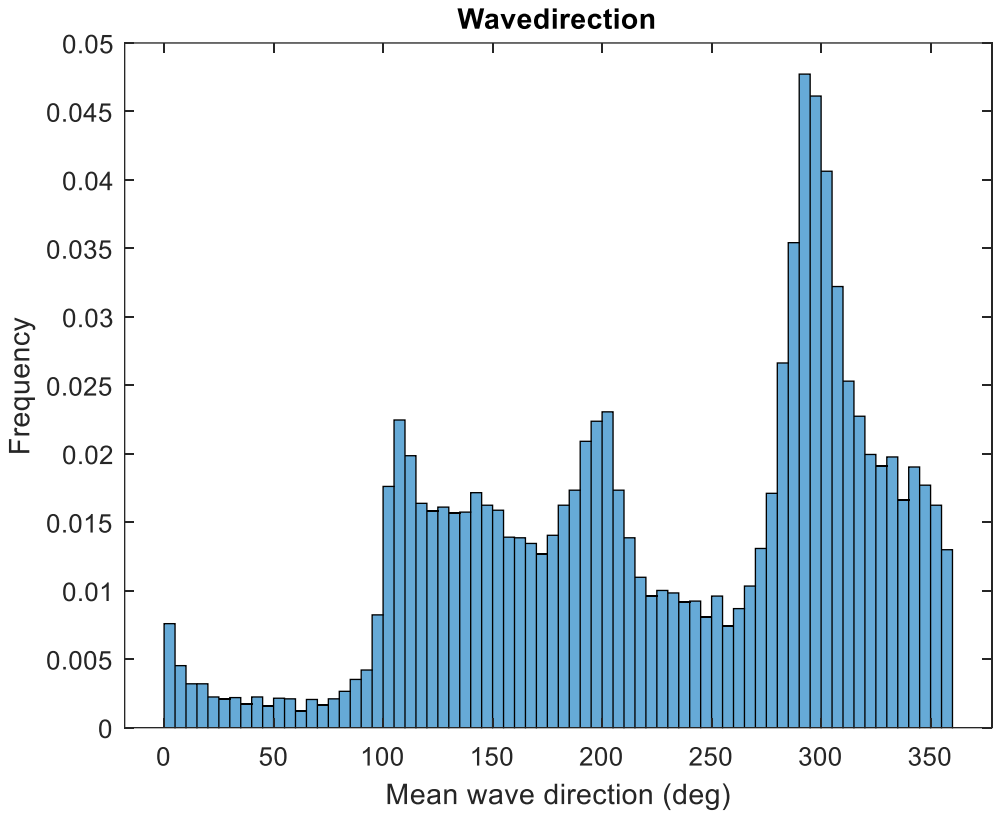

c.

Figure 25: Distribution of a: significant wave height, b: peak wave period, and c: mean wave direction. Normalised for probability with a bin width of 0.1, 0.12, and 5 respectively.

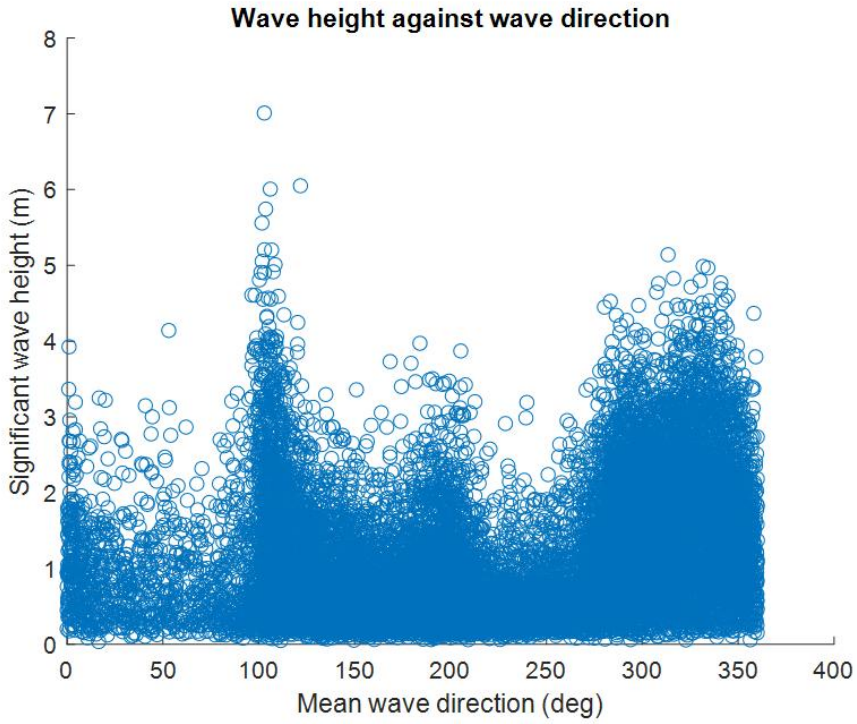

Figure 26: Significant wave height plotted against mean wave direction.

The wave data shows that the highest waves correspond to a wave direction of about 110 degrees (Figure 26). This coincides with the south-easterly winds that are associated with a long fetch, high waves, and that more often result in storms compared to the north/north-westerly winds. It is however notable that the difference in wave height between these waves and the waves with a direction between 280 and 360 degrees is not that big, especially since these north-westerly waves are associated with a short fetch and thus relatively small waves. These distributions agree with literature, as shown in Appendix F

Since the wave data is always taken at 00:00 UTC a possibility of a bias exists. As shown earlier in chapter 2.4, the tidal cycle is approximately 50 minutes longer than a solar day (NORA). Because of this, the tide will not always be in the same part of the tidal cycle at 00:00 UTC and will therefore not introduce a bias to the wave data. However, other phenomena such as wind speed and direction could introduce a bias to the wave data if they follow a certain diurnal pattern. To investigate this effect the wave data taken at 00:00 UTC is compared to wave data taken at 12:00 UTC. The resulting distributions of $H_{s,0}$, T_p, and the mean wave direction of both data sets are shown in Figure 27.

There are some differences between the two datasets. Notably, $H_{s,0}$ is on average slightly higher at 00:00 than it is at 12:00. Also, a higher percentage of the wave data have a wave direction between 100 and 250 degrees at 00:00 as compared to at 12:00. What causes these differences is unknown, but they are considered to be small enough not to be of concern.

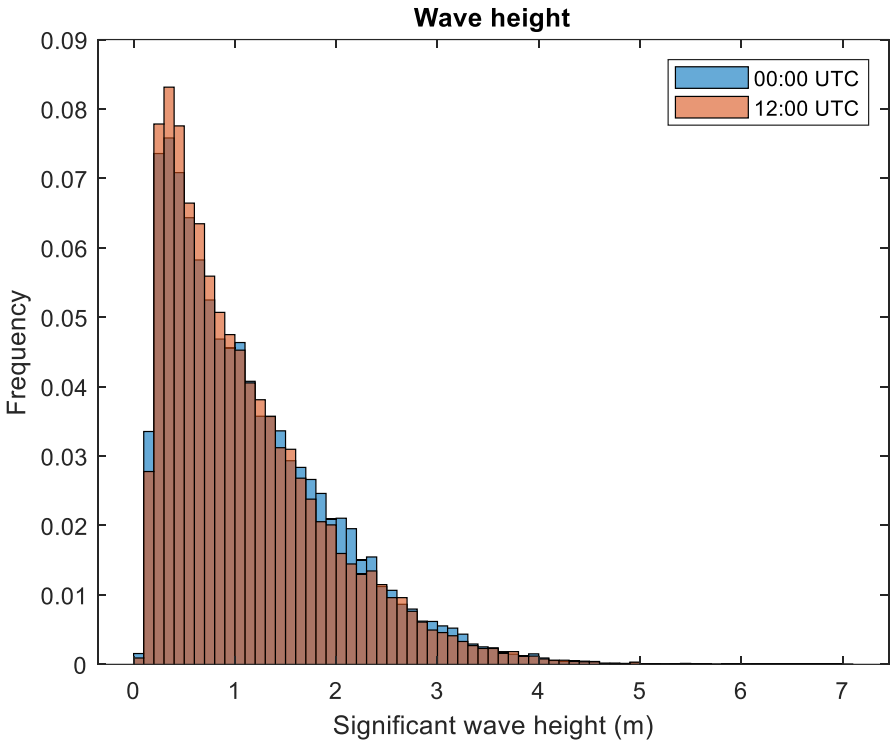

a.

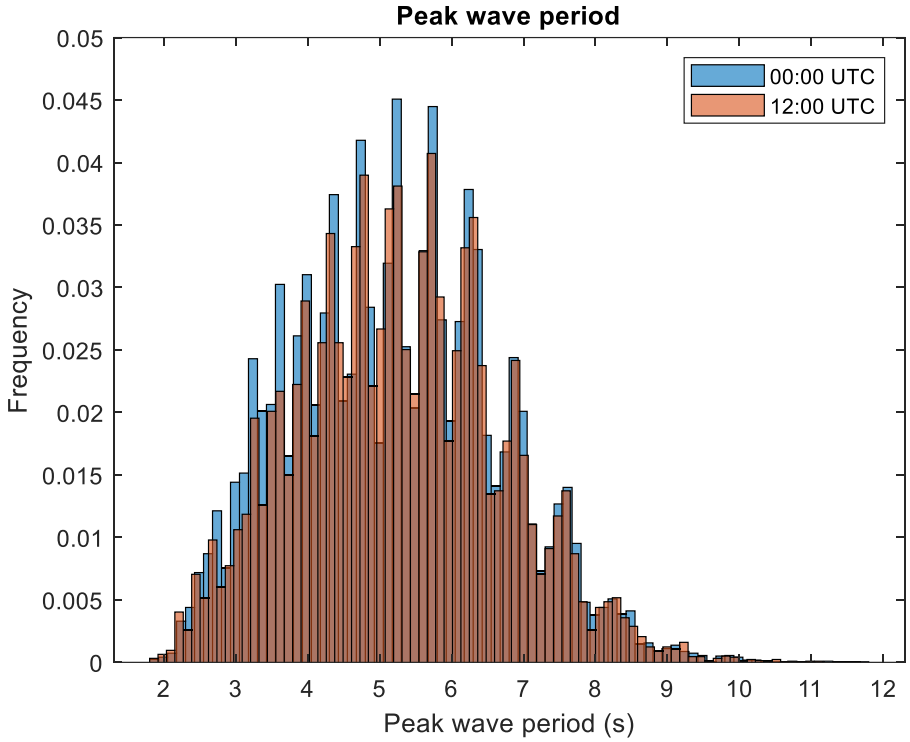

b.

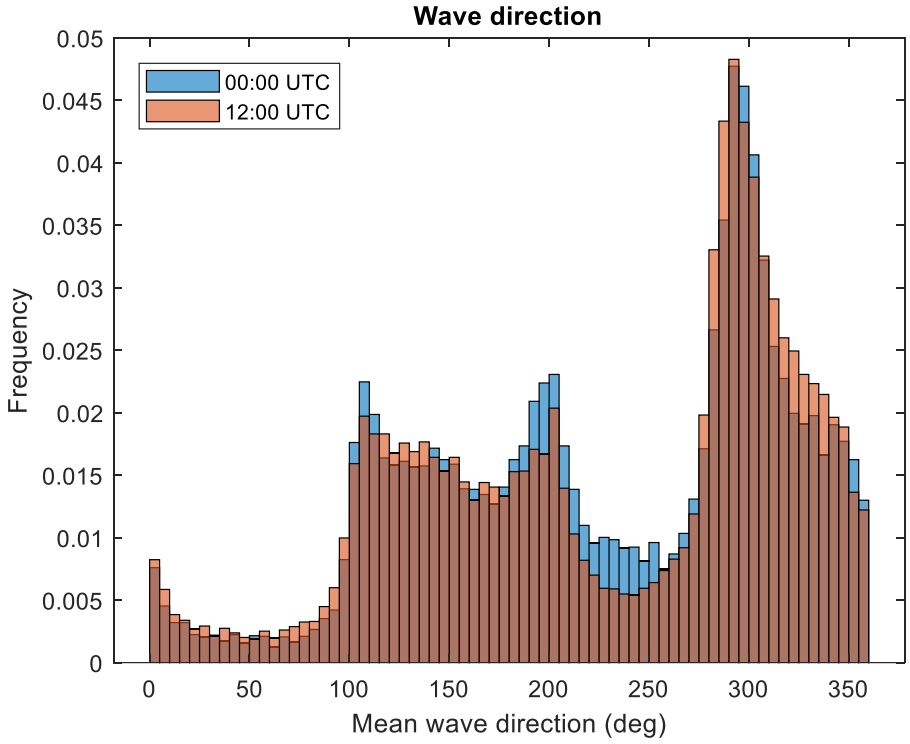

c.

Figure 27: Distribution of a: significant wave height, b: peak wave period, and c: mean wave direction for datasets taken at 00:00 and 12:00. Normalised for probability with a bin width of 0.1, 0.12, and 5 respectively.

It was found that some of the waves with a northerly wave direction were having an erroneous effect on the simulations. These waves erroneously caused all the sediment at the spits to be moved towards the south. This was possible because of the outward growing shape of the shoreline in combination with the beginning and end point of the section of shoreline that was considered.

Usually, if a part of the shoreline is sheltered by another part of the shoreline, ShorelineS prevents the waves from affecting the sheltered shoreline (Roelvink et al, 2020). ShorelineS does this since there would not be offshore waves coming from where the coast is. Because of this, waves with a northerly direction do not impact the simulation of the Rhône shoreline development since the coast lies to the north. However, in the model, this coast to the north stops at the western and eastern boundaries of the shoreline. This makes it possible for some waves to come from around the corner, as illustrated by the arrows in Figure 28.

To prevent the erroneous effect of some of the northerly waves in the model, the wave data needed to be filtered for waves in a certain wave direction band. Figure 29 shows the outer bounds of this wave direction band. These outer bounds were determined by considering under what angles waves could interact with the shoreline without coming from offshore. This means that waves with a wave direction between 291 and 91 degrees are considered to possibly have a negative impact on the simulation and any waves with wave directions outside of this wave direction band are considered to be offshore waves without any negative impact on the simulation.

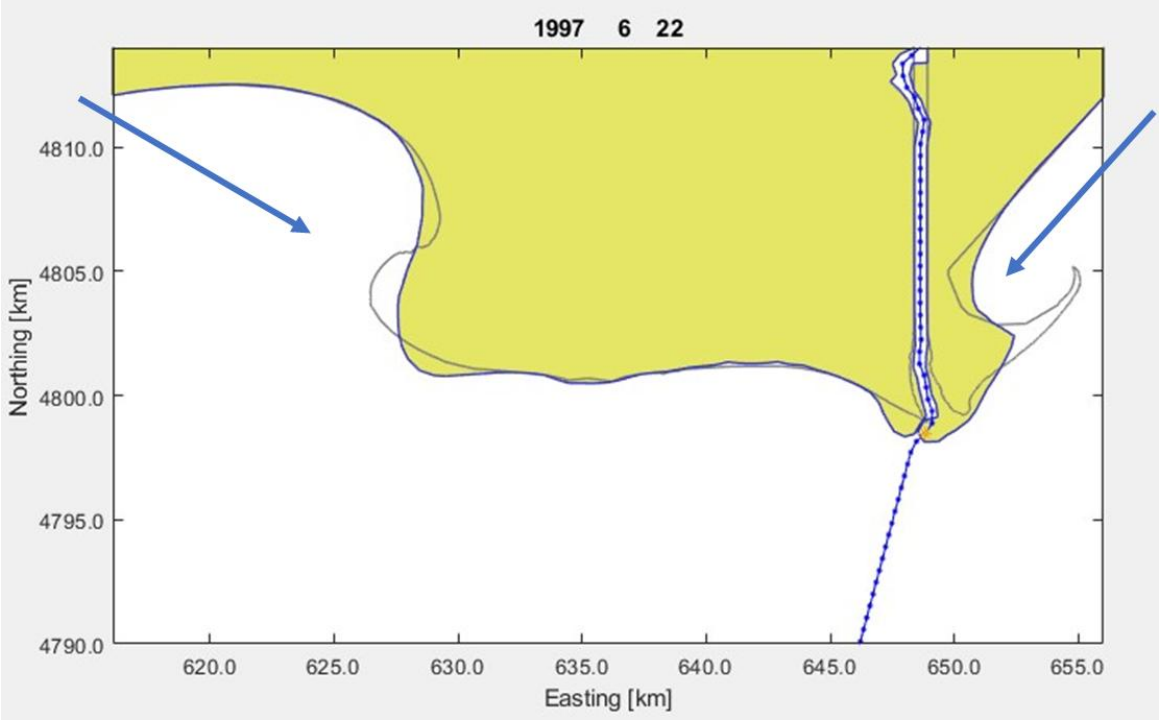

Figure 28: Illustration of how waves with wave directions as indicated by the arrows can result in erroneous interaction at the western and eastern spits by moving all the sediment towards the south. The depicted simulation started with the 1960 interpreted shoreline (grey).

Figure 29: The coast of the Rhône delta with the outer bounds of the wave directions that negatively impact the simulation illustrated. The maximum fetch of the waves in the gulf of Beauduc is also indicated (Google maps).

Since all the northerly wave data is filtered it is possible that a small error is introduced to the simulation because the waves generated by northerly winds in the gulf of Beauduc and the gulf of Fos could affect the northern side of the Beauduc and La Gracieuse spits. To understand the possible impact of these waves, the maximum significant wave height is determined.

The wave generation by local winds is governed by the wind speed, duration, and fetch. The wave growth can be limited by all three of these. However, since the maximum $H_{s,0}$ is of interest, the duration can be ignored as a limiting factor. When both the Tramontane and Mistral occur at the same time a sustained windspeed of 15 m/s can be reached at a height of 10 metres above the surface (Obermann et al, 2018). There is a maximum fetch in the gulf of Beauduc. This fetch is 20 kilometres (Figure 29). Under these circumstances the wave growth is limited by the fetch. The maximum $H_{s,0}$ in the bays can be calculated with equation 3-39 from the Shore Protection Manual (USACE, 1984). This equation is an adaptation of the JONSWAP equation (Hasselmann et al, 1973) specifically made for fetch limited cases.

$$\frac{gH}{U_A^2} = 0.283 \tanh\left[0.530\left(\frac{gd}{U_A^2}\right)^{3/4}\right] \tanh\left\{\frac{0.00565\left(\frac{gF}{U_A^2}\right)^{\frac{1}{2}}}{\tanh\left[0.530\left(\frac{gd}{U_A^2}\right)^{\frac{3}{4}}\right]}\right\} \qquad (11)$$

With a maximum fetch (F) of 20 kilometres and a maximum sustained windspeed (U_A) of 15 m/s this results in a maximum $H_{s,0}$ of 1.4 metres for the waves generated by northerly winds in the gulf of Beauduc and the gulf of Fos.

The filtering of the northerly wave data affects 9194 datapoints of the 21854 total datapoints. The distribution of $H_{s,0}$, T_p, and the mean wave direction within the dataset after filtering is shown in Figure 30. This shows that the wave data filtering removed waves that on average have a higher wave height as well as a higher wave period. The new mean $H_{s,0}$ and mean T_p are 0.9 metre and 5.0 seconds respectively.

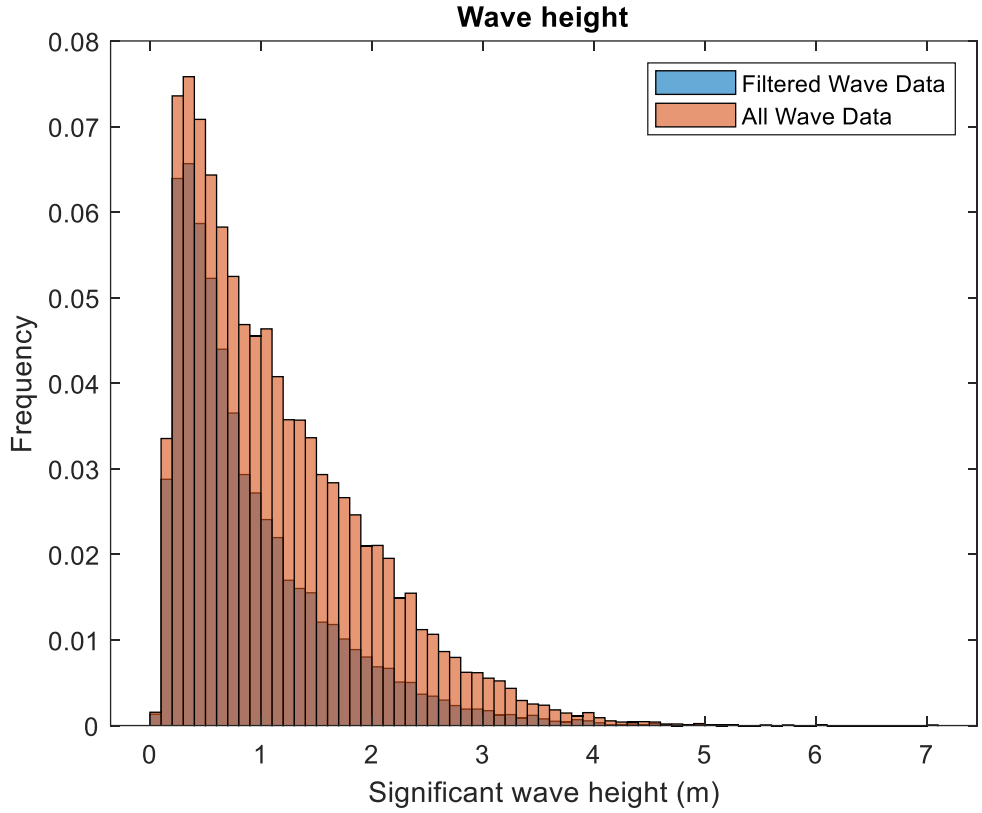
Wave height
Filtered Wave Data
All Wave Data
Frequency
0.08
0.07
0.06
0.05
0.04
0.03
0.02
0.01
0
0
1
2
3
4
5
6
7
Significant wave height (m)

a.

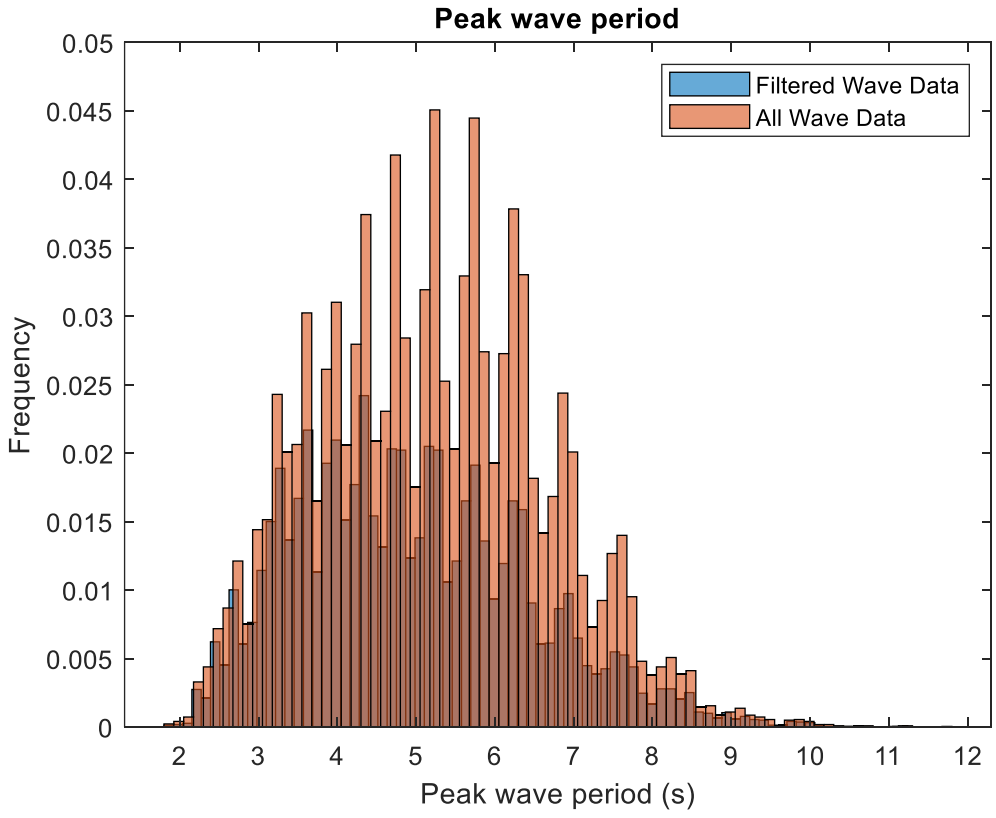
Peak wave period
Filtered Wave Data
All Wave Data
Frequency
0.05
0.045
0.04
0.035
0.03
0.025
0.02
0.015
0.01
0.005
0
2
3
4
5
6
7
8
9
10
11
12
Peak wave period (s)

b.

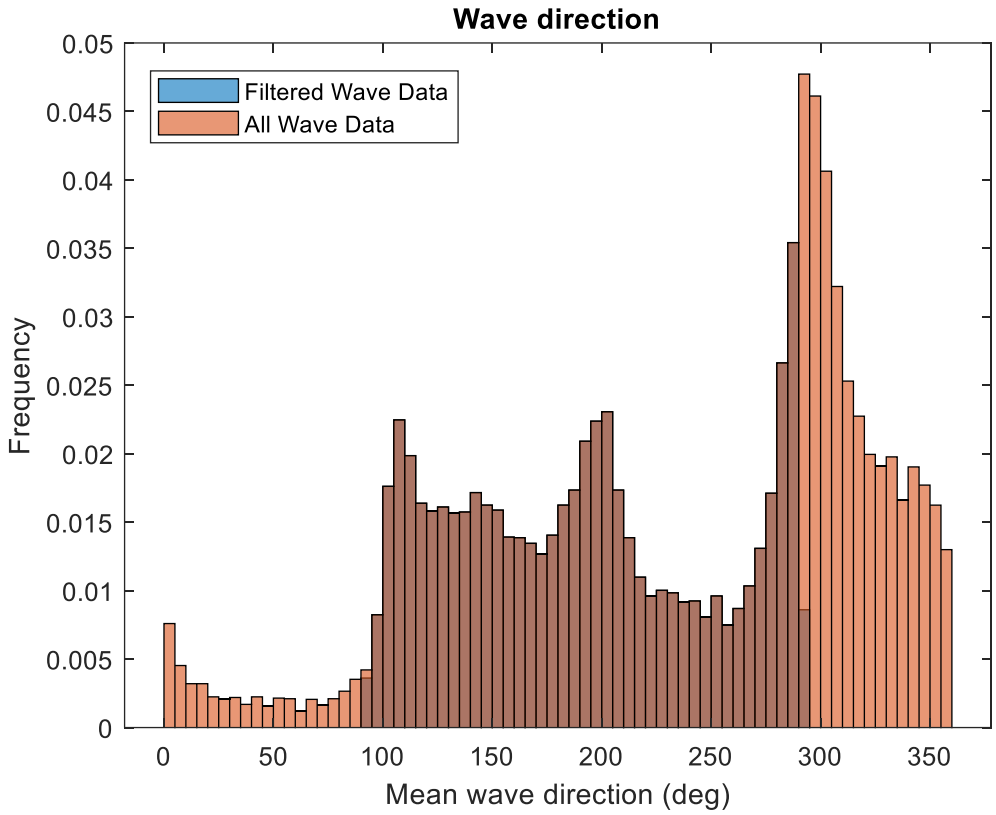

c.

Figure 30: Distribution of a: significant wave height, b: peak wave period, and c: mean wave direction for the wave data both pre and post filtering. Normalised for probability with a bin width of 0.1, 0.12, and 5 respectively.

With the wave data now being more in line with the in-situ conditions a final step is taken to further examine the wave data. To get a good understanding of how the size of the wave changes, the relation between $H_{s,0}$ and T_p is examined (Figure 31). Both a linear and quadratic fit are considered as representations of this relation. The quadratic fit is chosen to be the best representation because the data seems to corelate more for the waves with $H_{s,0}$ between 2.5 and 4.5 metres. Waves with $H_{s,0}$ higher than 4.5 metres are exceedingly rare and the fact that the correlation between the quadratic fit and the wave data falls of at such high $H_{s,0}$ is therefore not of great importance.

$$y = -0.23x^2 + 2.2x + 3.2 \tag{12}$$

This quadratic equation will be used later on to adjust both $H_{s,0}$ and T_p in a realistic manner when looking at the model behaviour.

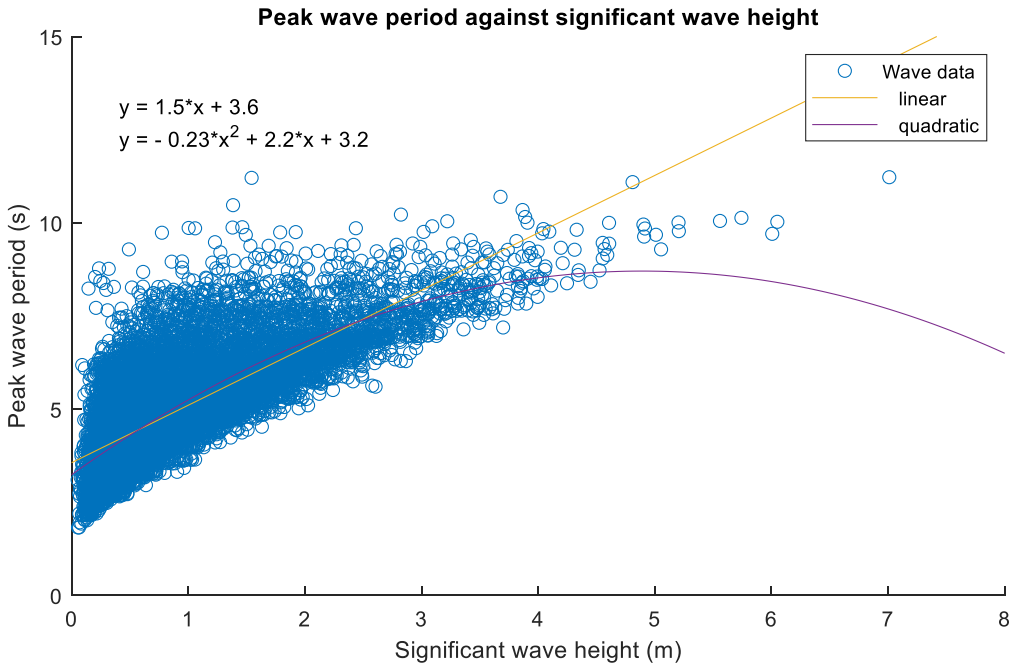

Figure 31: Relation between the peak wave period and the significant wave height illustrated with a linear and quadratic fit included.

4.3. Shoreline profile

The bathymetry is used to determine the profile of the shoreline. First, the slope of the shoreline is examined. Figure 32 shows the cross-shore distance to the 50m isobath from four points spread across the coast of the Rhône delta. This gives a notion of the difference in coastal slope alongshore. The slope near the mouth of the Rhône is very flat but then drops of sharply after about 1 km. This plateau is typical for a prograding delta.

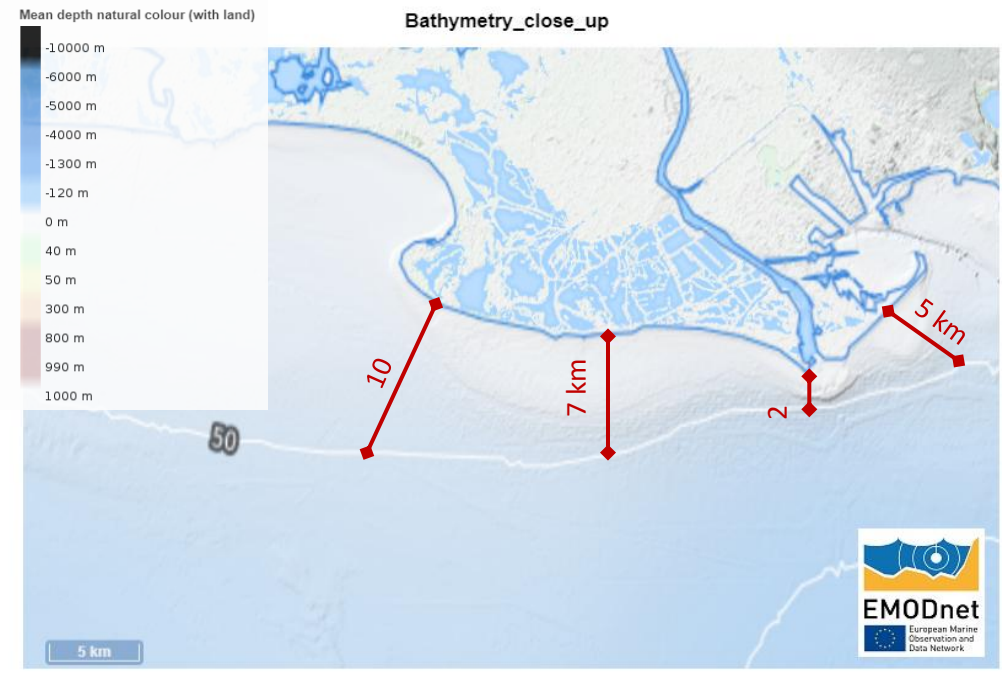

Figure 32: Map of the bathymetry near the coast of the Rhône delta with the cross-shore distance to the 50m isobath indicated (EMODnet).

When considering only the upper part of the profile, to a depth of 10 metres, the bathymetry looks quite different (Figure 33). There is still a difference in steepness of the slope along the shoreline, and the delta plateau is still clearly visible. However, the slope is also steeper near both the Beauduc spit and the La Gracieuse spit whereas the slope here is on average more gradual considering the profile up to a depth of 50 metres. This means that there is not only a difference in steepness of the profile along the shoreline. The steepness of the profile is also not consistent.

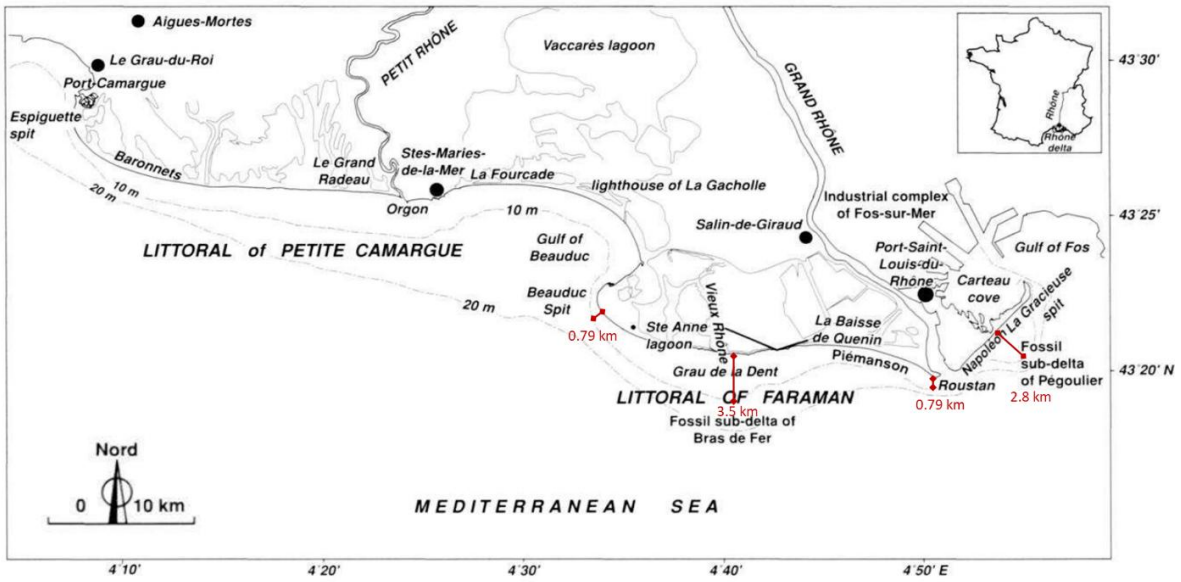

Figure 33: Map of the Rhône delta with the 10m and 20m isobaths. The cross-shore distance to the 10m isobath is indicated. Scale was adjusted (Adapted from Sabatier & Suanez, 2003)

ShorelineS uses a mean bed slope as input so despite the difference in steepness along the shoreline of the Rhône delta, a mean slope angle that is representative of the entire shoreline is determined. Since most of the longshore sediment transport takes place in the upper shoreface, the mean slope in this zone will be considered.

The boundary between the upper and lower shoreface is the depth of closure, which can be calculated based on the mean $H_{s,0}$. After filtering of the wave data, the mean $H_{s,0}$ is 0.9 metre. According to the simplified version of Hallermeier's formulation by Houston, that is especially suited for micro tidal environments, the mean depth of closure is 8 metre (Houston, 1995).

$$h_{in} = 8.9\overline{H_s} \tag{13}$$

To determine the mean slope in the upper shoreface, the profile to a depth of 10 metres was considered. This depth is used since it is the closest depth to the depth of closure while having an isobath available.

The distance from the shoreline to the 10-metre isobath was determined based on the shoreline between the Beauduc spit in the west and the La Gracieuse spit in the east (Figure 34), but not on the bay between the Beauduc spit and Saintes-Maries-de-la-Mer. This decision was made because the shallow bay would greatly influence the average distance to the 10-metre isobath, and therefore the average slope angle. Since the average slope angle is necessary for the longshore sediment transport, and since the longshore sediment transport is assumed to be limited to the area between the Beauduc and the La Gracieuse spits (Figure 40), only this area was considered for the determination of the average slope angle.

This determination was done by georeferencing the isobath map and tracing the 10-metre isobath in QGIS (Figure 34). Next, the part of the shoreline that is of interest was divided into 370 equidistant points. Since the isobath map is from 2003, the interpreted shoreline for 2003 was used. The minimal distance from each point on the interpreted shoreline for 2003 to the 10-metre isobath was determined (Figure 34) with a nearest-neighbour interpolation and the mean distance between the shoreline and the 10-metre isobath was found to be 1.51 km. With a depth of 10 metres, this results in a mean bed slope of 0.0066.

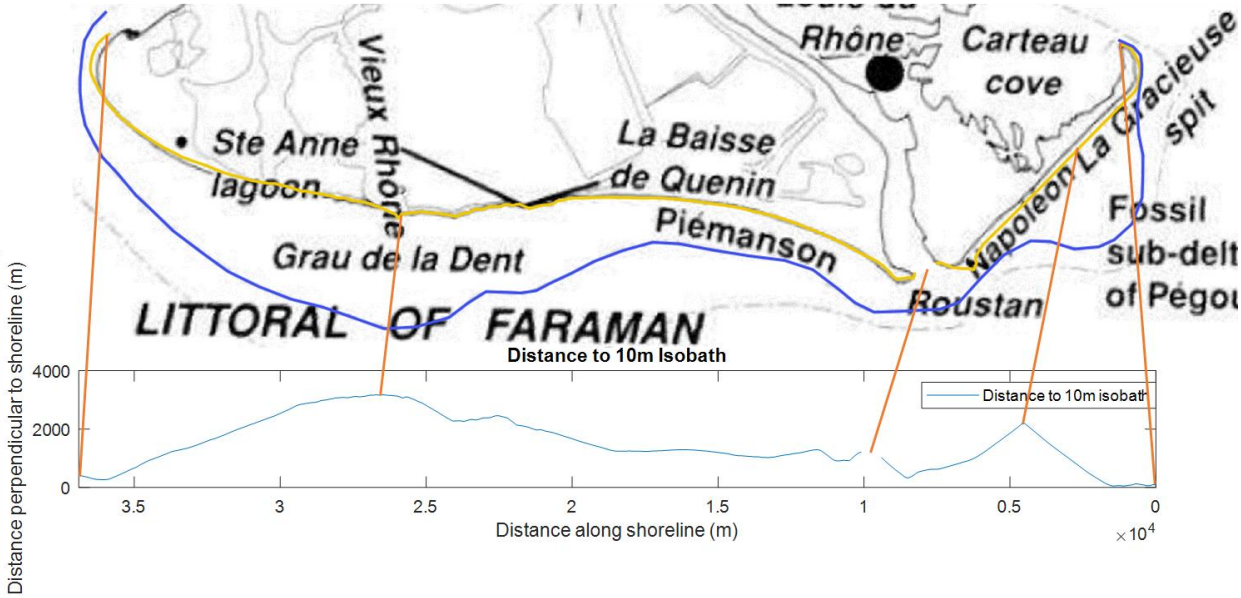

Figure 34: Isobath map with the 2003 interpreted shoreline (yellow) and the 10-metre isobath (blue) and the distance between them plotted along the shoreline. 5 points on the shoreline are indicated. From left to right these are: the Beauduc spit, the Bras de Fer relict sediment lobe, the mouth of the Grand-Rhône, the relict lobe of the Pégoulier mouth, and the La Gracieuse spit.

It is worth noting that the mean distance to the 10-metre isobath is 400 m for the Beauduc spit, and 80 m for the La Gracieuse spit, these are the points in the region of interest with the steepest bed slope. Resulting in a combined mean distance of 240 m which in turn results in a mean bed slope of 0.042 as a slope representative of the spits in the region of interest.

Similarly, it is worth noting that the mean distance to the 10-metre isobath is 2.83 km for the part of the shoreline at Grau de la Dent, where the Bras de Fer relict sediment lobe is located. The mean distance to the 10-metre isobath is 1.61 km at the Napoleon beach, where the Pégoulier relict sediment lobe is located. This results in a combined mean distance of 2.22 km and a mean bed slope of 0.0045 for the parts of the shoreline where the relict sediment lobes are located. These are the points in the region of interest with the gentlest bed slope.

The active profile extends from the depth of closure to the top of the beach berm. The mean berm height in the region of interest is about 2 m (Sabatier & Anthony, 2015). The combination of a mean bed slope of 0.0066 with a depth of closure of 8 m, and a berm height of 2 m results in the profile shown in figure 35. This gives an active profile height of 10 m.

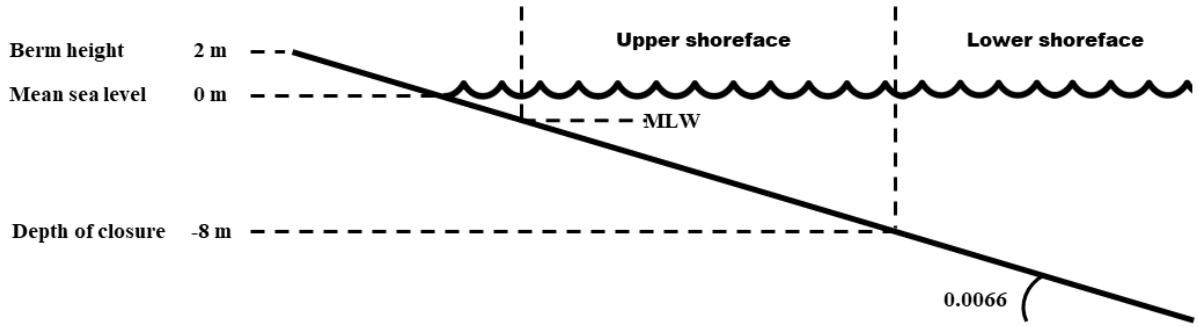

Figure 35: Average profile of the examined part of the Rhône delta, to be used in the simulation. With water depth of depth of closure, mean sea level, slope angle, and berm height indicated.

5. Synthetic case for development of a shoreline with a river mouth

5.1. Model setup

In order to better interpret the results of the simulation of the shoreline development of the Rhône delta, and to answer the question if ShorelineS can successfully simulate shoreline development of a shoreline with a river mouth in a simplified environment, a synthetic case with a simplified shoreline has been set up.

For the simulation of this synthetic case, the shoreline was treated as a region where the morphology is completely governed by natural processes, where the shoreline is sandy along its entire length, and where the sediment transported by the river is discharged at a constant rate throughout the simulation.

To allow for easy comparing between the result of this synthetic case and the hindcast of the Rhône shoreline later on, the default parameters will be the same for both cases where possible. This comes down to all input being the same except for the initial shoreline, the flow path of the river, and the wave parameters. All the different parameters used, and all the decisions made to set up the synthetic case will be discussed here. Table 3 shows all the default parameters. Unless specified, these are the parameters used in all the simulations of the synthetic case.

5.1.1. Input shoreline

The shoreline constructed for the synthetic case is a straight, 30 km long shoreline. At the centre is a river mouth perpendicular to the shoreline (Figure 36). The river channel is 1 km wide. The channel extends for 11 km to the North. Since ShorelineS considers the banks of the channel as part of the shoreline, this results in a total shoreline of 51 km made up of two segments of 25.5 km

For ShorelineS to correctly process the shoreline of the synthetic case (black line in Figure 36) it should go from east (right) to west (left). For ShorelineS to correctly process the river channel, the flow path of the river should go from boundary to boundary. In this case that is from the northern boundary to the southern boundary. Since the river channel separates the shoreline into two parts, the string of grid points that represents the initial shoreline is also separated into two parts.

5.1.2. Channel parameters

The implementation of a river in ShorelineS is done through specifying a flow path along the river channel and describing what the desired channel width is and how strongly the model should try to adhere to this width. The sediment discharged by the river is implemented in ShorelineS in the form of a nourishment in the river channel. ShorelineS checks at every timestep if the channel is still at the desired width and if that is not the case, because the channel is getting filled in by sediment from the nourishment, sediment is moved through the channel towards the mouth.

How well the channel width is maintained is controlled by a predefined adaptation factor. This makes it possible for the river channel to get filled in under certain circumstances, for instance if the waves keep pushing the sediment into the channel. For the synthetic case, the desired width will be 1 km, and the adaptation factor is set at 0.8. This is relatively high, but it should ensure that the channel will not get filled in from the nourishment. The nourishment that represents the sediment discharge will be a continuous supply of 0.51 Mm^3/yr for the entire sixty-year period, for a total of 30.4 Mm^3. This is according to the sediment budget described in section 3.4.

Here, the river flow path is right in the middle of the channel and extends to the southern limit of the simulation area (Figure 36). This results in the final setup for the simulation of the synthetic case.

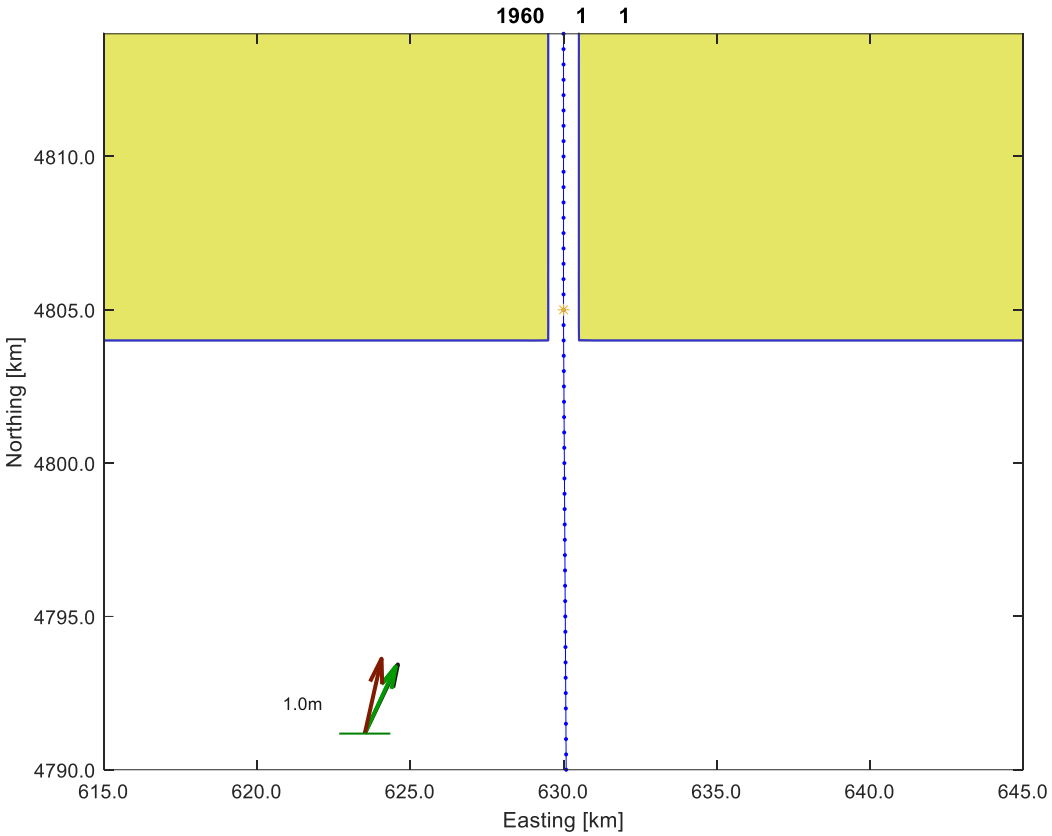

Figure 36: Starting position for simulation of the synthetic case. The yellow area is the coastal area bounded by the shoreline in black, the blue dotted line is the flow path of the river, and the arrows signify the wave direction (offshore, nearshore, and breaking in black, green and red respectively).

5.1.3. Wave climate

For the synthetic case, a constant wave climate is used with a constant $H_{s,0}$ and T_p as well as a constant wave direction. Although a uniform spread can be added to the wave direction to more closely resemble a real-world wave climate, this is not done for most simulations in the synthetic case since having a constant wave direction eliminates random outcomes which is helpful for the model behaviour analysis. To stay as close to the hindcast as possible, the means of $H_{s,0}$ and T_p (0.9 metre and 5.0 seconds respectively) from the offshore wave data for the hindcast are used as constant wave climate in the synthetic case.

5.1.4. Relative sea level rise

For the synthetic case, no rise in relative sea level was included to keep the simulation as simple as possible in order to focus on the model behaviour concerning the development of the river mouth. The model behaviour under standard conditions with the relative sea level rise as predicted in the shared socio-economic pathways is also analysed.

5.1.5. Transport formula

The bulk longshore transport formula used in the simulation under standard conditions is the VR14 formula (eq. 8). This formula is used since it is expected to have the best performance based on comparisons to the other bulk transport formulas (van Rijn, 2014). The performance under standard conditions of the other five longshore transport formulas implemented in ShorelineS (Table 1) is also analysed.

5.1.6. Shoreline profile

For the best insight into the results from the hindcast, the same parameters that define the shoreline profile of the Rhône shoreline (Figure 35) will be used for the synthetic case. These are the mean bed slope of 0.0066, the depth of closure of 8 m, the berm height of 2 m, and the active profile height of 10 m. The orientation of the foreshore is not specified which causes ShorelineS to derive it from the orientation of the shoreline by assuming depth contours parallel to the shoreline.

5.1.7. Model parameters

Just like the hindcast, the simulation will be run for 60 years (from 1960 to 2020). The fixed timestep is set at 0.05 yr. The initial grid size is set at 500 m. According to the stability criterion (eq. 10), the simulation is stable under these circumstances up to a maximum transport rate of 12.5 Mm^3/yr. This is more than sufficient for most simulations in the synthetic case. Nevertheless, whenever instability is encountered, the simulation is instead run with a timestep of 0.01 yr. When this is the case, it will be specified.

The lateral boundary conditions that are set on either ends of the shoreline are Neumann boundaries. This means that a free in and outflow of sediment across the boundary is possible. This boundary condition is chosen to make sure that the sediment transport at the boundary does not interfere with the simulation of the development of the shoreline and river mouth.

The median grain diameter d50 and d90 were set to 0.2 and 0.3 millimetre respectively. These are the values representative of the Rhône shoreline according to the grain size analysis by Masselink et al (1992). These values are used to allow for easier comparison between the synthetic case and the hindcast.

5.2. Default synthetic case parameters

The parameters used to simulate the shoreline development for the synthetic case are given in Table 3. The different values represent the different simulation runs for that specific parameter. The bolded values represent the default values. Unless specified otherwise, only one parameter is changed per simulation.

Parameter	Value
Wave Parameters	
Significant wave height	0.5 m **0.9 m** 1.3 m
Peak wave period	3.0 s **5.0 s** 7.0 s
Deepwater wave angle	**180°** 150° 120°
Wave spreading	**0°** 45° 90°
Water depth offshore	80 m
Active profile height	6 m **10 m** 14 m
Transport Parameters	
Transport formula	CERC CERC2 CERC3 KAMP MILH **VR14**
CERC coefficient	0.5 E^{6}
Median grain diameter d50	2 E^{-4} m
Median grain diameter d90	3 E^{-4} m
Porosity	0.4
Mean bed slope	0.0045 **0.0066** 0.042
Density of sand	2650 kg/m^3
Density of water	1025 kg/m^3
Gravitational acceleration	9.81 m^2/s
Depth of closure	4 m **8 m** 12 m
Time steps & numerical	
Timestep	0.01 yr **0.05 yr**
Reference (Starting) time	1960-01-01
End of simulation	2020-01-01
Initial grid size	100m **500 m** 1000 m
Boundary conditions	
Boundary condition at start of shoreline	Neumann
Boundary condition at end of shoreline	Neumann
Climate change impact	
Sea level rise	**0 mm/yr** 5.5 mm/yr 11 mm/yr
Nourishments	
Total nourishment	3.0 E^{7} m^3
Channel physics	
Channel width	1000 m
Channel adaptation factor	0.8

Table 3: Default simulation parameters for the synthetic case. Bolded values are the default values.

5.3. Results from the synthetic case

To test the performance of ShorelineS to simulate a prograding river mouth, the first test is limited to a nourishment in the flow path of the river but without any wave interaction. For this test all the default parameters as specified in Table 3 are used, but with a wave height of 0 metre and with three different total nourishments of 2.1 E^7 m^3, 4.2 E^7 m^3, and 8.4 E^7 m^3 respectively. This gives the results shown in Figure 37. These results show that the sediment deposited by the river is pushed out seawards while the channel is maintained. Furthermore, the increasing total nourishments result in extra sediment being deposited on the shoreline in the form of thin outward growing land ridges. These protruding sediment deposits can only grow in such a way because there are no waves to spread their sediment out along the shoreline.

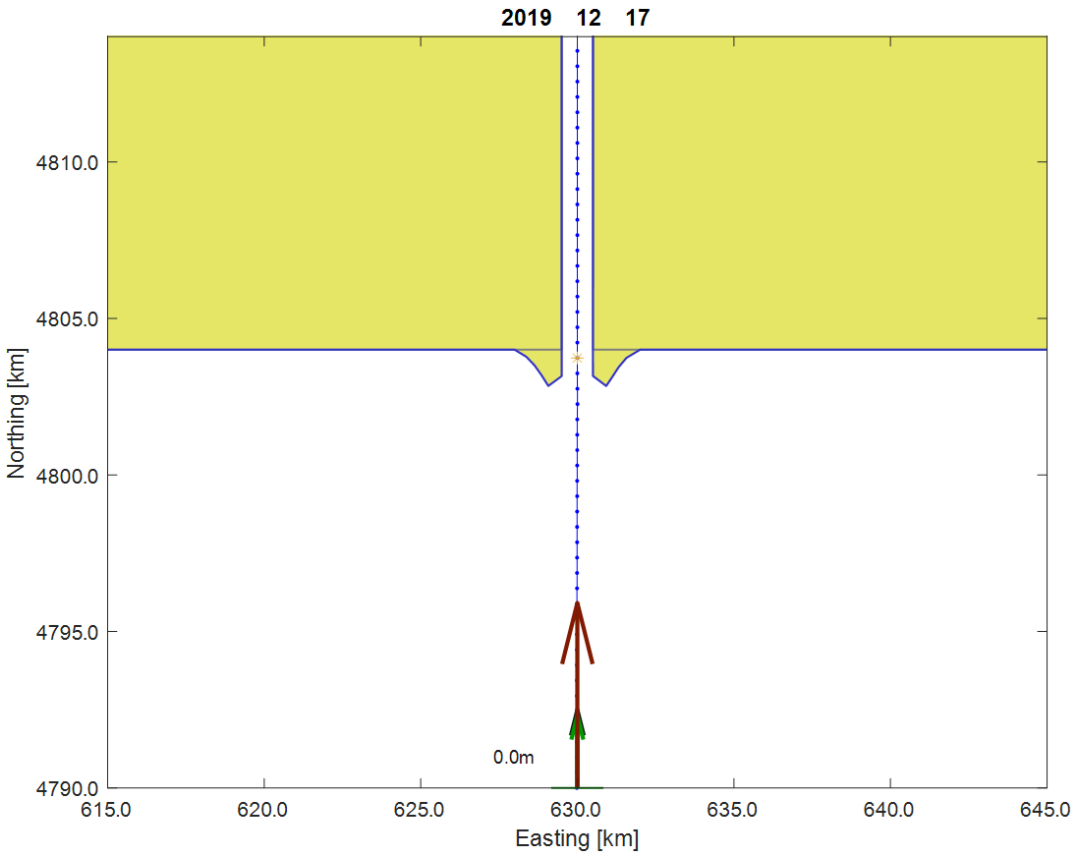

a.

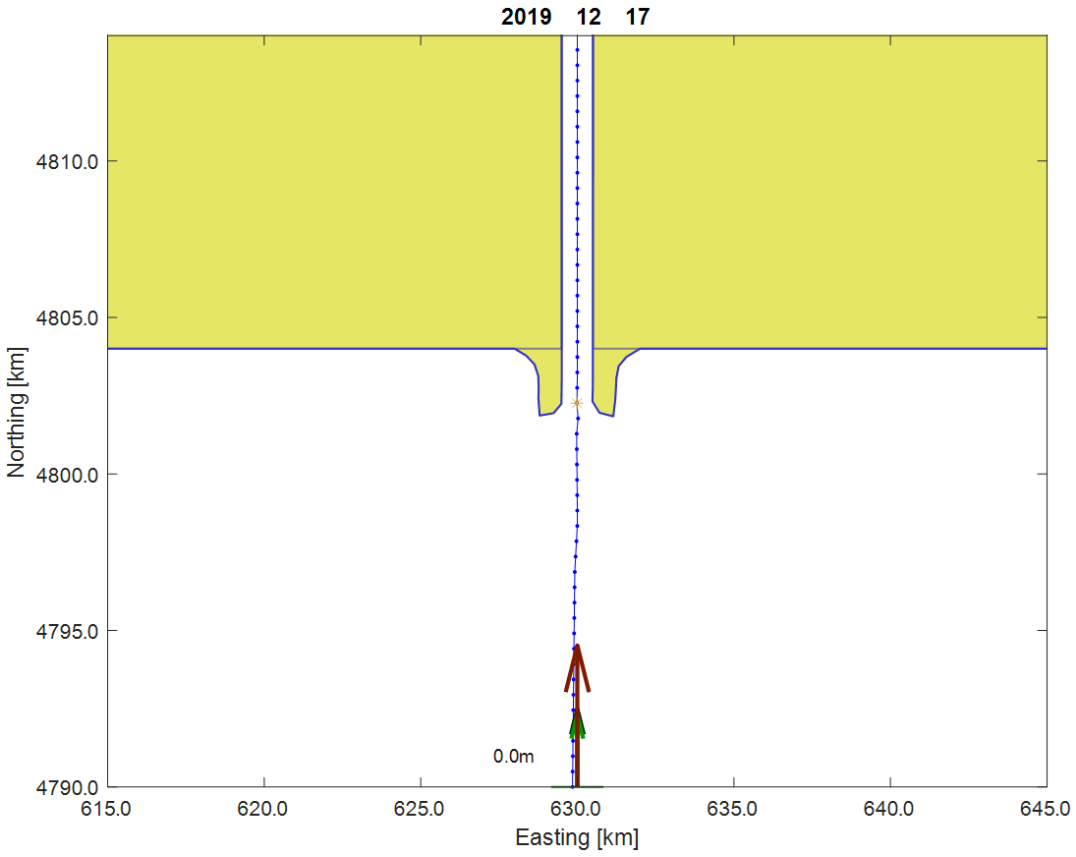
2019 12 17
4810.0
4805.0
4800.0
4795.0
4790.0
Northing [km]
0.0m
615.0
620.0
625.0
630.0
635.0
640.0
645.0
Easting [km]

b.

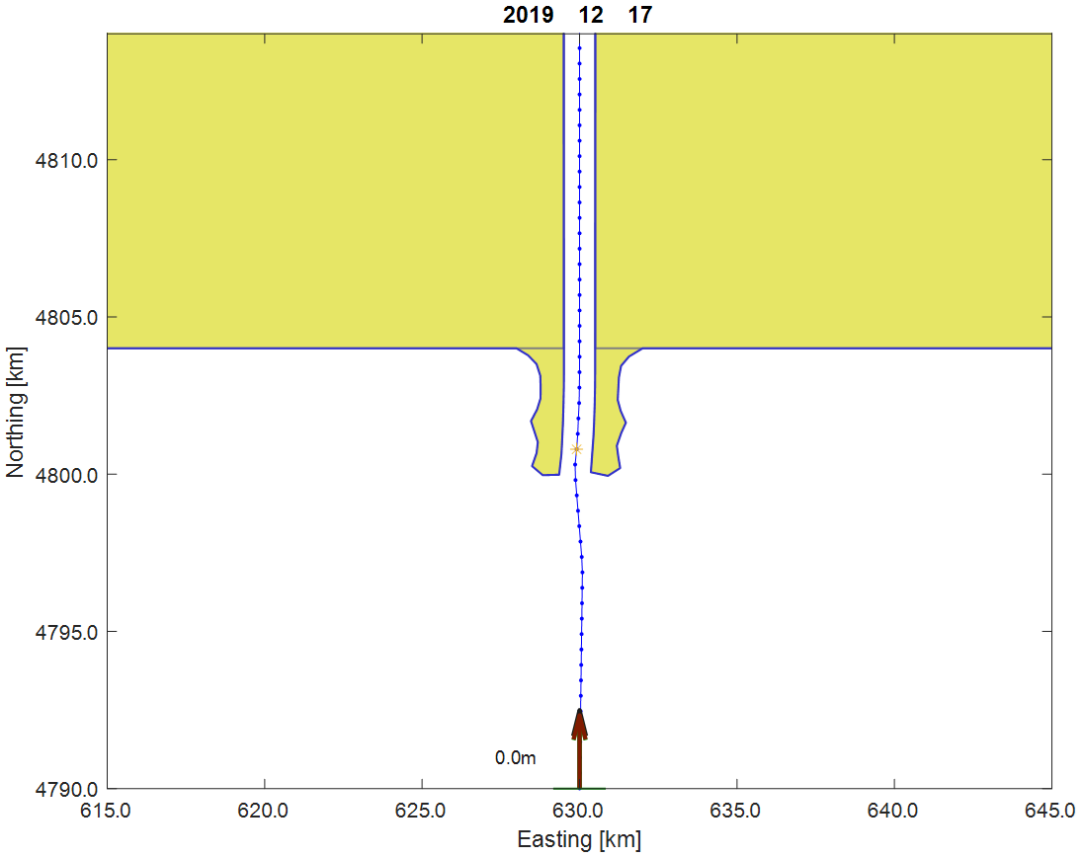
2019 12 17
4810.0
4805.0
4800.0
4795.0
4790.0
Northing [km]
0.0m
615.0
620.0
625.0
630.0
635.0
640.0
645.0
Easting [km]

c.

Figure 37: Result of the simulation for the synthetic coast with a river mouth but without wave interaction. Nourishment used as sediment deposited by the river is a: 2.1 E^7 m^3, b: 4.2 E^7 m^3, and c: 8.4 E^7 m^3.

5.3.1. Standard Simulation

When the simulation is instead run with the default parameters for the synthetic case, including the default wave parameters, the result is quite different (Figure 38). the sediment deposit is now spread out much more evenly across the shoreline near the river mouth. With wave interaction, this is the expected behaviour. It is worth noting that the channel is still maintained meaning that the waves are not impactful enough to push the sediment into the channel and clog the river.

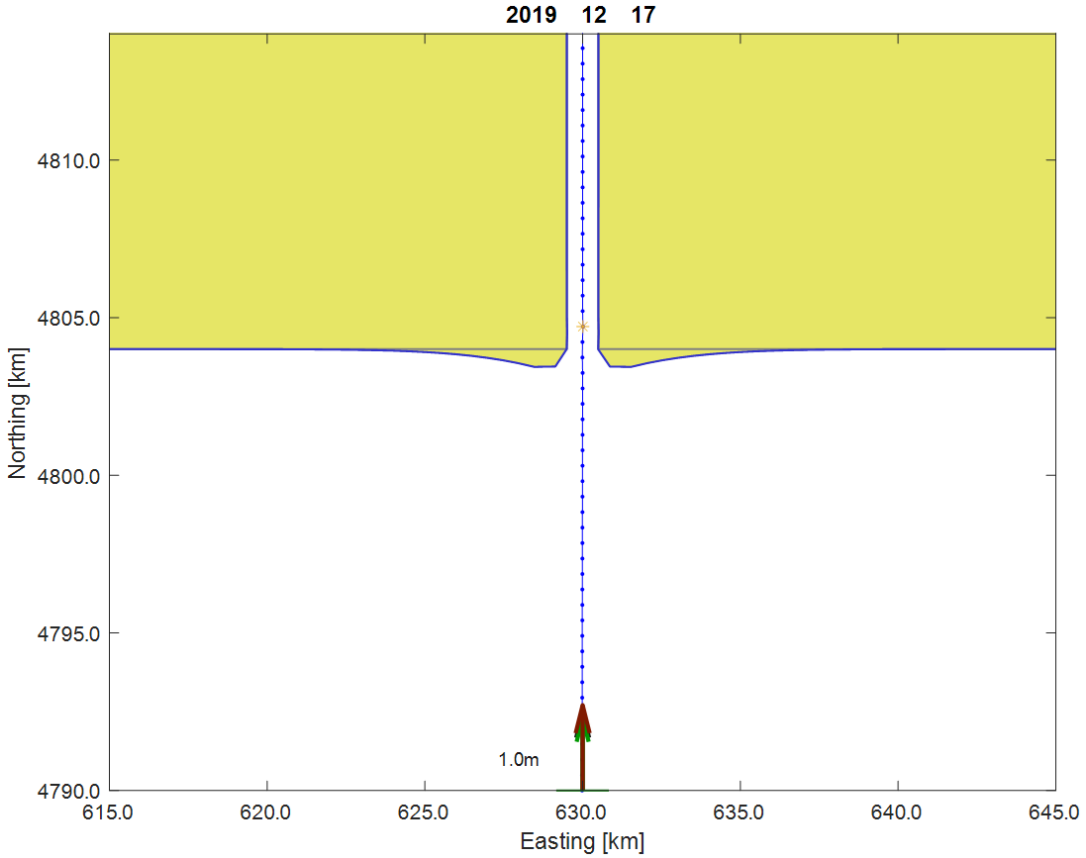

Figure 38: Result of the simulation for the synthetic case when run with the default parameters.

Since this is a fictional case, it cannot be compared to any real-world data. Instead, the different simulation results will be compared to the result of this standard simulation. The simulated shoreline that is the result of this standard simulation will be included in the other simulation results in the form of a red dashed line, to be used as a reference. When there is no perceivable difference between the result of a synthetic case simulation and the synthetic case standard simulation the result will not be shown here. It can however still be found in Appendix B.

5.3.2. Model parameters

Timestep:

The synthetic case simulation with the default timestep of 0.05 yr shows no signs of instability. Nevertheless, the stability is still examined by running the simulation at both a lower timestep of 0.01 yr and at a higher timestep of 0.2 yr. According to the stability criterion (eq. 10), the timestep has an upper limit depending on the grid size and the transport rate. On the other hand, a lower

timestep requires a lot more computing time and power and is therefore limiting in its own way. The results are the same as the standard simulation, which is to be expected when changing the timestep within the stability criterion. The results can be found in Appendix B.

Grid size:

Similarly to the timestep, the grid size plays an important role in the stability of the simulations. When running the simulation with an initial grid size of 100 m, but with the default time step of 0.05 yr, the simulation becomes unstable and crashes after 17 simulated years. Figure 39 a. shows the result with a zoomed in view at the final moment before the simulation crashed. This was almost certainly because of the overlapping of the shoreline due to the instability. The stability criterion (eq. 10) limits the timestep based on the square of the grid size. When retroactively calculating the critical timestep for this simulation based on the maximum transport rate throughout the simulation, a critical timestep of 0.05 yr was found. Therefore, the timestep was indeed too large when combined with the smaller grid size and instability could be expected.

When the timestep is reduced to 0.01, the simulation with an initial grid size of 100 m is stable (Figure 39 b). However, the simulations take exponentially more time to run under these conditions. The result of this simulation shows that the sediment deposit at the mouth of the river does not get rounded down to the extent that happens with the other simulations in the synthetic case.

When the simulation is instead run with an initial grid size of 1000 m, the simulation is stable. The resulting shoreline (Figure 39 c) is however much less smooth. This is to be expected when the distance to the next grid point is twice as big.

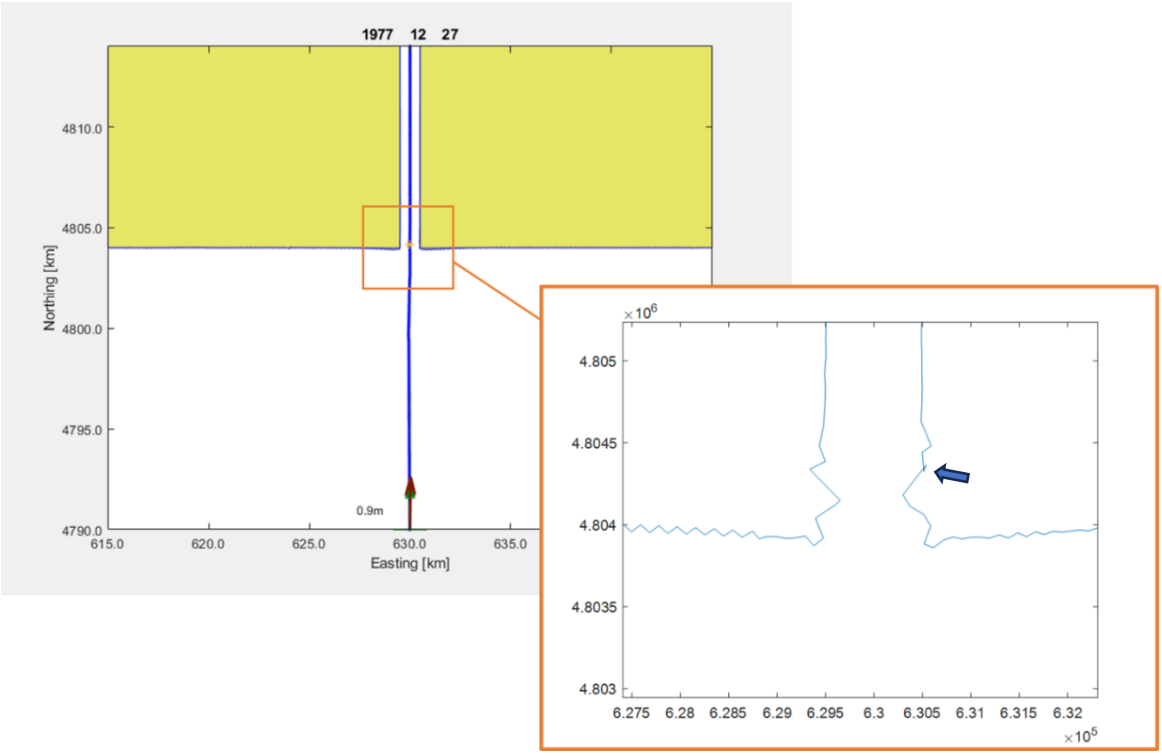

a.

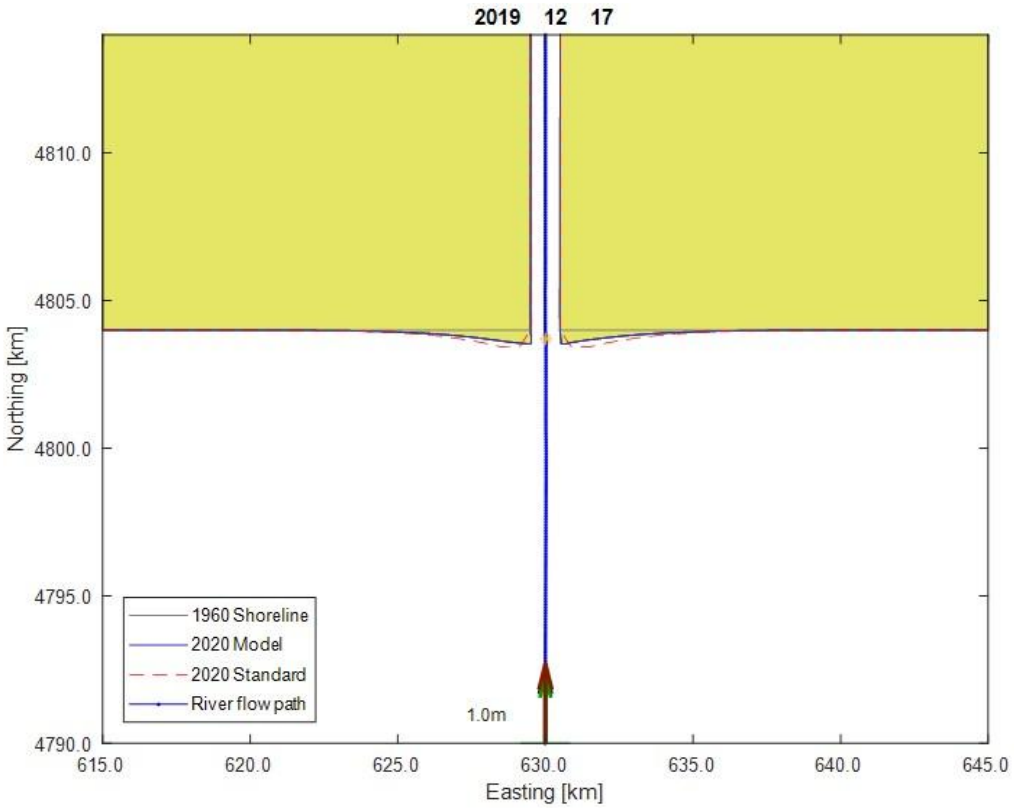

b.

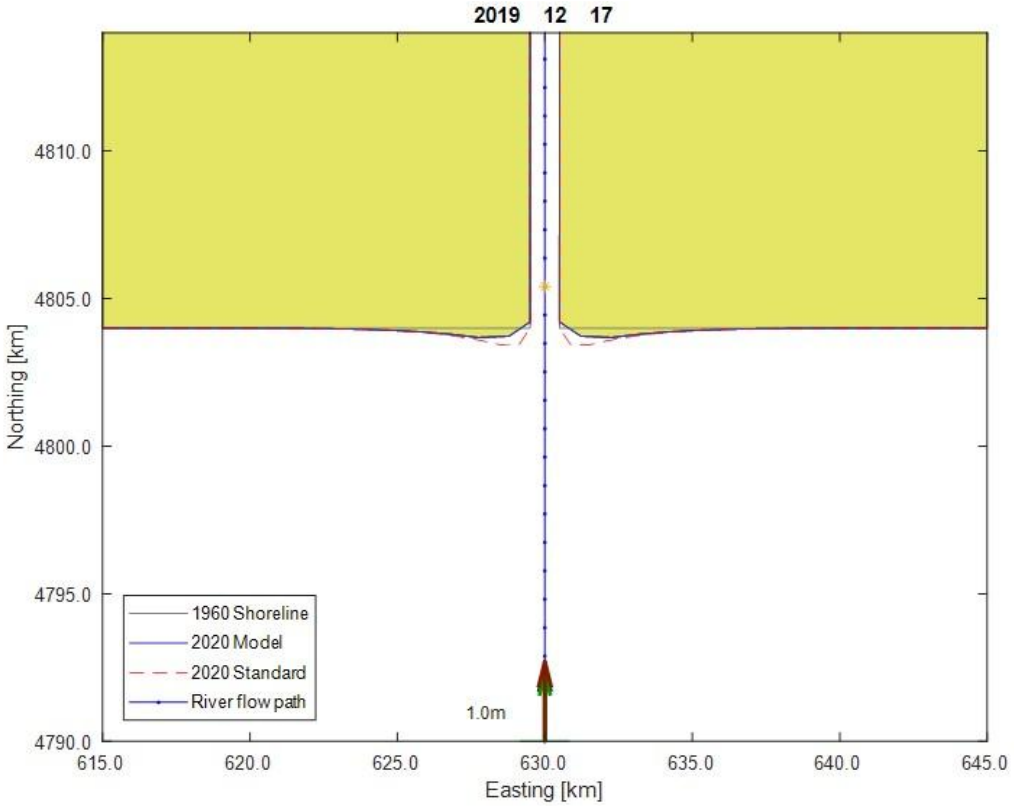

c.

Figure 39: Results of the simulations of the synthetic case with an initial grid size of a: 100 m (unstable, arrow shows overlapped shoreline), b: 100 m (but with timestep = 0.01 yr), and c: 1000 m.

5.3.3. Transport parameters

Transport formula

The default longshore transport formula used in this study is the van Rijn formula (eq. 8). For the analysis of the effect of the longshore transport formula on the simulations, simulations are run for all five other longshore transport formulas implemented in ShorelineS (listed in Table 1). The implementation of the KAMP and MILH formulas in ShorelineS appears to be incorrect, as both use $H_{s,0}$ instead of $H_{s,br}$. The adapted versions of the KAMP and MILH formulas use $H_{s,br}$ as intended. Both simulations with the original and the adapted implemented formulas for KAMP and MILH will be analysed just in case.

The result of the simulation with the CERC formula (Figure 40 a) is very similar to the result of the standard simulation. It has a similar amount of sediment buildup at the river mouth, but the resulting shoreline is slightly less symmetric.

The result of the simulation with the CERC2 formula (Figure 40 b) shows that there is hardly any buildup of sediment at the river mouth. Instead, the western and eastern banks of the river mouth have been slightly eroded before a small amount of sediment was deposited back at the mouth. The wave driven longshore transport of sediment has been more impactful throughout this simulation compared to the standard simulation and the simulation with the CERC formula.

The result of the simulation with the CERC3 formula (Figure 40 c) shows that there is again hardly any buildup of sediment at the river mouth and again there is erosion of both banks of the river mouth in early stages of the simulation. However, in this simulation the deposition of sediment in a later stage only happens on the eastern bank of the river mouth, resulting in an asymmetric shoreline.

The result of the simulation with the originally implemented KAMP formula (Figure 40 d) shows a clear buildup of sediment at the river mouth. Compared to the result of the standard simulation, this sediment deposit protrudes out further from the original shoreline, and the deposited sediment is spread out less along the shoreline.

The result of the simulation with the adapted KAMP formula (Figure 40 e) also shows a clear buildup of sediment at the river mouth. There is less sediment buildup at the mouth compared to the originally implemented KAMP formula. The result is now closer to the result of the standard simulation. The difference being that the sediment deposits on both sides of the river mouth extend slightly further seaward and the sediment is slightly less spread out along the shoreline.

The results of the simulations with the originally implemented MILH formula (Figure 40 f) and the adapted MILH formula (Figure 40 g) are very similar to the results of the simulations with the original and adapted KAMP formulas respectively. However, the simulations with the MILH formulas result in a sediment buildup that extends further seaward and is not spread out as far along the shoreline compared to their respective KAMP formulas.

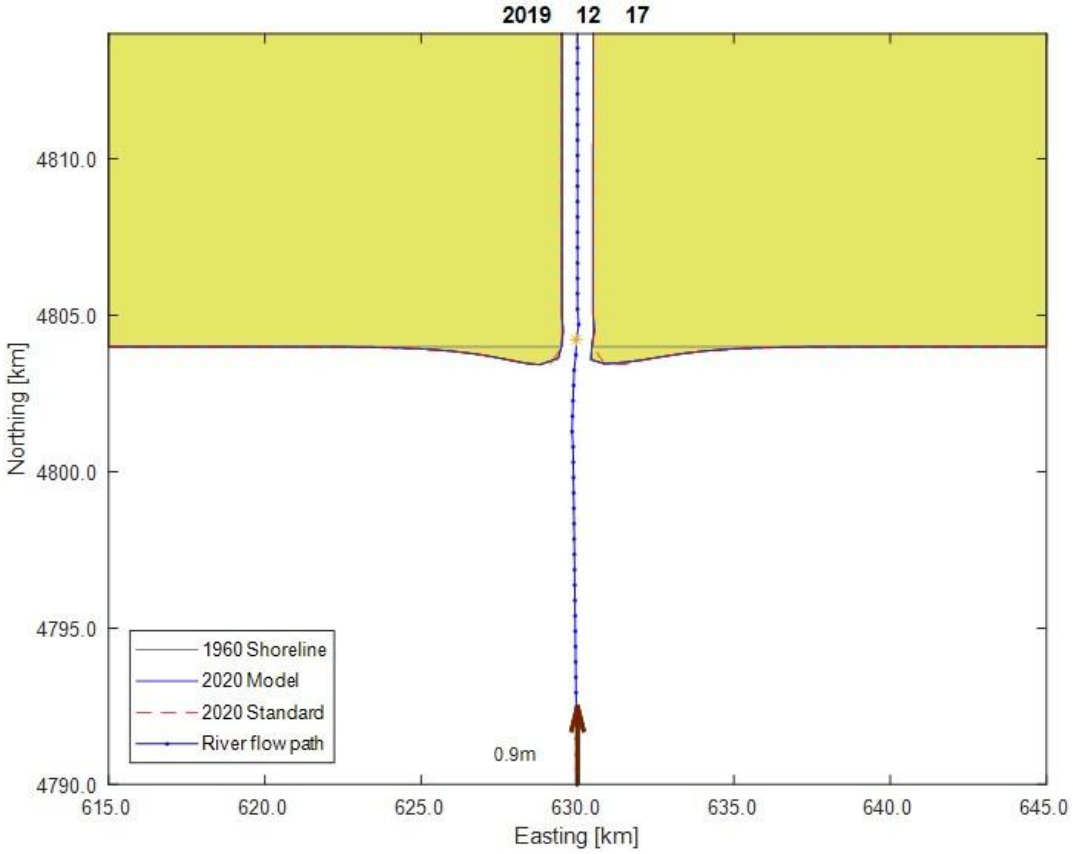
2019 12 17
4810.0
4805.0
4800.0
4795.0
4790.0
Northing [km]
615.0
620.0
625.0
630.0
635.0
640.0
645.0
Easting [km]
1960 Shoreline
2020 Model
2020 Standard
River flow path
0.9m

a.

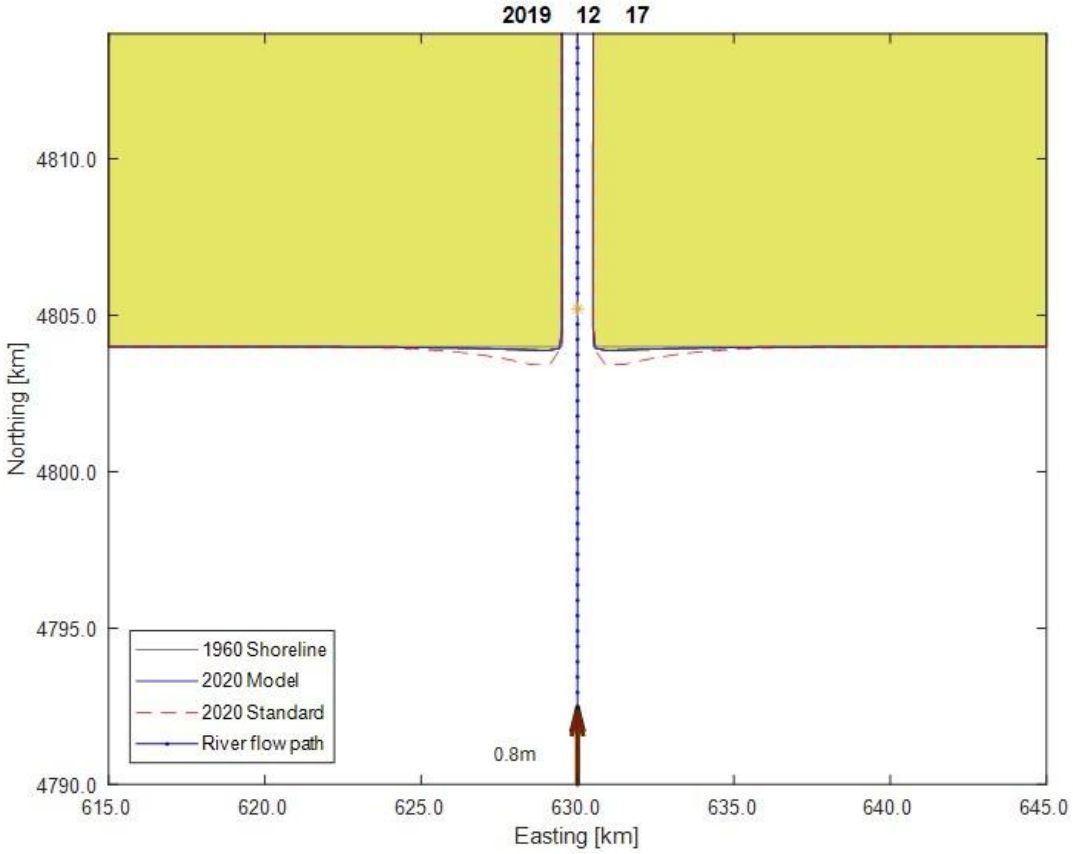
2019 12 17
4810.0
4805.0
4800.0
4795.0
4790.0
Northing [km]
615.0
620.0
625.0
630.0
635.0
640.0
645.0
Easting [km]
1960 Shoreline
2020 Model
2020 Standard
River flow path
0.8m

b.

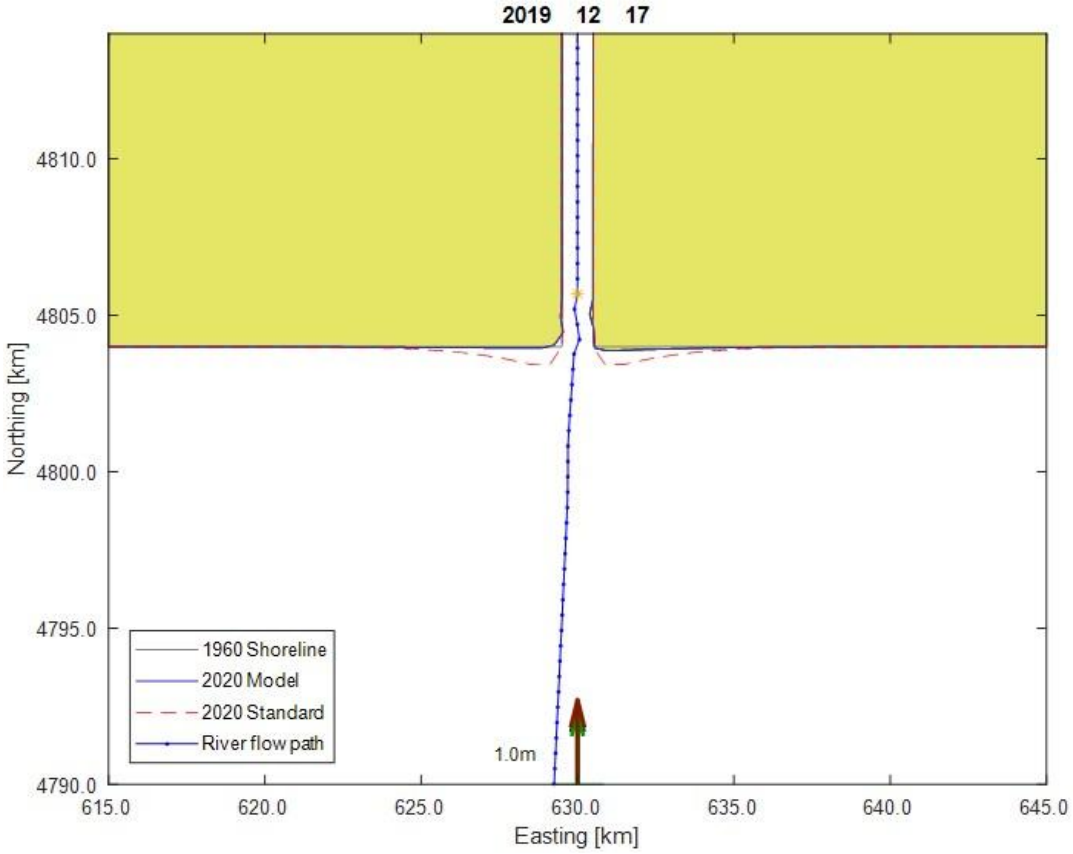
2019 12 17
4810.0
4805.0
4800.0
4795.0
4790.0
Northing [km]
615.0
620.0
625.0
630.0
635.0
640.0
645.0
Easting [km]
1960 Shoreline
2020 Model
2020 Standard
River flow path
1.0m

c.

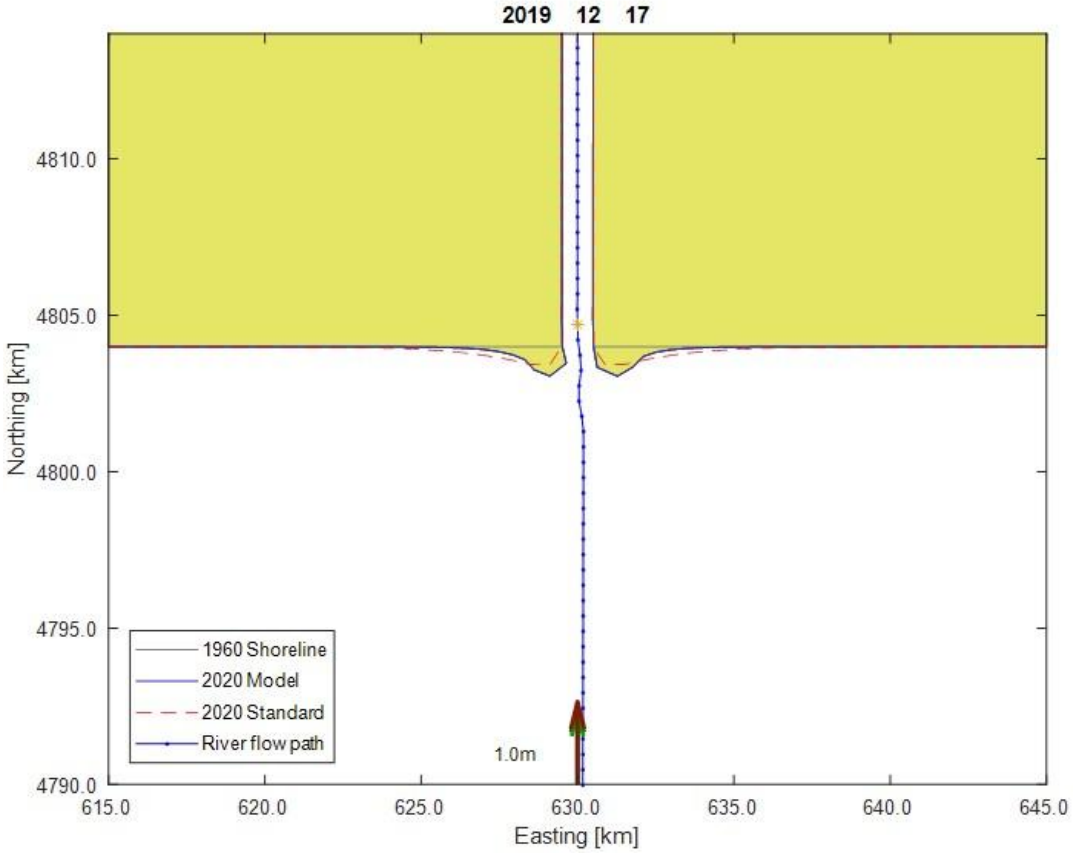
2019 12 17
4810.0
4805.0
4800.0
4795.0
4790.0
Northing [km]
615.0
620.0
625.0
630.0
635.0
640.0
645.0
Easting [km]
1960 Shoreline
2020 Model
2020 Standard
River flow path
1.0m

d.

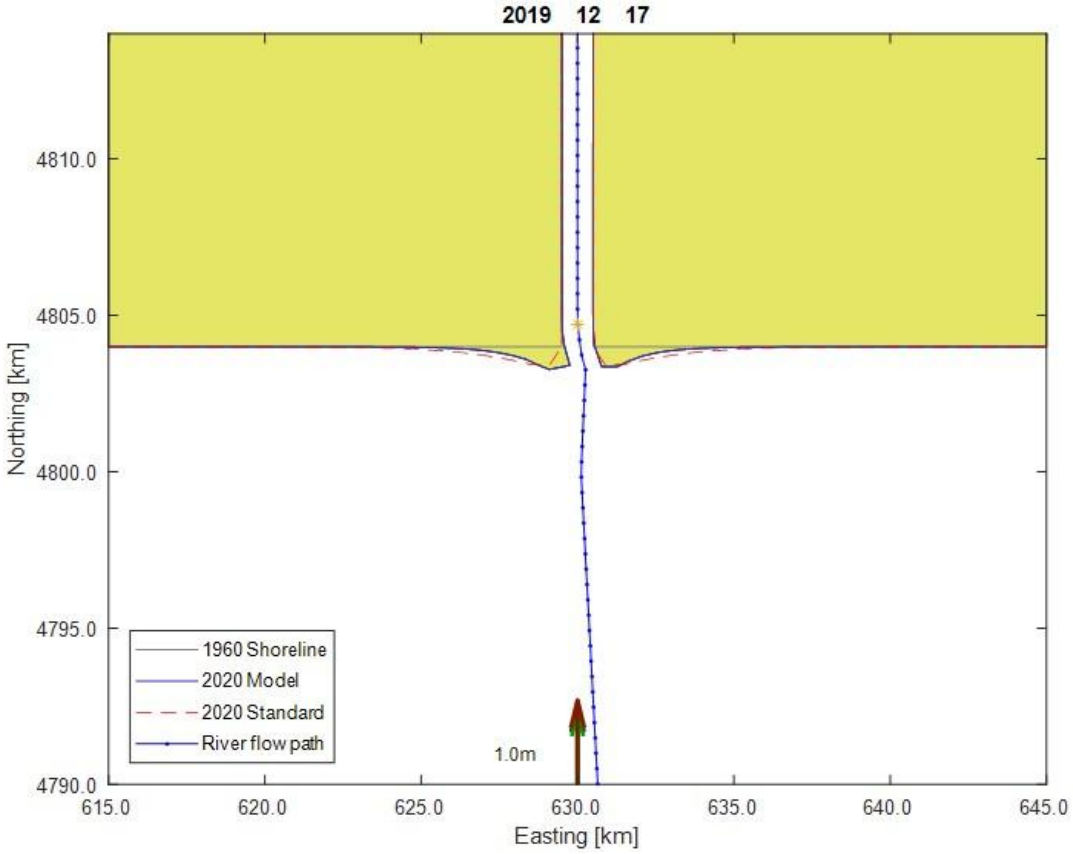
2019 12 17
4810.0
4805.0
4800.0
4795.0
4790.0
Northing [km]
615.0
620.0
625.0
630.0
635.0
640.0
645.0
Easting [km]
1960 Shoreline
2020 Model
2020 Standard
River flow path
1.0m

e.

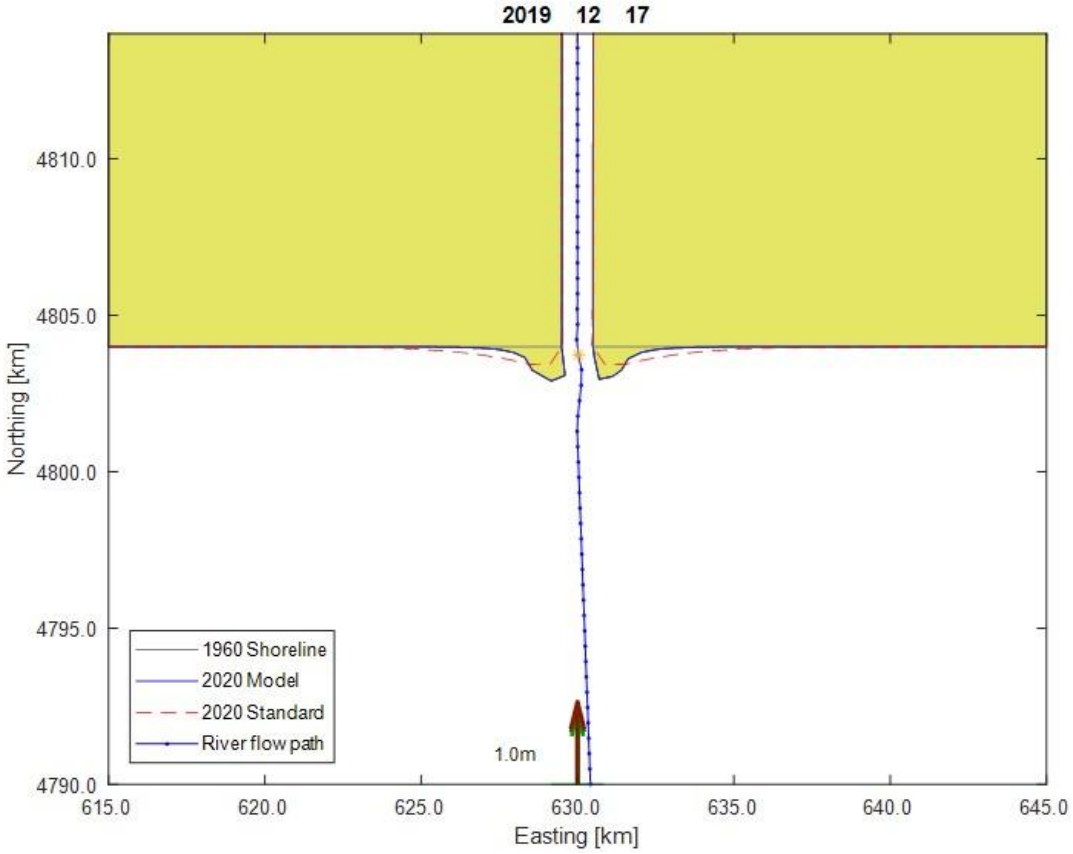
2019 12 17
4810.0
4805.0
4800.0
4795.0
4790.0
Northing [km]
615.0
620.0
625.0
630.0
635.0
640.0
645.0
Easting [km]
1960 Shoreline
2020 Model
2020 Standard
River flow path
1.0m

f.

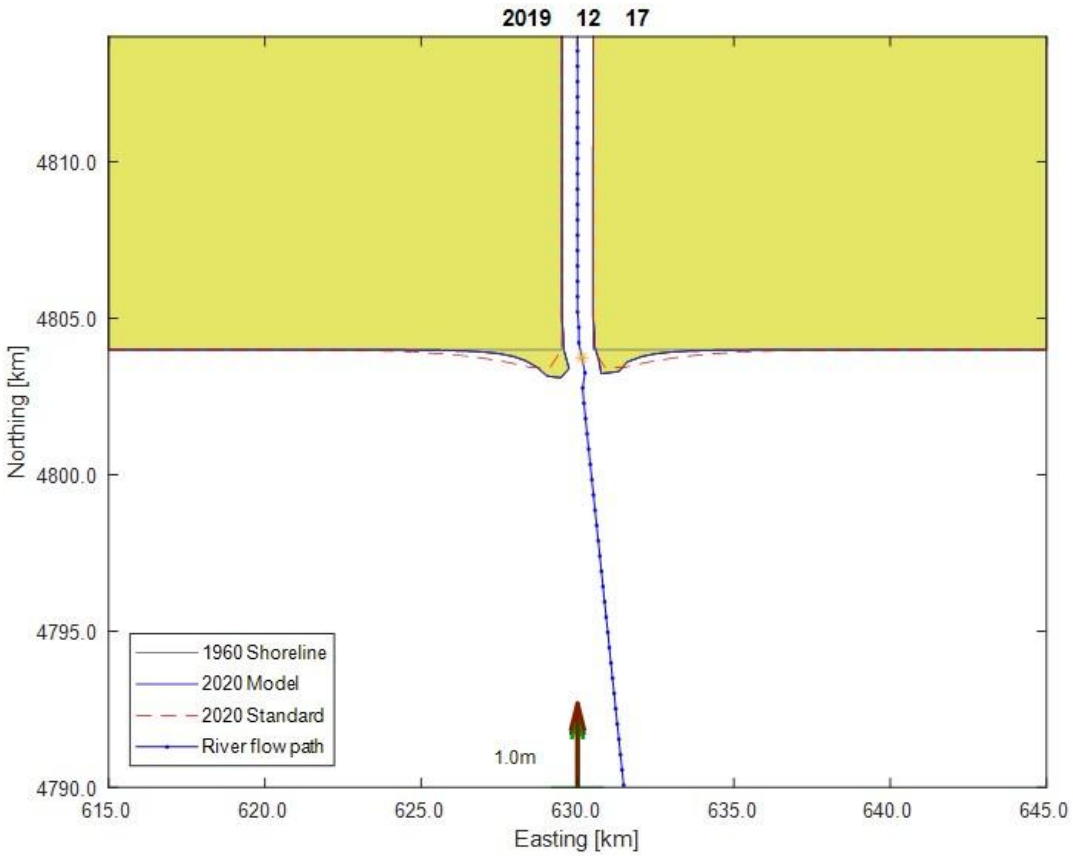

g.

Figure 40: Results of the simulations being run with the a: CERC, b: CERC2, c: CERC3, d: KAMP, e: Kamp adapted, f: MILH, and g: MILH adapted transport formulas.

Mean bed slope

For the analysis of the effect of the slope angle on the simulations, the slope angles are used that represent different parts along the Rhône shoreline. The default bed slope of 0.0066 is the mean value for the part of the shoreline in the region of interest where longshore sediment transport takes place. However, a lower value of 0.0045 is representative of the slope at the relict sediment lobes while a higher slope angle of 0.042 is more representative of the slope at the spits.

The result of the simulation with a mean bed slope of 0.0045 (Figure 41 a) differs from the result of the standard simulation by having a slightly bigger buildup of sediment at the river mouth. The result of the simulation with a mean bed slope of 0.042 (Figure 41 b) differs much more from the result of the standard simulation. It barely has any buildup of sediment at the river mouth. This shows a relation where the buildup of sediment increases with a decrease in bed slope angle. The difference between the result of the standard simulation and the result of the simulation with the bed slope of 0.042 is much bigger than the difference between the result of the standard simulation and the result of the simulation with the bed slope of 0.0045. This makes sense since the bed slope of 0.0045 that is representative of the slope at the relict sediment lobes is much closer to the mean bed slope than the bed slope of 0.042, representative of the slope at the spits.

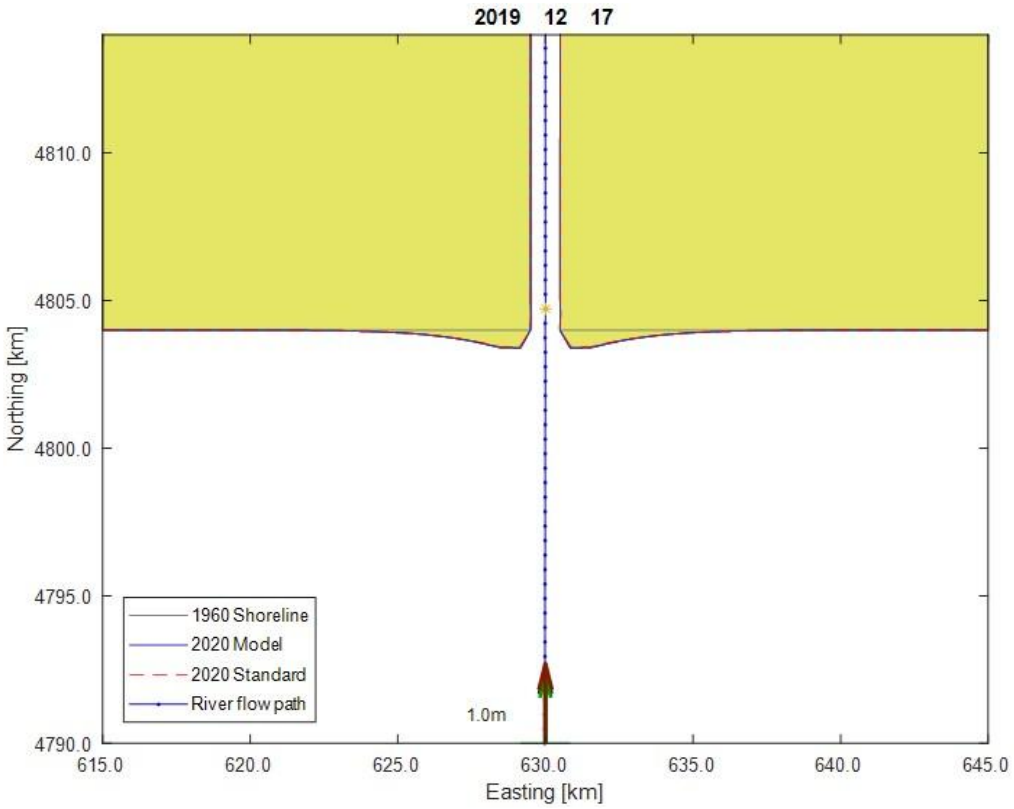

a.

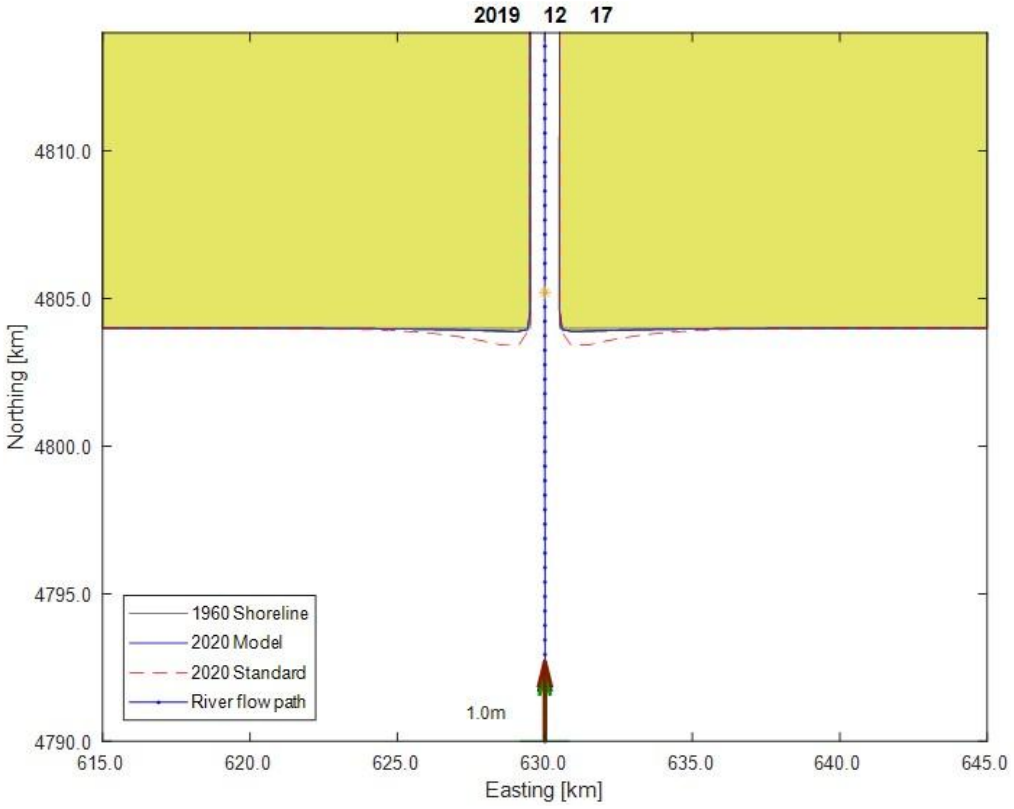

b.

Figure 41: Results of the simulations of the synthetic case with a mean bed slope of a: 0.0045 and b: 0.042.

Depth of closure

For the analysis of the effect of the depth of closure on the simulations both a shallower and deeper depth of closure are simulated. At a depth of 4 m and 12 m respectively. This also impacts the active profile height in these simulations which will be set at 6 m and 14 m respectively. The results show a small deviation from the standard simulation. A shallower depth of closure leads to more buildup of sediment. The results can be found in Appendix B.

5.3.4. Wave climate

Wave height

For the analysis of the effect of $H_{s,0}$ on the simulations both a simulation with a lower and higher $H_{s,0}$ were carried out. A constant $H_{s,0}$ of 0.5 m and a constant $H_{s,0}$ of 1.3 m were used in these simulations. The results are very similar to the results of the wave size simulations. To avoid cluttering the results of the synthetic case only the results for the wave size simulations are shown here. The results for the wave height simulations can be found in Appendix B.

Wave period

For the analysis of the effect of the wave period on the simulations a constant T_p of 3 s and a constant T_p of 7 s were used in these simulations. The results do not differ much from the standard simulation. The sediment buildup in the simulation with a constant T_p of 3 s protrudes out further from the shoreline compared to the constant T_p of 7 s. The results can be found in Appendix B.

Wave size

When the wave height of an offshore wave increases, typically its wave period will also increase. Changing only $H_{s,0}$ or T_p while leaving the other constant is therefore not a very realistic simulation. These simulations are still carried out to analyse the model behaviour. However, for a more realistic simulation both $H_{s,0}$ and T_p should be changed. This is done with the quadratic formula that relates $H_{s,0}$ to T_p (eq. 12). This combination of significant wave height and peak wave period will be referred to as wave size. The default combination of $H_{s,0}$ and T_p of 0.9 m and 5 s respectively will be called wave size 2. According to this formula, lowering $H_{s,0}$ to 0.5 m corresponds to a reduction in T_p to 4.2 s. This combination will be called wave size 1. Increasing $H_{s,0}$ to 1.3 m corresponds to an increase in T_p to 5.7 s. This combination will be called wave size 3.

The results of the simulations with wave size 1 (Figure 42 a) and wave size 3 (Figure 42 b) are very similar to the results of the simulations with altered significant wave heights (Appendix B). The result of the simulation with the lower wave size of 1 shows a prograding river mouth. The result of the simulation with the higher wave size of 3 shows that the sediment deposited by the river at the river mouth is spread across the shoreline and into the river channel, preventing progradation of the river mouth.

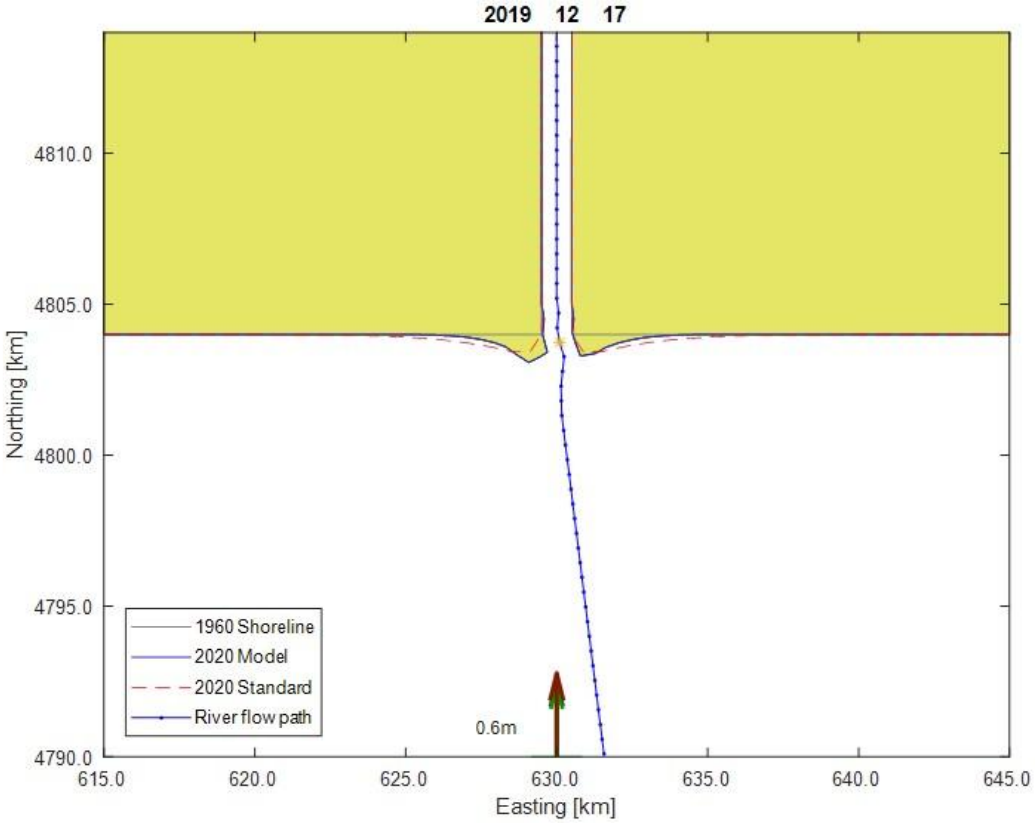

a.

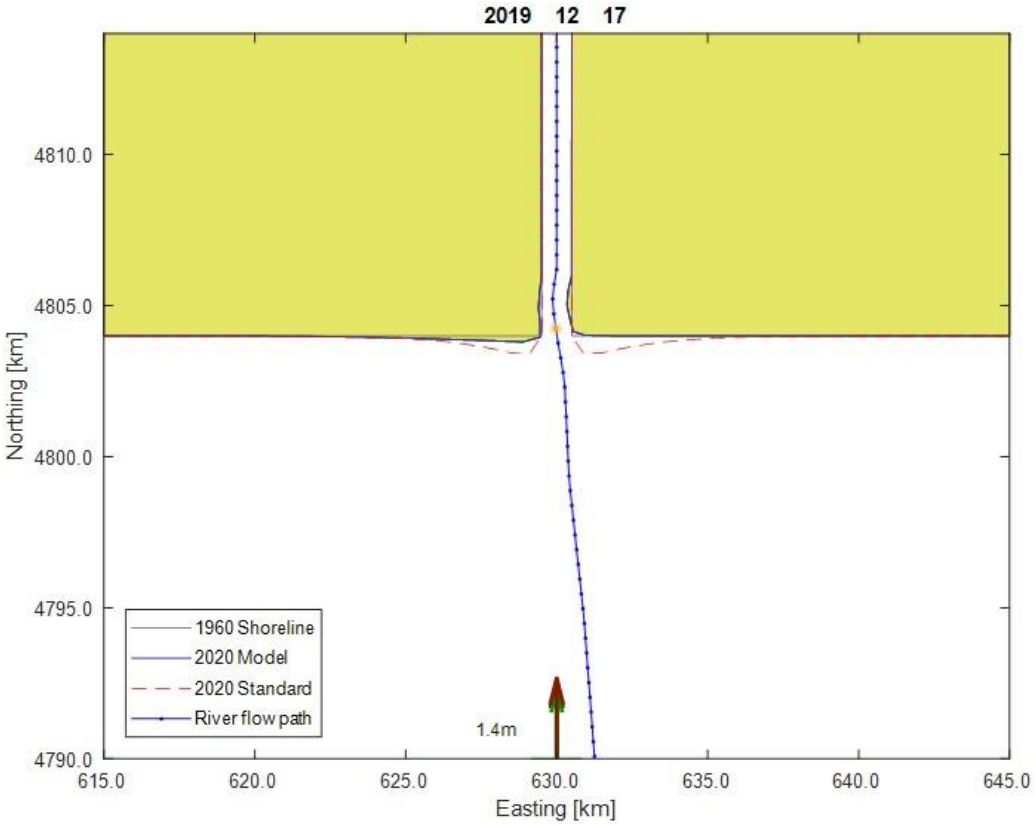

b.

Figure 42: Results of the simulations of the synthetic case with a wave size of a: 1 and b: 3.

Wave direction

The effect of the wave direction on the simulation is analysed by changing the default constant wave direction of 180° to a constant wave direction of 150° and to a constant wave direction of 120°. Since the shoreline is a straight line from east to west, this corresponds with a wave angle of incidence of 30° and 60° respectively. It should be noted that the 60° angle of incidence is higher than the critical 45° angle of incidence that would lead to instability if a central scheme was used. The wave arrows visible in the results of these simulations show the offshore wave direction, the nearshore wave direction, and the wave direction at the point of breaking in black, green, and red respectively.

The result of the simulation with the wave direction of 150° and the angle of incidence of 30° (Figure 43 a) shows that the buildup of sediment at the river mouth gets pushed over to the west. The buildup of sediment on the western bank of the river mouth is spread out very evenly over the western part of the shoreline. The sediment on the eastern bank of the river mouth instead forms a spit that extends from the eastern bank towards the west. This spit crosses the flow path of the river channel. In an effort to maintain the channel, the river flow path is adjusted to flow around the spit. This erodes part of the western bank of the river mouth.

When considering the result of the simulation with the wave direction of 120° and the angle of incidence of 60° (Figure 43 b), a result is seen that is similar to the result of the simulation with the 150° wave direction. However, there is one major difference. A sort of sawtooth pattern appears everywhere along the shoreline that is not sheltered from the waves. Although such a sawtooth pattern usually points to instability of the simulation, that is not the case here. It is instead the result of the angle of incidence higher than the critical angle of 45°. At such high angles of incidence, the shoreline starts to form protrusions that accrete and eventually become spits. This is possible because of the local upwind scheme that ShorelineS uses instead of a central scheme when the angle of incidence is higher than the critical angle.

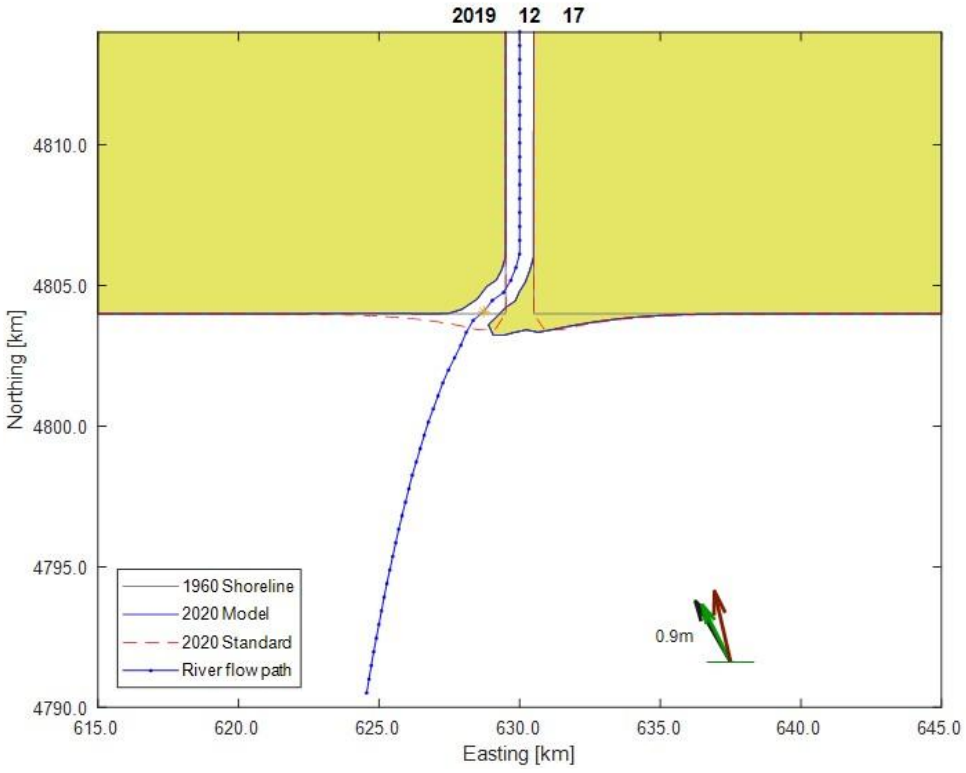

a.

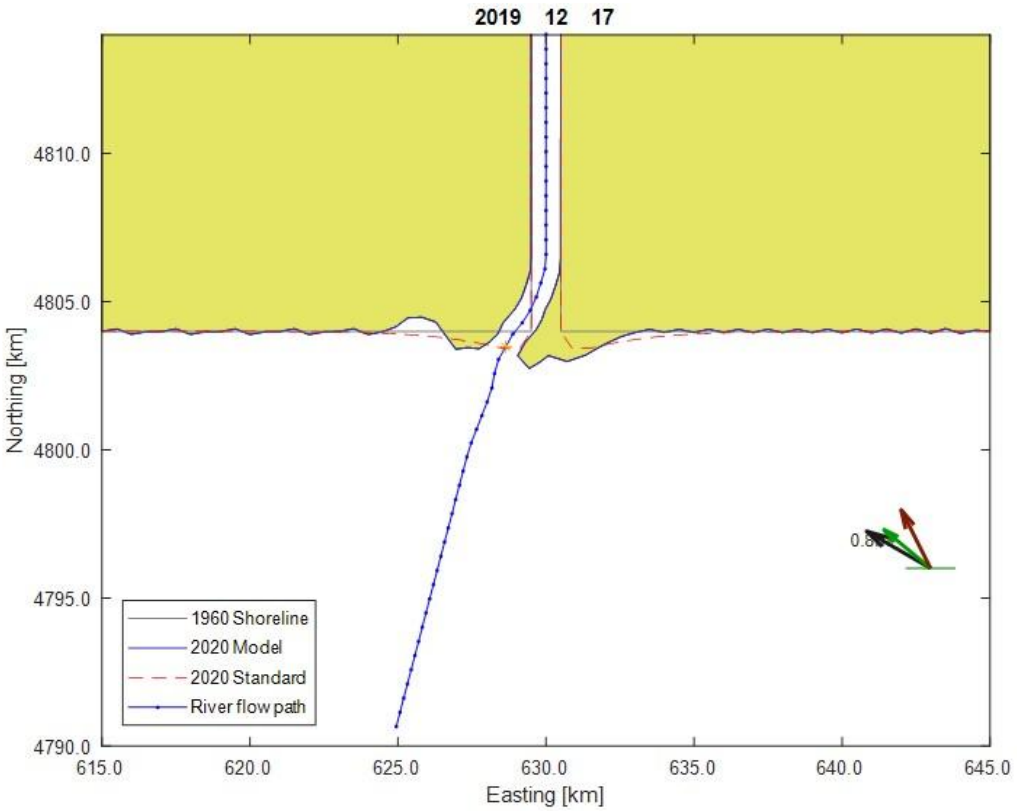

b.

Figure 43: Results of the simulations of the synthetic case with a constant wave direction of a: 150° and b: 120°.

Wave spread

The standard simulation has a constant wave direction of 180° which is useful for model behaviour analysis since no random element is introduced into the simulation. This means that all the simulations are perfectly reproduceable. Nevertheless, a uniform spread added to the constant wave direction allows for a more realistic wave climate and analysing the simulation of the shoreline development with a wave climate that more closely resembles a real-world case is valuable.

The results for the simulation with a wave spread of 45° and 90° (Appendix B) show almost no difference compared to the standard simulation. There is however a slight deviation from the perfectly straight channel.

5.3.5. Relative sea level rise

The shared socio-economic pathways developed by the IPCC (2023) illustrate a range of possible scenarios. The sea level rise predicted for the remainder of this century ranges from about 5.5 mm/yr for SSP1 to about 11 mm/yr for SSP5 (IPCC, 2023).

The shoreline development in the simulation with a relative sea level rise of 5.5 mm/yr (Figure 44 a) differs from the result of the standard simulation by showing almost no sediment deposition at the river mouth. There is also a slight amount of erosion along the banks of the river channel.

The shoreline development in the simulation with a relative sea level rise of 11 mm/yr (Figure 44 b) shows even more erosion compared to the SSP1 simulation. There is so much erosion that there is no visible sediment deposited at the mouth. Besides this, the entire shoreline has slightly transgressed.

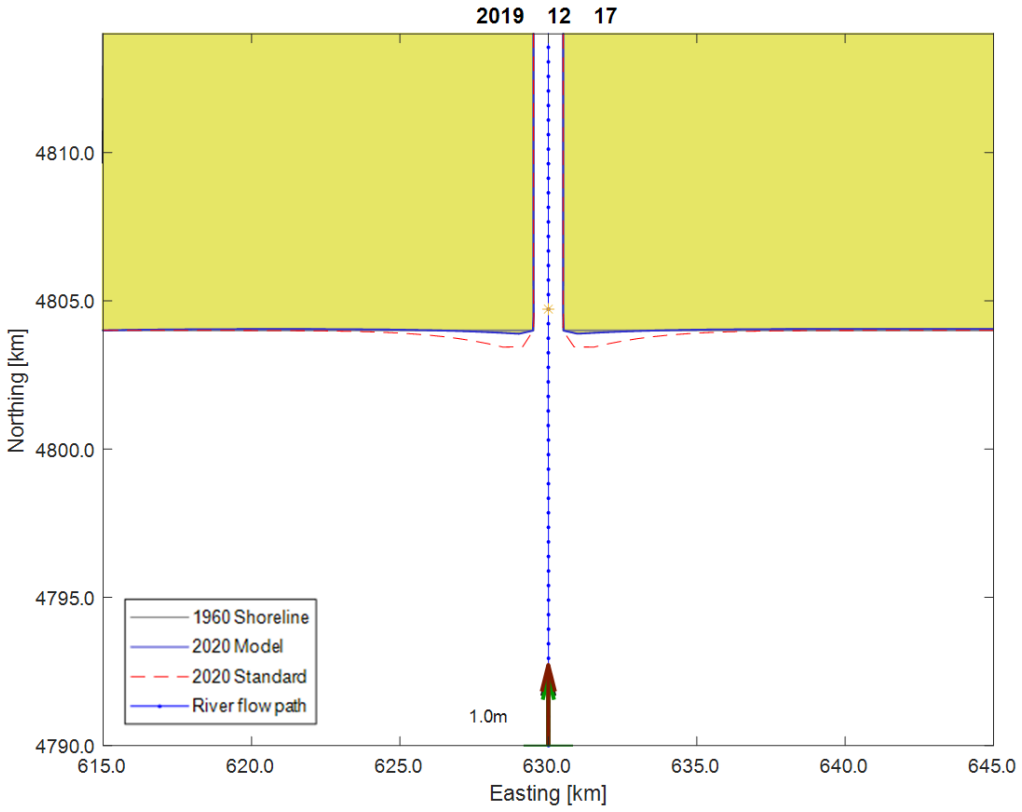

a.

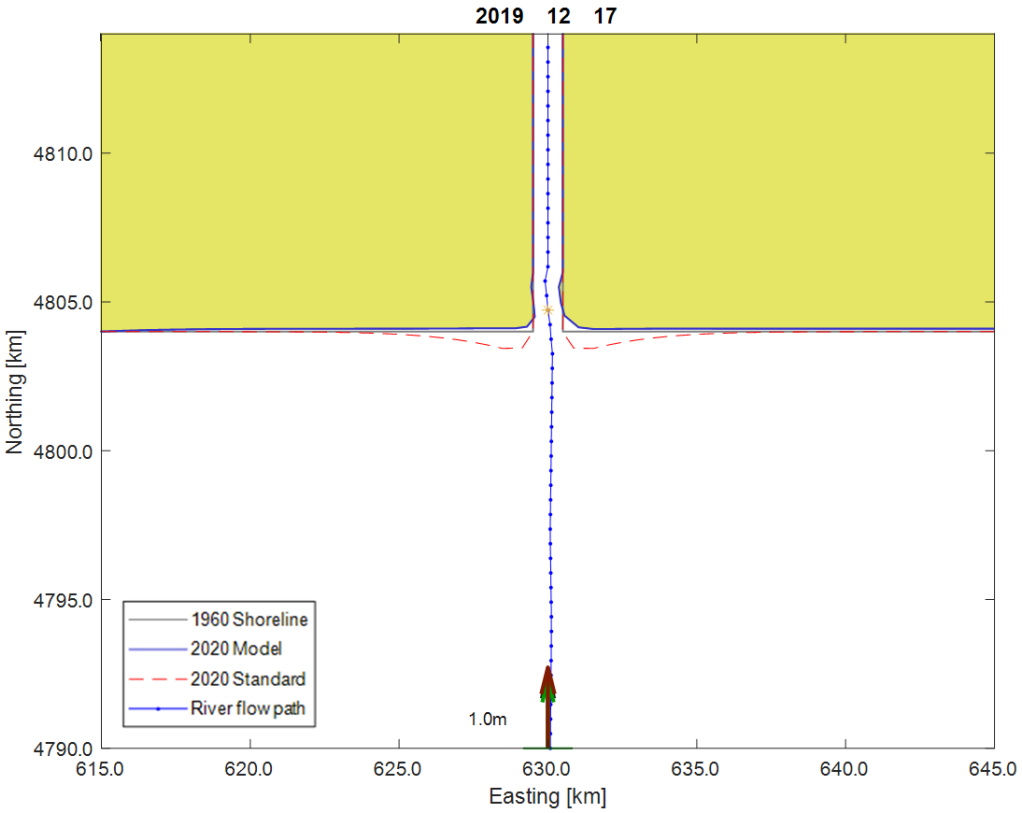

b.

Figure 44: Results of the simulations of the synthetic case with a relative sea level rise of a: 5.5 mm/yr and b: 11 mm/yr.

5.4. Discussion

The synthetic case was set up to answer the question if ShorelineS can successfully simulate shoreline development of a shoreline with a river mouth in a simplified environment. It was also set up to better understand the model behaviour of ShorelineS for a shoreline with a river mouth, which will help interpret the results of the hindcast. The results of the synthetic case will be discussed here.

The synthetic case was set up based on many assumptions. The assumptions of a constant shoreline profile and no cross-shore transport are necessary to use the ShorelineS model. It was further assumed that the shoreline was treated as a region where the morphology is completely governed by natural processes, where the shoreline is sandy along its entire length, and where the sediment transported by the river is discharged at a constant rate throughout the simulation. It was set up with a constant wave climate without any spread in the wave direction. The results should therefore not be compared directly to real-world data. However, trends in the results can still be compared.

5.4.1. Stability

The stability of the simulations is defined by the stability criterion (Eq. 10). This criterion shows that the stability depends on the time step and grid size, but also on the maximum transport rate. With the default time step of 0.05 yr and the default initial grid size of 500 m, a maximum transport rate of 12.5 Mm^3/yr still results in a stable simulation. The maximum transport rate during the simulation can be checked retroactively. The maximum transport rate in the standard simulation is 0.5 Mm^3/yr. Even the simulations with a higher transport rate, such as in the simulation with a higher $H_{s,0}$ which has a maximum transport rate of 1.5 Mm^3/yr, are still well within the stability criterion. With the grid size at 100 m but with the default time step of 0.05 yr, the maximum transport rate within the range defined by the stability criterion is 0.5 Mm^3/yr. The maximum transport rate during this simulation was 0.506 Mm^3/yr. This is just outside of the stability range and therefore an unstable simulation is the expected result.

5.4.2. Shoreline profile

The shoreline profile as implemented in ShorelineS is mostly defined by the angle of the profile and the depth of closure, which determines to what depth the active profile zone extends. The results of the simulations with varied bed slope and varied depths of closure show a pattern where the river progrades further when the slope angle is lower and when the depth of closure is shallower. The lower bed slope causing an increase in progradation makes intuitive sense, since there is effectively less space for the same amount of sediment.

The decrease in progradation with a deeper depth of closure, however, is not as intuitive. With a constant slope angle this means that the active profile zone becomes bigger, which means there is more space along the shoreline profile where longshore transport can take place. However, when looking at the fundamental formula used for the updating of the coastal section (eq. 1) based on the conservation of sediment this relation makes sense. The transport rate in this equation is divided by the height of the active profile, which depends on the depth of closure. Eq. 1 is always used in ShorelineS for the updating of the shoreline throughout the simulation. Therefore, a deeper depth of closure will inevitably lead to a lower amount of progradation.

5.4.3. Wave interaction

The results of the wave size simulations are very similar to the results of the significant wave height simulations. Both sets of simulations use the same $H_{s,0}$ of 0.5 m and 1.3 m, albeit with different T_p. While the significant wave height simulations use the default T_p of 5 s, the wave size simulations use peak wave periods corresponding to their significant wave height. The results of the peak wave

period simulations differ less. The shape of the sediment buildup at the mouth is the same, but the amount of sediment is lower for the higher wave period.

This shows that a smaller wave has less energy to move sediment away from the river mouth, causing the river mouth to prograde sooner. The larger wave has more energy to move the sediment away from the river mouth, causing the river mouth to stay at the same point or even retrograde. This is true for both wave parameters that affect the wave size, however the effect that $H_{s,0}$ has is bigger than the effect T_p has. This is reflected by the importance of $H_{s,0}$ in the longshore transport compared to T_p which is not included in the CERC, CERC3 and VR14 formulas.

A local upwind scheme is used by ShorelineS instead of the standard central scheme when waves with an angle of incidence beyond the critical angle of incidence of 45° are detected. Because of this local upwind scheme, it is possible to simulate the formation of spits along the shoreline that are formed under angles of wave incidence larger than the critical angle. The result of the simulation with the angle of incidence of 60° shows the start of this form of shoreline development. The model is capable of simulating this behaviour and simulating the development of the river mouth without the two different processes hindering each other.

It is surprising that the result of the simulation with the spread of 45° added to the wave direction does not lie between the results of the simulations with the spreads of 0° and 90° added to the wave direction. It is not known what causes this. The asymmetry of the channel in the results of the simulations with spreads of 45° and 90° is due to the random nature of the uniform spread added to the constant wave direction of 180°

5.4.4. Relative sea level rise

The results of the simulations with the SSP1 and SSP5 scenario related relative sea level rise are similar to the results with higher wave energy. This is an interesting result since transgression of the shoreline is expected with a rise in relative sea level, according to the Bruun rule. However, since ShorelineS assumes a constant bed slope, it would perhaps be expected that the shoreline had transgressed in such a way that the resulting shoreline would be parallel to the original shoreline. Just like the result the passive inundation method would produce. The fact that this is not the case illustrates the importance of the shoreline development processes that the passive inundation method does not take into account.

5.4.5. Bulk longshore transport formula

Three different sets of similar simulation results can be distinguished. The results of the simulations with the CERC and VR14 formulas are the first set. These results exhibit a similar shoreline development with a similar amount of progradation as well as spreading out of sediment along the shoreline in both directions. This is surprising since the two longshore transport formulas are quite different. One being a simplified formula that only accounts for $H_{s,0}$ and the angle of wave incidence, as well as the breaking coefficient. The other being the formula that takes the most different parameters into account out of all the implemented longshore transport formulas. Namely $H_{s,br}$, the angle of wave incidence at the breaking line, the median grain size, the mean bed slope, and the swell percentage.

The results of the simulations with the CERC2 and CERC3 formulas form the second set of similar simulation results. The shoreline development in both of these results has barely any progradation and in fact has slight retrogradation in early stages of the simulation. The results of these two simulations being similar is not as surprising since the CERC2 and CERC3 formulas are themselves similar, with CERC2 being an adaptation of CERC3 that accounts for refraction and shoaling. Since

the wave direction in this synthetic case is fixed at a constant 180°, refraction does not change the angle of incidence at the breaking line compared to the offshore angle of incidence. This means that one of the differences between the two formulas is not relevant in this situation.

The third set of similar simulation results is formed by the results of the simulations with the KAMP and MILH formulas, both the original and adapted implementations. The shoreline development in these results has significant progradation of about 1 km. The sediment is spread out along the shoreline for about 4 km in both directions. The similarity here is no surprise because the MILH formula is a re-evaluation of the KAMP formula. Depending on the exact same parameters, but to a slightly different degree.

The small difference between the results of the simulations with the KAMP formulas and the MILH formulas respectively is that the progradation of the river mouth is slightly less and the sediment is spread out slightly further along the shoreline in the case of the KAMP formulas. This means there is more longshore sediment transport with the KAMP formulas under the standard conditions.

The difference between the original and adapted formulas is purely caused by the use of $H_{s,0}$ or $H_{s,br}$ respectively. The results of the simulations with the adapted formulas show less progradation and more sediment spread out across the shoreline. These formulas use $H_{s,br}$. This is the case for both the adapted KAMP and MILH formulas. Since a less protruding and more spread-out sediment deposit points to higher wave energy, the conclusion can be drawn that $H_{s,br}$ is higher than $H_{s,0}$. When retroactively checking both significant wave heights throughout the simulation it becomes clear that $H_{s,br}$ is indeed slightly higher. The constant $H_{s,0}$ of 0.90 m results in a $H_{s,br}$ of 0.98 m. This is only the case outside of the channel.

The difference in shoreline development between the three sets of similar simulation results is interesting. The use of longshore transport formulas CERC2 and CERC3 result in very different shoreline development compared to the simulations for all other formulas, with hardly any progradation of the river mouth present. The CERC2 and CERC3 formulas are quite different but still give a similar result. Because of the major difference between the results of this set of simulations and all the simulations with the other four formulas, it is likely that the longshore transport rate calculated with these formulas is too high. Resulting in too much of the deposited sediment from the river being transported along the shoreline.

The difference between the results of the CERC and CERC3 simulations is also interesting. The CERC and CERC3 formulas are identical except for the substitution of $H_{s,0}$ for $H_{s,br}$ and the substitution of the offshore angle of incidence for the angle of incidence at the breaking line to get from CERC3 to CERC. Combining this with the fact that $H_{s,0}$ and $H_{s,br}$ only differ about 0.1 m, such a big difference in shoreline development is unexpected.

The results of the CERC, VR14, KAMP (adapted), and MILH (adapted) simulations all show similar shoreline development that seem like logical results.

5.4.6. Summation of findings

The main takeaway from the results from the synthetic case is that the simulation by ShorelineS of the development of a shoreline with a river mouth, where the river is implemented as an algorithm that keeps the river channel open while moving sediment towards the river mouth, works well in a simplified environment. The results from the model behaviour tests mostly returned the expected results. These results can be crudely summarised by comparing the effect of the parameters on the progradation of the river mouth. The progradation lessens as the slope angle, the depth of closure, the significant wave height, the peak wave period and the relative sea level rise increase.

The model stability is also not negatively influenced by the presence of the river mouth. Even under wave angles of incidence beyond the critical 45° angle of incidence that would lead to instability if a central scheme was used.

The results further showed that a relative rise in sea level will not automatically lead to a cross-shore shift of the shoreline as it would with passive inundation. This is not even the case with the constant shoreline profile that is assumed by ShorelineS.

The results also showed a surprising performance from the different implemented bulk longshore transport formulas. The van Rijn (2014) formula performed best, which is according to expectations. However, the simplified CERC formula also performed surprisingly well, considering how limited the formula is.

There are, however, also limitations to the use of ShorelineS, even for a simplified shoreline. The model cannot simulate natural processes related to river dynamics that develop under natural circumstances such as avulsion or the formation of a mouth bar. This limits the applicability of ShorelineS for simulating shorelines with channels where these processes occur. Where this is not the case, however, ShorelineS should find applicability. For example, a canal that is constantly being dredged.

6. Hindcast of Rhône shoreline development

6.1. Model setup

6.1.1. Assumptions

The simulating of the hindcast as part of the validation of ShorelineS with respect to shorelines with a river mouth is based on several assumptions. The region of interest is defined as the active coastal zone of the shoreline between Saintes-Maries-de-la-Mer and the La Gracieuse spit. It is assumed that all the sediment in this region consists of sand, that all the longshore transport of sediment happens in the predetermined active coastal zone, and that the cross-shore sediment transport is negligible. This allows for the use of the fundamental formula used for the updating of the coastal section based on the conservation of sediment (eq. 1) without any additional sediment sink terms.

It is assumed that the sediment transported by the Rhône and discharged at the mouth can be represented as a constant discharge rate throughout the simulation. In reality, the sediment discharged by the Rhône is not discharged at a constant rate throughout the time interval that is simulated, 1960 to 2020. The construction of dams both on the Rhône and on its tributaries has caused a significant reduction of sediment discharge (Piégay et al, 2022), (Provansal et al, 2014). However, the assumption of constant discharge was still made to prevent further complicating of the simulations and thereby the interpretation of the results of the simulations.

It is further assumed that the region of interest can be treated as a region where the morphology is completely governed by natural processes and where there is no interference from manmade engineering, even though there are some coastal defence engineering works present. ShorelineS has the option to incorporate hard structures such as groynes or revetments but the decision to not include these structures was made because the capability of ShorelineS to handle a shoreline with a river mouth is the main focus of this study and any unexpected model behaviour that could jeopardise this is avoided. Also, the capabilities of ShorelineS to handle groynes and other coastal structures has already been researched.

All the different parameters used, and all the decisions made to set up the simulations of the shoreline of the Rhône will be discussed here. Table 4 shows all the default parameters. Unless specified, these are the parameters used in all the simulations.

6.1.2. Input shoreline

The shoreline used as input in the simulations for the hindcast is the extracted shoreline discussed in section 4.1. For ShorelineS to correctly process the shoreline of the Rhône, it should go from east (right) to west (left). A few modifications need to be made to the extracted shoreline in order for it to be used in the simulations.

First, an additional grid point has to be added at the start of the shoreline to make sure that the shoreline extends further towards the east than the La Gracieuse spit. This is necessary for the spit to have space to grow. This should not affect the development of the shoreline in the simulations as the part of the shoreline behind the La Gracieuse spit is sheltered from all wave action and any longshore transport of sediment from the mouth to the east ends up on the La Gracieuse spit.

The next modification to the extracted shoreline is made at the part of the extracted shoreline that incorporates the banks of the Grand-Rhône channel. The point where the Grand-Rhône is cut off, about 3.5 km inland, is extended all the way to the northern boundary of the simulation. Because of this, the river channel will be approximated as a straight channel. This is done because river dynamics related to the curvature of the river cannot be taken into account by ShorelineS and the

curvature could result in unexpected model behaviour, which should be avoided. The Grand-Rhône channel splits the shoreline, and therefore the string of grid points representing the shoreline, into two parts (Figure 45).

6.1.3. Channel parameters

In order for ShorelineS to correctly simulate the channel of the Grand-Rhône, the flow path of the river needs to be defined from one boundary to another. In this case that is from the northern boundary to the southern boundary. The flow path of the river is right in the middle of the channel. This results in the following starting position for the simulation of the hindcast (Figure 45).

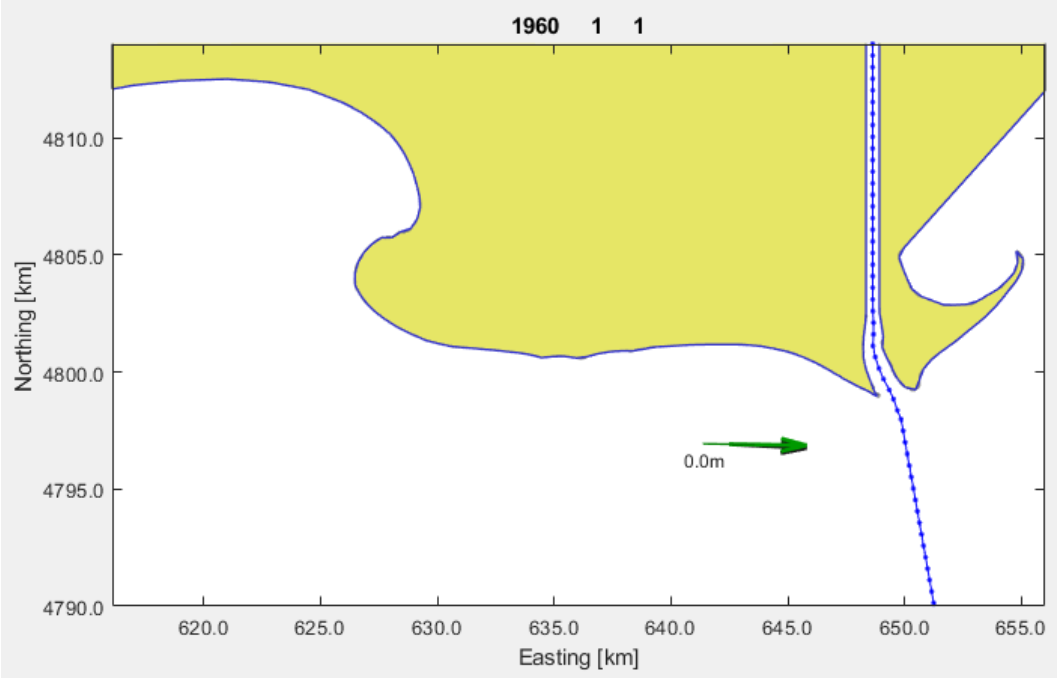

Figure 45: Starting position for simulation of the hindcast. The yellow area is the coastal area bounded by the shoreline in black, the blue dotted line is the flow path of the river, and the arrows signify the wave direction (offshore, nearshore, and breaking in black, green and red respectively).

The sediment discharged by the river is approximated in the simulations by a nourishment in the river channel. ShorelineS checks at every timestep if the channel is still at the desired width and if that is not the case, sediment is moved through the channel towards the mouth. How well the channel width is maintained is controlled by a predefined adaptation factor. For the simulations for the hindcast, the desired width of the channel is set at 500 m. The adaptation factor is set at 0.8. This is relatively high, but the discharge of the Rhône is also relatively high, and it should ensure that the channel will not get filled in from the nourishment. The nourishment that represents the sediment discharge will be a continuous supply of 0.51 Mm^3/yr for the entire sixty-year period, for a total of 30.4 Mm^3. This is according to the sediment budget of the Grand-Rhône determined in section 3.4.

6.1.4. Wave climate

The wave climate used in the simulations for the hindcast is the wave climate described in section 4.2 after filtering of the northerly wave data.

6.1.5. Relative sea level rise

For the hindcast, no rise in relative sea level was included for the default parameters as the rise in relative sea level in the Gulf of Lion was found to be not representative. Nevertheless, the model behaviour under standard conditions with the relative sea level rise as predicted in the shared socio-economic pathways is still analysed.

6.1.6. Transport formula

The bulk longshore transport formula used in the standard simulation of the hindcast is the VR14 formula (eq. 8). This formula is used since it is expected to have the best performance based on comparisons to the other bulk transport formulas (van Rijn, 2014). Since the shoreline of the Rhône delta in the region of interest is far from a straight shoreline it would not be reasonable to assume that the wave conditions at the point of breaking are constant along the shoreline. This means that the simplified CERC formula, CERC1, should not be used.

It is important that the bed slope is considered in the bulk longshore transport formula used for the hindcast since the bed slope varies significantly along the shoreline of the Rhône delta. The shoreline profile near the mouth of the Rhône is variable due to the Bras de Fer and Pégoulier relict sediment lobes as well as the delta plateau of the current mouth of the Grand-Rhône.

Allowing for the use of a predetermined bed slope and the possibility of analysing model behaviour with different bed slopes that represent different parts of the shoreline is important. Because of this, the CERC2 and CERC3 formulas cannot be used as these do not account for the bed slope angle.

Of the formulas that take the bed slope into account (KAMP, MILH, and VR14), the van Rijn formula has performed best in tests (van Rijn, 2014). The performance under standard conditions of the other five longshore transport formulas implemented in ShorelineS (Table 1) is also analysed.

6.1.7. Shoreline profile

The parameters that define the shoreline profile and that will be used in the simulations for the hindcast are described in section 4.3. These are the mean bed slope of 0.0066, the depth of closure of 8 m, the berm height of 2 m, and the active profile height of 10 m (Figure 35). The mean bed slopes representative of the steepest and gentlest parts of the shoreline, the spits and relict lobes respectively, will also be considered. The orientation of the foreshore is not specified which causes ShorelineS to derive it from the orientation of the shoreline by assuming depth contours parallel to the shoreline. Even though the profile is varied along the shoreline, this is a good approximation.

6.1.8. Model parameters

The simulation will be run for 60 years (from 1960 to 2020). The fixed timestep is set at 0.05 yr. The initial grid size is set at 500 m. According to the stability criterion (eq. 10), the simulation is stable under these circumstances up to a maximum transport rate of 12.5 Mm^3/yr. Although the maximum transport rate in the hindcast is on average about 10 times higher compared to the synthetic case simulations, it is still well within the safe range defined by the stability criterion.

With respect to longshore sediment transport, the study area can be approximated as a closed box system, and the town of Saintes-Maries-de-la-Mer is effectively an impermeable wall. Because of this the lateral boundary conditions that govern the sediment transport across the borders of the simulation were initially chosen as Dirichlet boundaries with zero longshore transport across the boundaries. This resulted in incorrect model behaviour which is why the lateral boundary conditions set on either ends of the shoreline are Neumann boundaries. This means that a free in and outflow of sediment across the boundary is possible. This means that longshore transport at the edge of the

closed box system is in theory possible. However, because the boundaries on either side are protected from the waves by spits, this is not expected to happen.

The median grain diameter d50 and d90 were set to 0.2 and 0.3 millimetre respectively, according to the grain size analysis by Masselink et al (1992) that was conducted in the region of interest.

6.2. Model comparison

In order to quantify how well ShorelineS simulates the coastal morphology, a tool is used that compares the change in shoreline over time. This can be done between two simulations when the performance of the model needs to be compared to another model, or between a simulation and real-world data. The latter is the case for the validation of ShorelineS in this study.

A comparison is made between two shorelines, a reference shoreline and the modelled shoreline. The way this tool works is by taking the two shorelines, in the form of strings of grid points, as input. These strings of grid points are the output of the ShorelineS simulation and are provided at certain points in time throughout the simulation. The cross-shore distance between the reference and modelled shoreline is determined (A detailed description of how this is done can be found in Appendix C). Because of this it is possible to quantify the change in shorelines throughout the simulation.

After the difference in cross-shore distance between the two shorelines has been determined, it is used to calculate the Brier score. This is the mean of the squared differences between two predictions (Brier, 1950).

$$BS = \frac{1}{N}\sum_{t=1}^{N}(f_t - o_t)^2 \tag{14}$$

Where BS is the Brier score, f_t is the modelled result, and o_t is the observed result.

This can in turn be used to calculate the Brier skill score, which reflects the relative performance of one forecast over a reference forecast. It is a common way of measuring accuracy and skill of forecasts that is often used for probability-based forecasts. The Brier skill score can quantify the predictive performance of the ShorelineS simulations.

$$BSS = 1 - \frac{BS}{BS_{ref}} \tag{15}$$

The Brier skill score is used to compare the performance of one model to a reference model. However, in this study the performance of the ShorelineS model is compared to the real-world observation. This means that there is no room for improvement over the reference model. Therefore, the model performance is best when BS approaches BS_{ref}, or when BSS is closest to 0.

6.3. Default hindcast parameters

The default parameters used to simulate the shoreline development are given in Table 4. The different values represent the different simulation runs for that specific parameter. The bolded values represent the default values. Unless specified otherwise, only one parameter is changed per simulation.

Parameter	Value
Wave Parameters	
Significant wave height	-
Peak wave period	-
Deepwater wave angle	-
Wave spreading	-
Water depth offshore	80 m
Active profile height	10 m
Transport Parameters	
Transport formula	CERC CERC2 CERC3 KAMP MILH **VR14**
CERC coefficient	0.5 E^{6}
Median grain diameter d50	2 E^{-4} m
Median grain diameter d90	3 E^{-4} m
Porosity	0.4
Mean bed slope	0.0045 **0.0066** 0.042
Density of sand	2650 kg/m^3
Density of water	1025 kg/m^3
Gravitational acceleration	9.81 m^2/s
Depth of closure	8 m
Time steps & numerical	
Timestep	0.01 yr **0.05 yr**
Reference (Starting) time	1960-01-01
End of simulation	2020-01-01
Initial grid size	100m **500 m** 1000 m
Boundary conditions	
Boundary condition at start of shoreline	Neumann
Boundary condition at end of shoreline	Neumann
Climate change impact	
Sea level rise	**0 mm/yr** 5.5 mm/yr 11 mm/yr
Nourishments	
Total nourishment	3.0 E^{7} m^3
Channel physics	
Channel width	1000 m
Channel adaptation factor	0.8

Table 4: Default simulation parameters for the hindcast. Bolded values are the default values.

6.4. Results from the hindcast

6.4.1. Standard Simulation

The simulation of the development of the shoreline of the Rhône delta under the conditions specified in Table 4 results in Figure 46. The yellow area with the blue border shows the final result of the shoreline evolution at the end of the simulation. The grey line shows the interpreted shoreline as it was in 1960, which is the starting position of the simulation. The interpreted shoreline for 2020, which is used as reference, is shown in red. This is the shoreline that the simulation should approximate.

Figure 47 shows the cross-shore distance plot for this same simulation. Here, the shoreline of the Rhône in 1960, which is used as the starting shoreline and is represented by the dashed line, is used as the x axis. The cross-shore distance from both the simulated shoreline and the interpreted shoreline to the 1960 shoreline has been determined. The simulated shoreline is shown as a scatter plot which colour depends on the distance from the 1960 shoreline. The interpreted shoreline is shown with the solid black line. The correlation between the cross-shore distance plot and the top-down view of the shoreline is shown in Figure 48.

Both figures 46 and 47 show that for the simulation, the biggest changes in shoreline occur near the mouth of the Rhône. Here, the difference between the 1960 and the simulated 2020 shoreline is much bigger than at the Beauduc spit, where there is hardly any change in the position of the shoreline. The cross-shore distance plot shows that the change in shoreline near the mouth of the Rhône happens at an early stage in the simulation but does not change much after this initial change.

However, when looking at the difference between the interpreted shoreline and the simulated shoreline, both shorelines show a big contrast. The interpreted shoreline has changed significantly more at the Beauduc spit compared to the modelled shoreline. Also, the interpreted shoreline has changed significantly less at the mouth of the Rhône. This points to two discrepancies in the simulation. Figures 49 a-g show three zoomed in versions of Figure 46 as well as Figure 47 for more clarity.

The Brier skill score starts at 0, decreases to -1.64 for the year 1985, and then increases again to a final score of -0.44 for the year 2020. The Brier skill score of 0 signifies the theoretical best performance. This is of course because the simulated and interpreted shorelines have the same starting location. The initial decrease in score shows that the simulation initially departs from the shoreline development as laid out by the interpreted reference shorelines but approaches this path again after the initial departure.

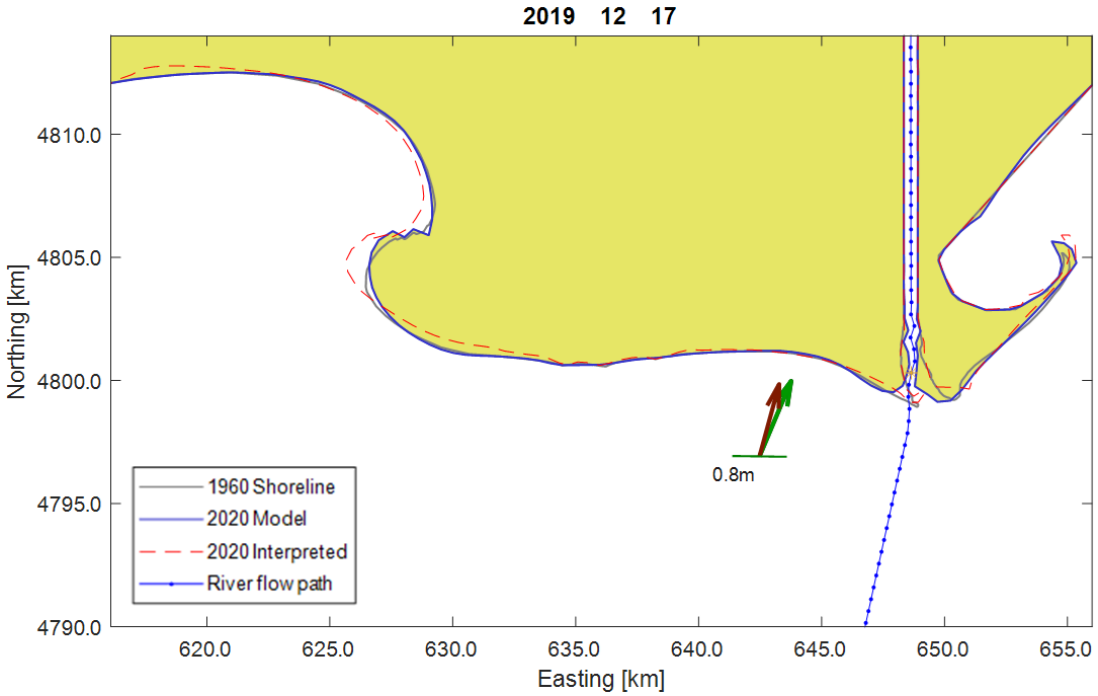

Figure 46: Top-down view of the final result of the simulation of the development of the Rhône shoreline under standard conditions as listed in Table 4.

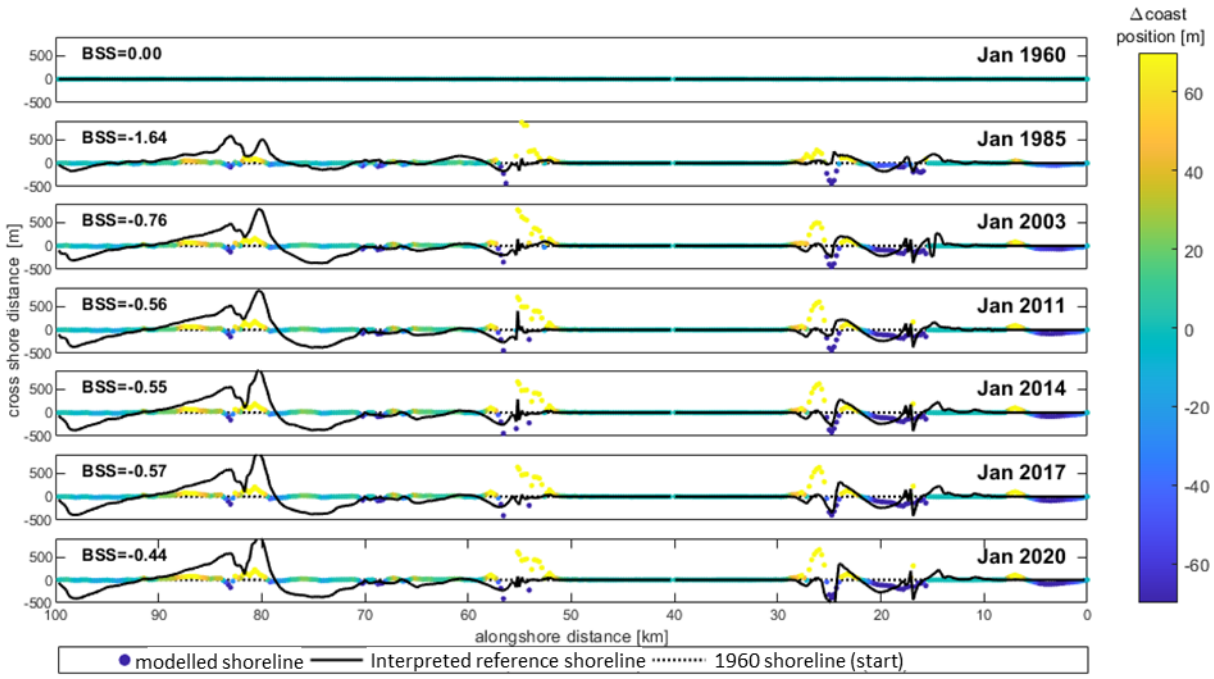

Figure 47: Cross-shore distance plot of the final result for simulation of Rhône shoreline under standard conditions as listed in Table 4.

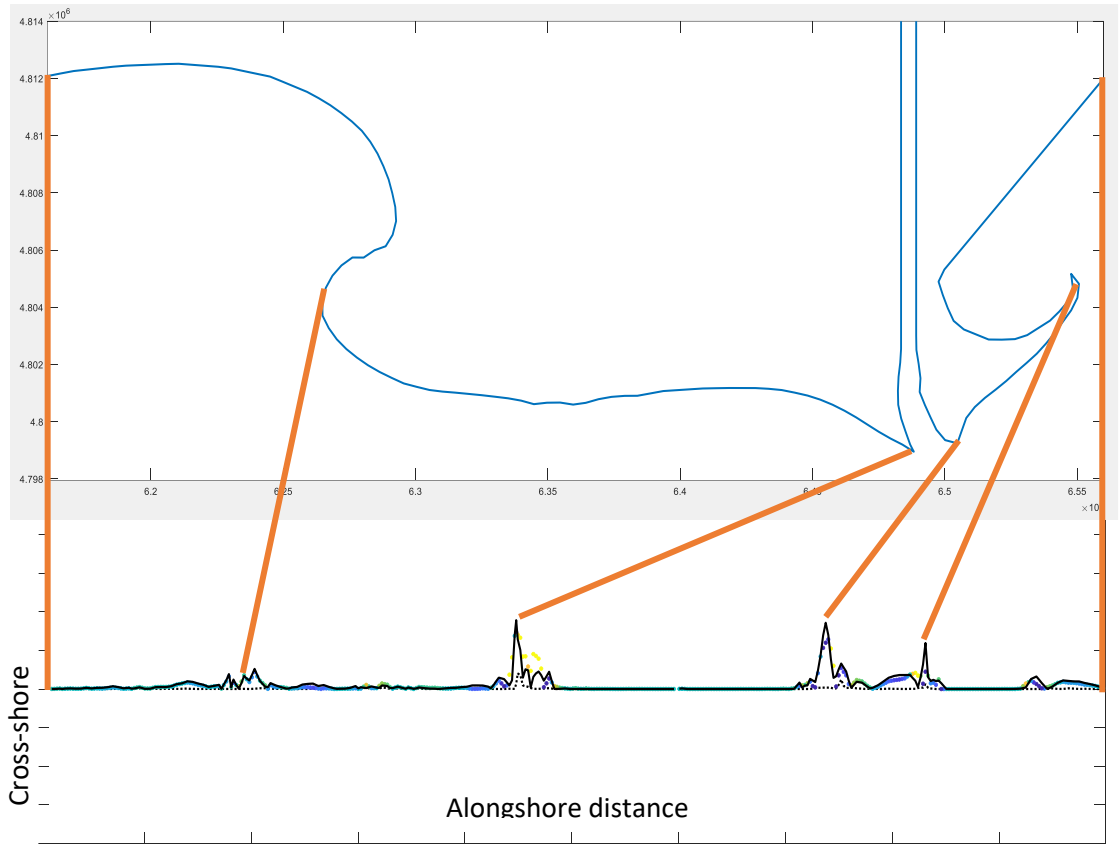

Figure 48: Correlation between the cross-shore distance plot and the shoreline it is based on.

Figures 49 b and c show that the interpreted shoreline at the Beauduc spit has been flattened at the southern part and has extended to the northwest. The point where the interpreted shoreline intersects with the 1960 shoreline signifies a shift from accretion to erosion over the span of 60 years. This point is indicated in both figures with a small arrow. This points to longshore transport of the sand at the south along the spit to the northwest. The contrast between the modelled and interpreted shoreline at the Beauduc spit points to a significant misrepresentation of the longshore transport at this position by the model.

Figures 49 d and e show the situation at the mouth of the Rhône. The interpreted shoreline shows a mouth bar that has grown and moved about 1 km to the northeast, partially blocking the Roustan mouth. The Piémanson shore has eroded and some of the sediment at the eastern side of the Roustan mouth has been transported along the coast to the east. The simulated shoreline on the other hand has changed a lot more. Both on the western and eastern sides of the mouth the shoreline has been pushed land inward. Even though the amount of sand distributed at this particular spot seems close to the correct amount, the interaction between the wave climate and the shape of the shoreline in the model have resulted in an incorrect distribution of the sand.

Figures 49 f and g show the situation at the La Gracieuse spit. Although the tip of the spit is wider in the simulation than it is for the interpreted shoreline, the spit has grown to about the correct length while maintaining the correct width.

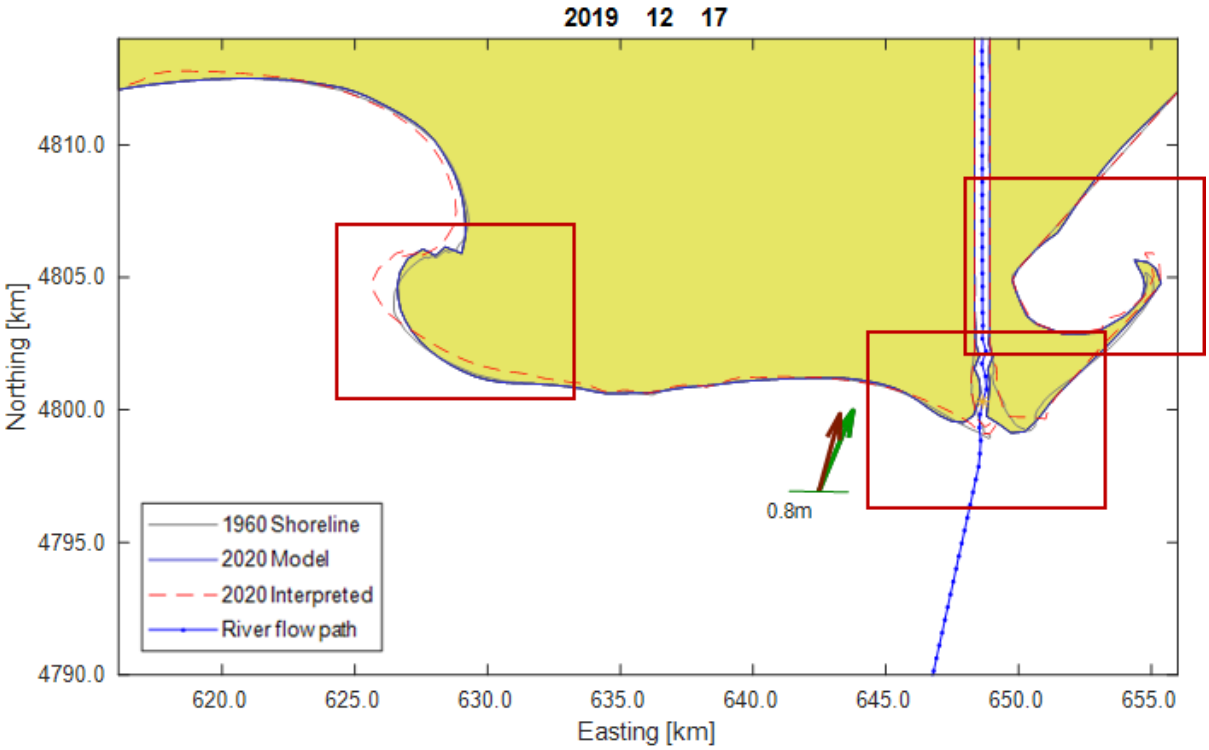
2019 12 17
4810.0
4805.0
4800.0
4795.0
4790.0
Northing [km]
620.0
625.0
630.0
635.0
640.0
645.0
650.0
655.0
Easting [km]
0.8m
1960 Shoreline
2020 Model
2020 Interpreted
River flow path

a.

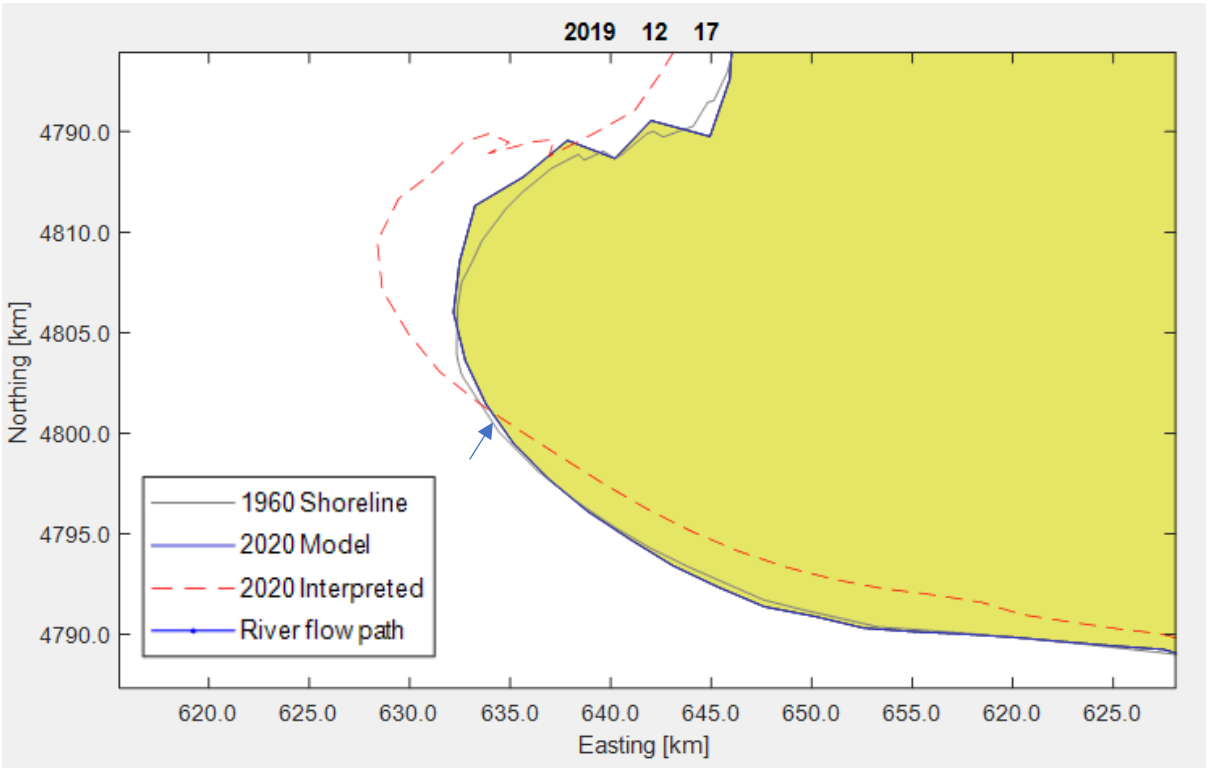
2019 12 17
4790.0
4810.0
4805.0
4800.0
4795.0
4790.0
Northing [km]
620.0
625.0
630.0
635.0
640.0
645.0
650.0
655.0
620.0
625.0
Easting [km]
1960 Shoreline
2020 Model
2020 Interpreted
River flow path

b.

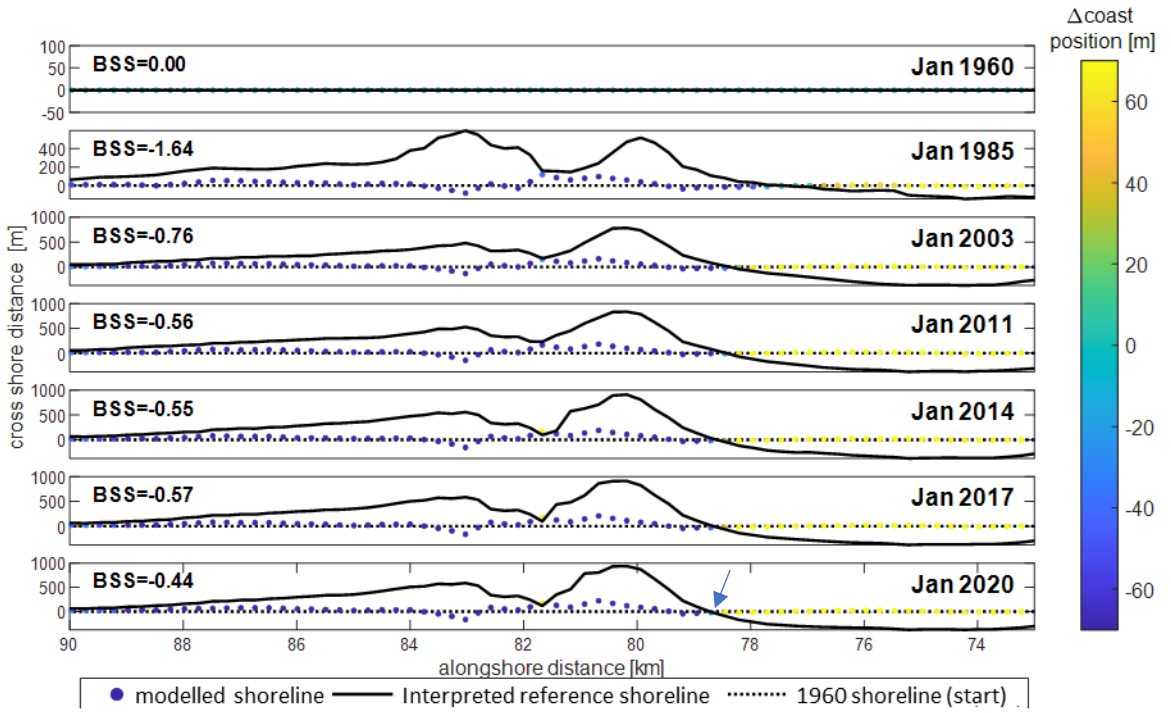
Δcoast position [m]
BSS=0.00
Jan 1960
BSS=-1.64
Jan 1985
BSS=-0.76
Jan 2003
BSS=-0.56
Jan 2011
BSS=-0.55
Jan 2014
BSS=-0.57
Jan 2017
BSS=-0.44
Jan 2020
cross shore distance [m]
alongshore distance [km]
modelled shoreline
Interpreted reference shoreline
1960 shoreline (start)

c.

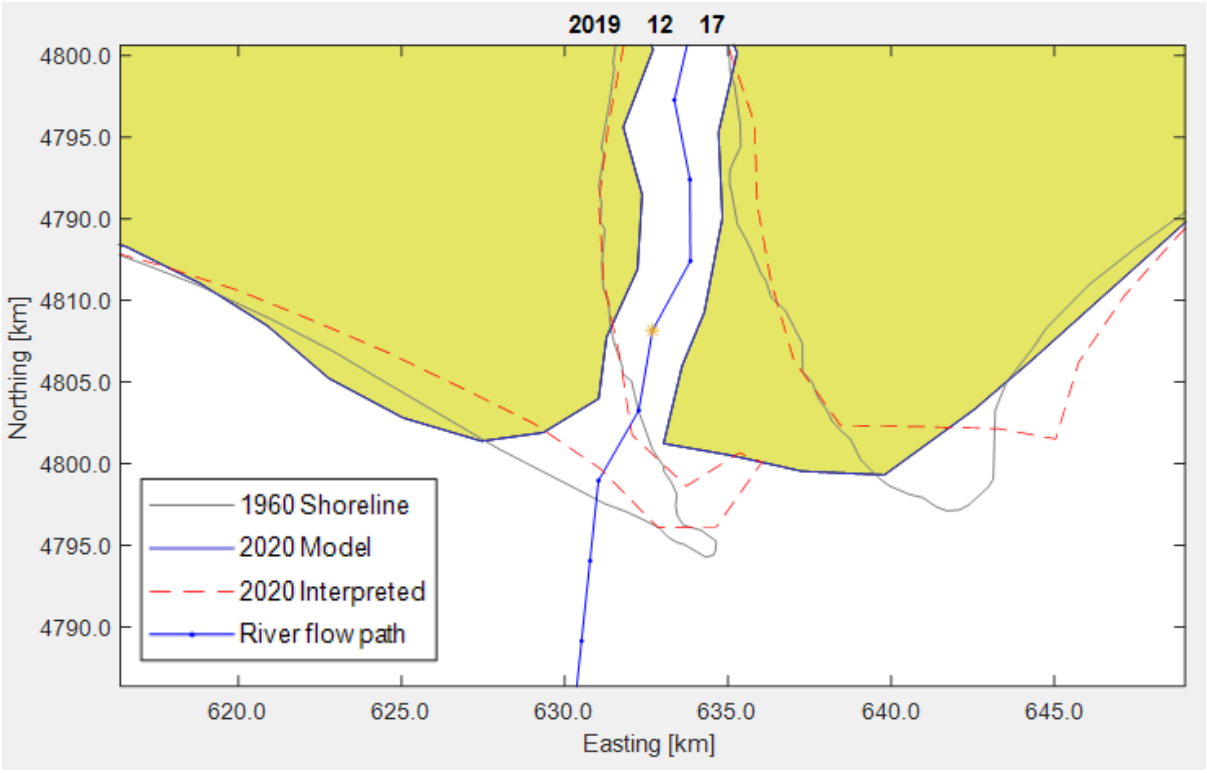
2019 12 17
Northing [km]
Easting [km]
1960 Shoreline
2020 Model
2020 Interpreted
River flow path

d.

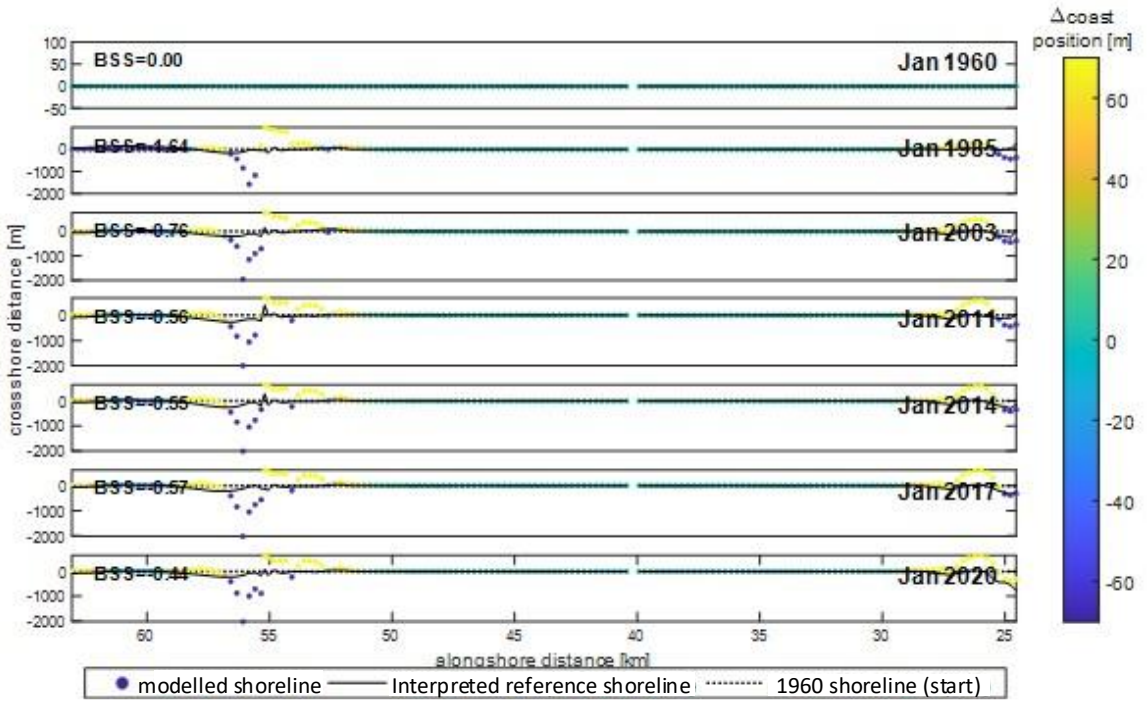
Δcoast position [m]
BSS=0.00
Jan 1960
BSS=-4.64
Jan 1985
BSS=-0.76
Jan 2003
BSS=-0.56
Jan 2011
BSS=-0.55
Jan 2014
BSS=-0.57
Jan 2017
BSS=-0.44
Jan 2020
crosshore distance [m]
alongshore distance [km]
modelled shoreline
Interpreted reference shoreline
1960 shoreline (start)

e.

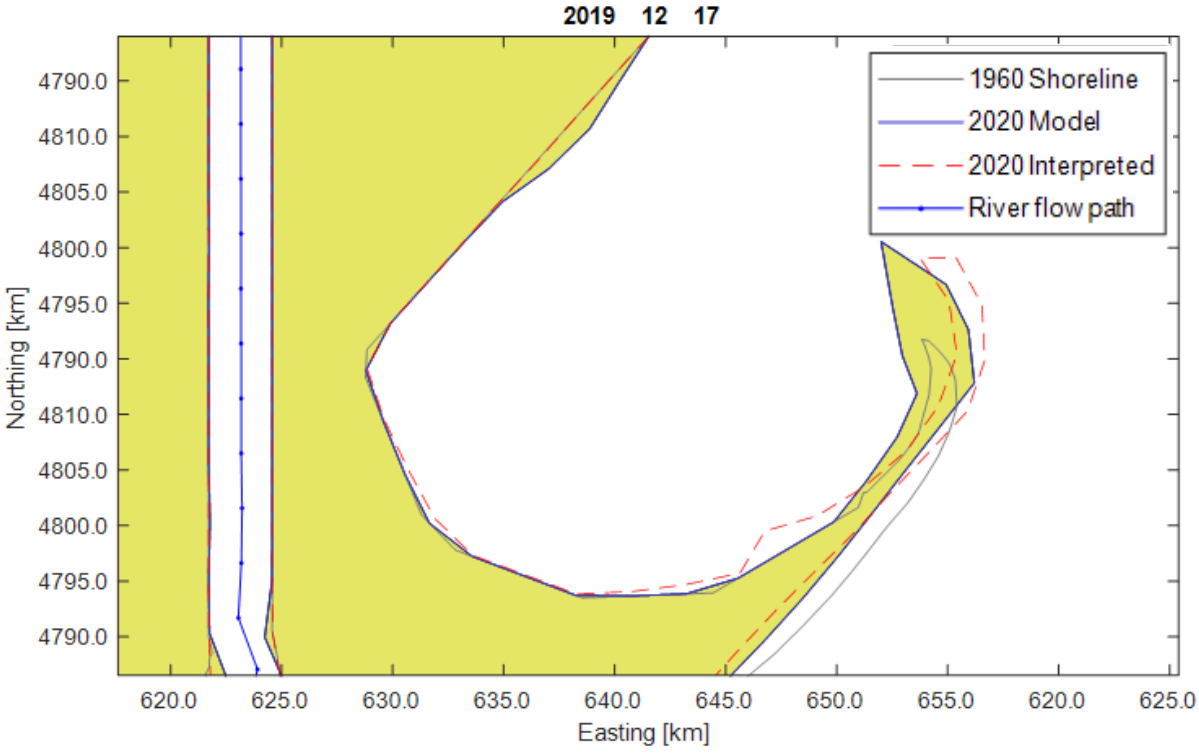
2019 12 17
1960 Shoreline
2020 Model
2020 Interpreted
River flow path
Northing [km]
Easting [km]

f.

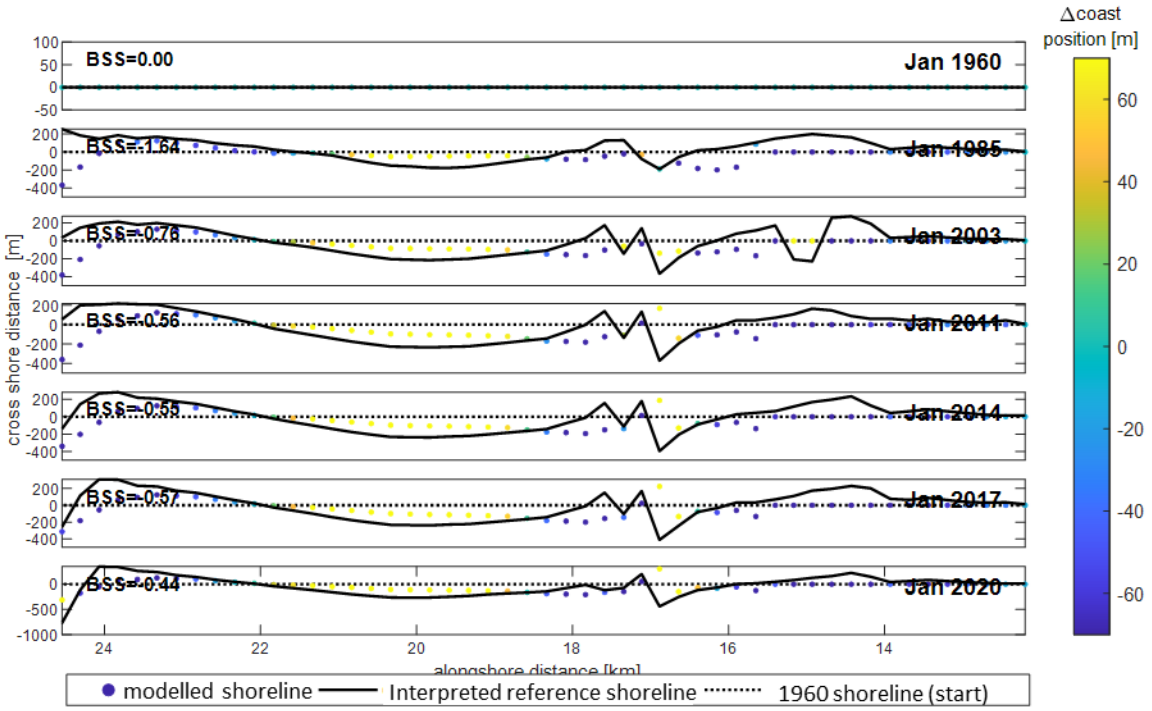

g.

Figure 49: Results of simulation of Rhône shoreline in the form of a: a top down view with areas of special interest highlighted with red rectangles, b and c: the top down view and the cross shore distance plot of the Beauduc spit respectively, d and e: the top down view and the cross shore distance plot of the mouth of the Rhône respectively, f and g: the top down view and the cross shore distance plot of the La Gracieuse spit respectively.

6.4.2. Model parameters

The shoreline development in the simulation with a timestep of 0.01 yr (Figure 50) has a slightly different result compared to the result of the standard simulation. There is less accretion at the Beauduc and La Gracieuse spits. At the same time there is more accretion at the mouth of the Grand-Rhône. This is the case for both banks of the mouth. The simulation with a timestep that is larger than the default timestep is unstable.

The simulation with an initial grid size of 100 m is also unstable, even when lowering the timestep to 0.01 yr. When the initial grid size is instead increased to 1000 m, the result is similar in general shoreline development trend (Figure 51). However, the result is much more jagged, much less precise, and therefore less usable.

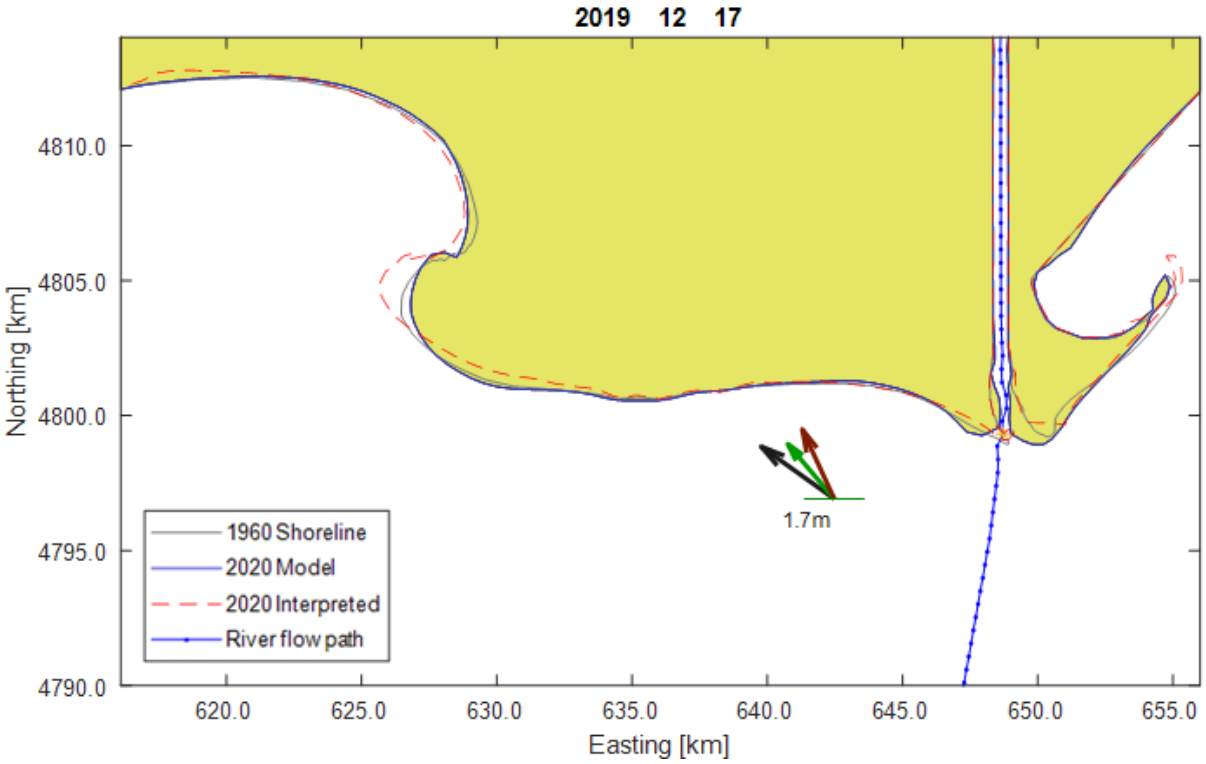

Figure 50: Result of the simulation with a timestep of 0.01 yr

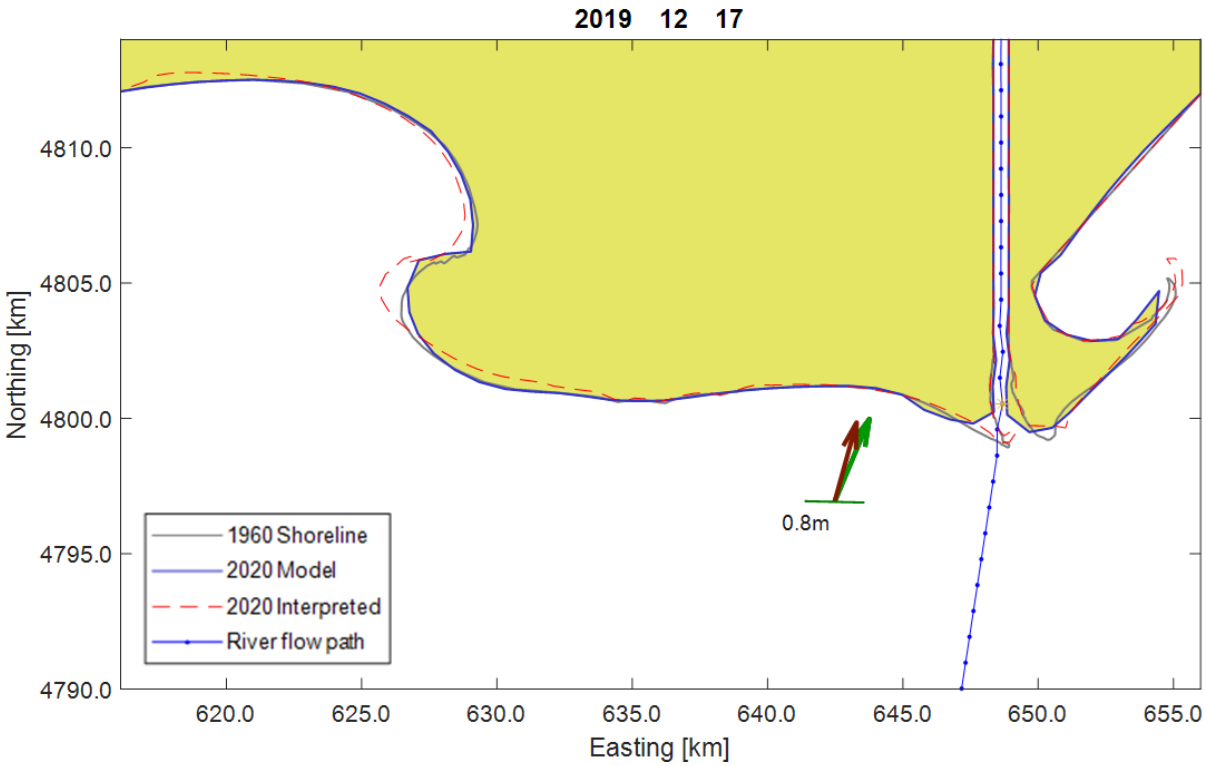

Figure 51: Result of the simulation with an initial grid size of 1000 m.

6.4.3. Transport formulas

The default longshore transport formula used in this study is the van Rijn formula (eq. 8). For the analysis of the effect of the longshore transport formula on the simulations, simulations are run for

all five other longshore transport formulas implemented in ShorelineS (listed in Table 1), including the adapted versions of the KAMP and MILH formulas.

The result of the simulation with the CERC formula (Figure 52 a) is very similar to the result of the standard simulation. The main difference is visible at the eastern bank of the Grand-Rhône mouth and at the La Gracieuse spit, where the sediment deposits are less angular compared to the standard simulation.

The simulation with the CERC2 formula crashed due to the channel getting filled in. This happened at the point in the simulation corresponding to the beginning of the year 2004. The final stable simulation result (Figure 52 b) shows that a protrusion from the western bank of the river channel is about to block of the river. It further shows that there is substantially more sediment accumulation at both the Beauduc and the La Graciesue spit when compared to the results of the standard simulation or the simulation with the CERC formula. Especially considering that the simulation with the CERC2 formula has not reached the end of the simulation due to crashing.

The simulation with the CERC3 formula (Figure 52 c) is similar to the simulation with the CERC2 formula. Again, there is substantial accretion at both the spits. There is even more accretion visible in the CERC3 simulation, but this is because this simulation has continued to the end while the CERC2 simulation did not. The main difference is that the river channel has managed to stay open. The same protrusion from the western bank of the river channel is visible but its growth was just a bit slower, allowing the algorithm that controls the flow path of the river to adjust before getting filled in.

The results of the simulations with the originally implemented KAMP formula (Figure 52 d) and the adapted KAMP formula (Figure 52 e) are very similar. The difference between the two results is that there is slightly more sediment buildup at the eastern bank of the mouth of the Grand-Rhône in the simulation with the adapted KAMP formula. It can further be noticed that there is virtually no change to the original shoreline that represents the shoreline of the Rhône delta in 1960. This applies to both the original and adapted KAMP simulations, although the latter exhibits a slight increase in length of the La Gracieuse spit.

The simulations with the originally implemented MILH formula (Figure 52 f) and the adapted MILH formula (Figure 52 g) are very similar and show a similar pattern as both KAMP simulations. Again, there is slightly more sediment buildup at the eastern bank of the mouth and on the La Gracieuse spit for the adapted version and, again, there is no visible change to the starting shoreline except at the mouth and at the La Gracieuse spit.

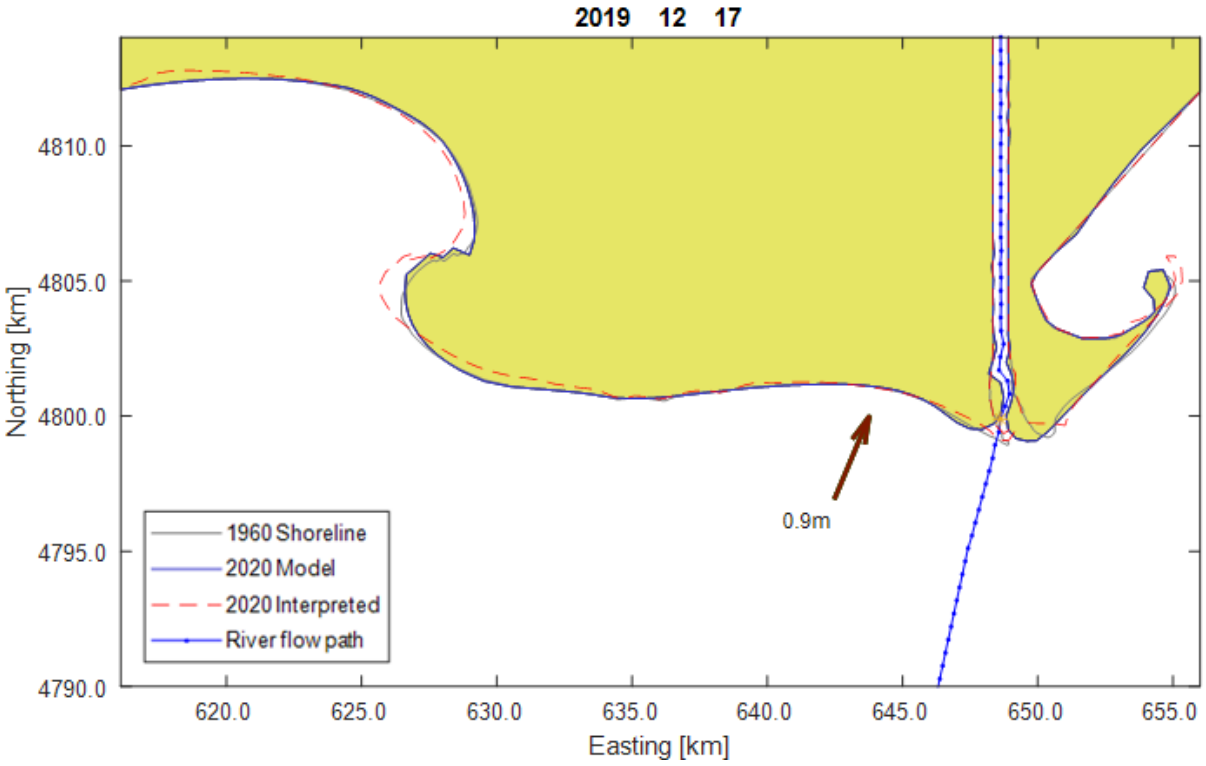
2019 12 17
4810.0
4805.0
4800.0
4795.0
4790.0
Northing [km]
620.0
625.0
630.0
635.0
640.0
645.0
650.0
655.0
Easting [km]
0.9m
1960 Shoreline
2020 Model
2020 Interpreted
River flow path

a.

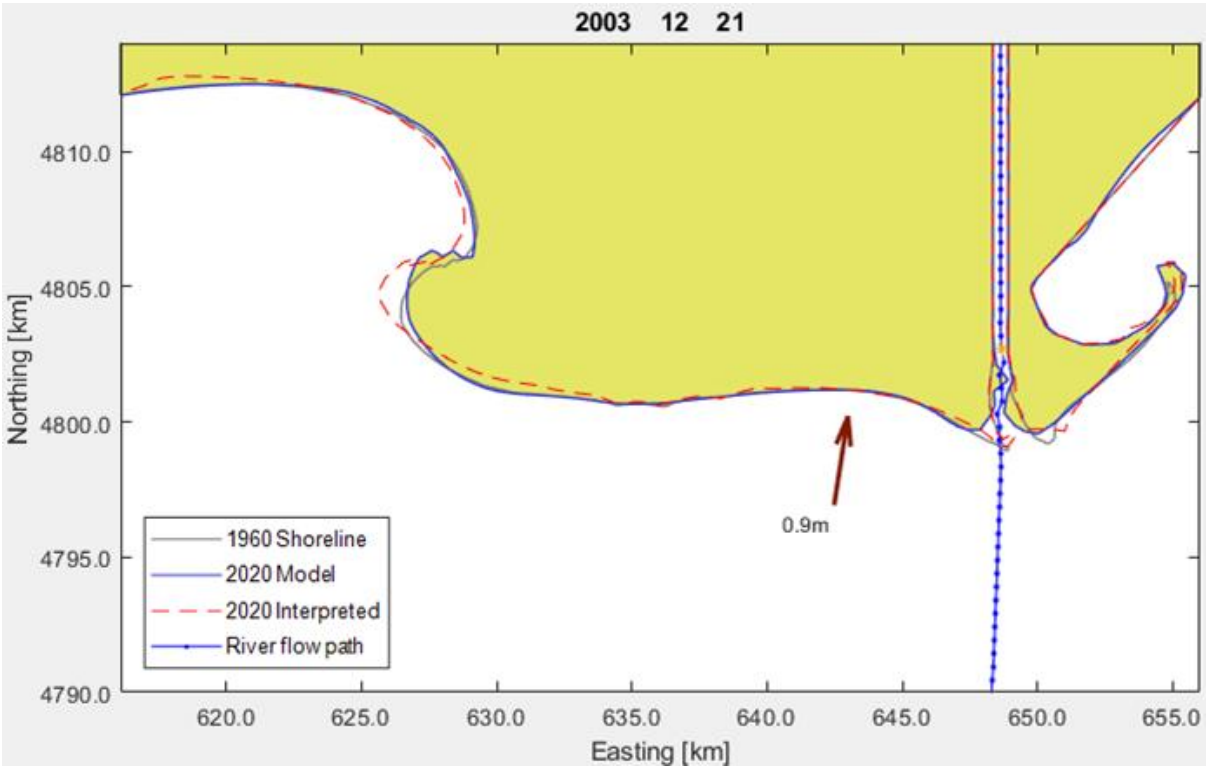
2003 12 21
4810.0
4805.0
4800.0
4795.0
4790.0
Northing [km]
620.0
625.0
630.0
635.0
640.0
645.0
650.0
655.0
Easting [km]
0.9m
1960 Shoreline
2020 Model
2020 Interpreted
River flow path

b.

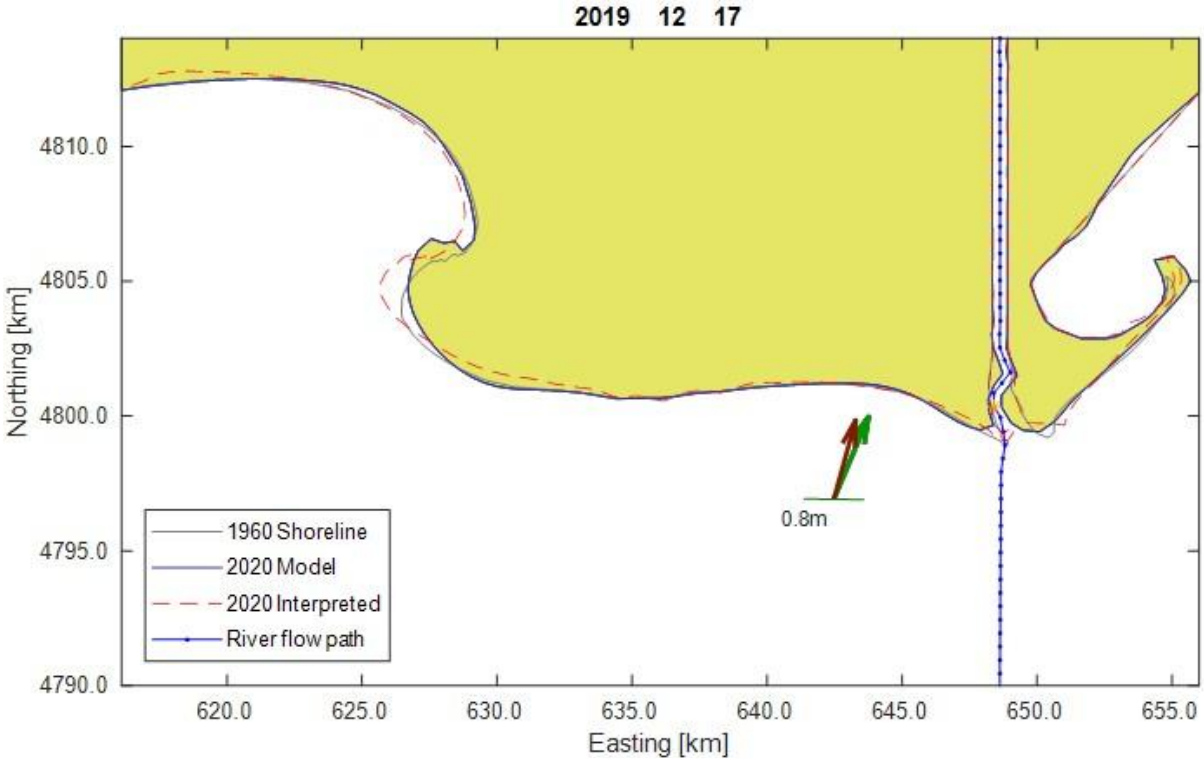
2019 12 17
4810.0
4805.0
4800.0
4795.0
4790.0
Northing [km]
620.0
625.0
630.0
635.0
640.0
645.0
650.0
655.0
Easting [km]
0.8m
1960 Shoreline
2020 Model
2020 Interpreted
River flow path

c.

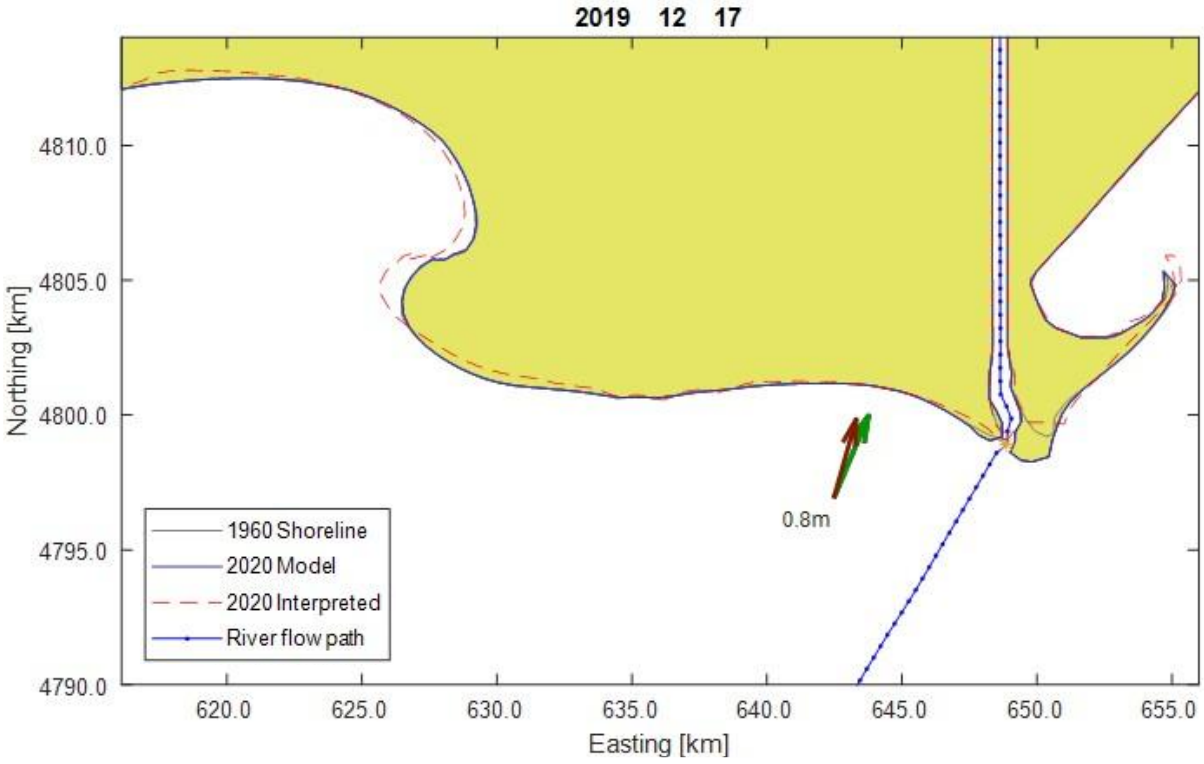
2019 12 17
4810.0
4805.0
4800.0
4795.0
4790.0
Northing [km]
620.0
625.0
630.0
635.0
640.0
645.0
650.0
655.0
Easting [km]
0.8m
1960 Shoreline
2020 Model
2020 Interpreted
River flow path

d.

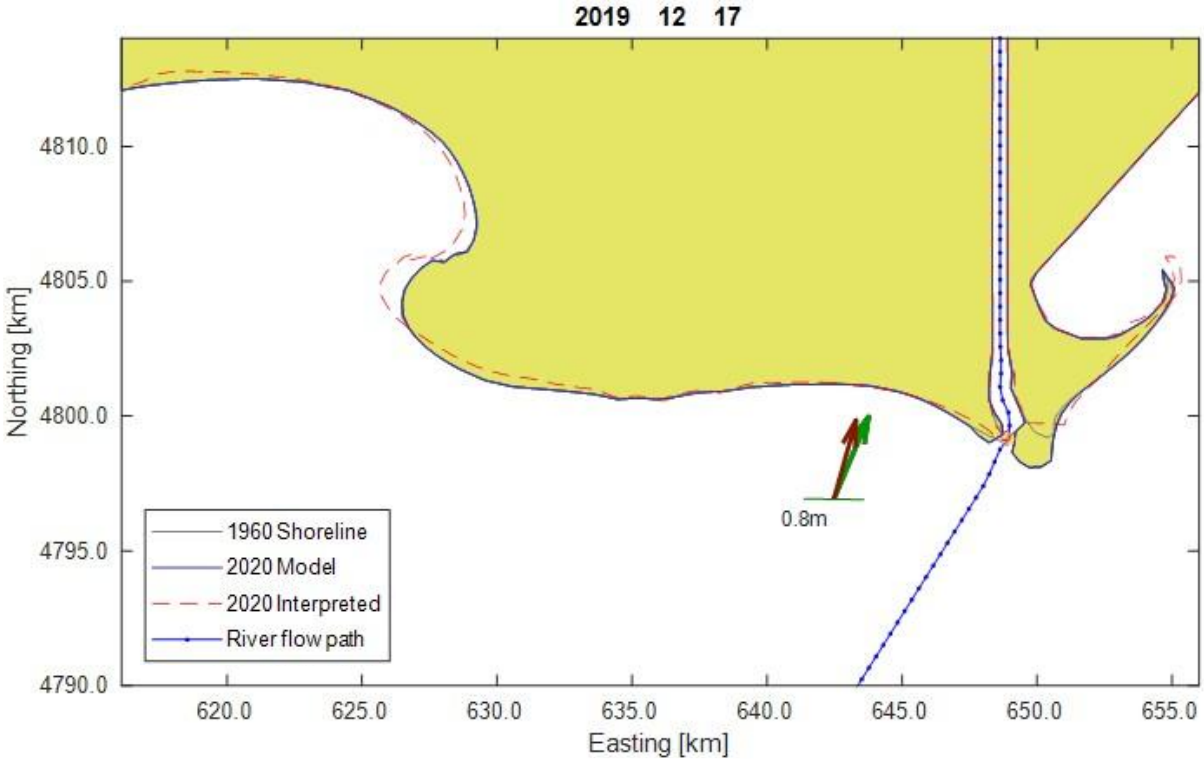
2019 12 17
4810.0
4805.0
4800.0
4795.0
4790.0
Northing [km]
620.0
625.0
630.0
635.0
640.0
645.0
650.0
655.0
Easting [km]
0.8m
1960 Shoreline
2020 Model
2020 Interpreted
River flow path

e.

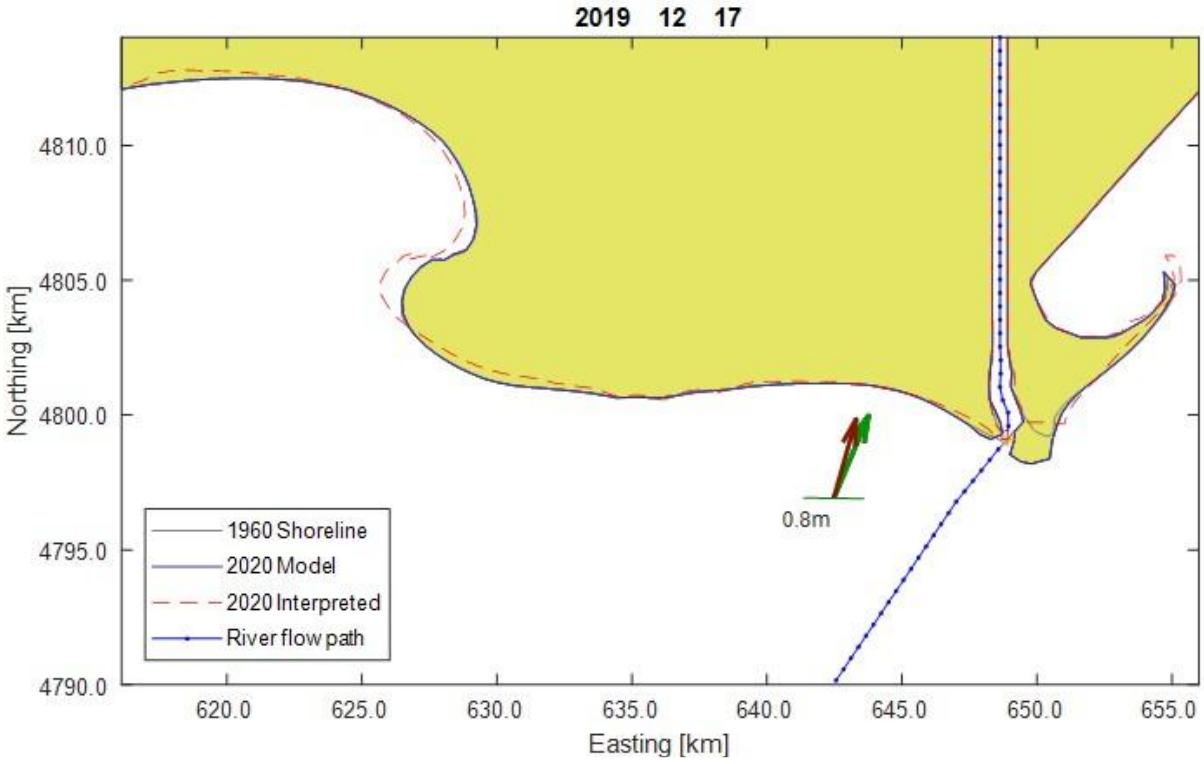
2019 12 17
4810.0
4805.0
4800.0
4795.0
4790.0
Northing [km]
620.0
625.0
630.0
635.0
640.0
645.0
650.0
655.0
Easting [km]
0.8m
1960 Shoreline
2020 Model
2020 Interpreted
River flow path

f.

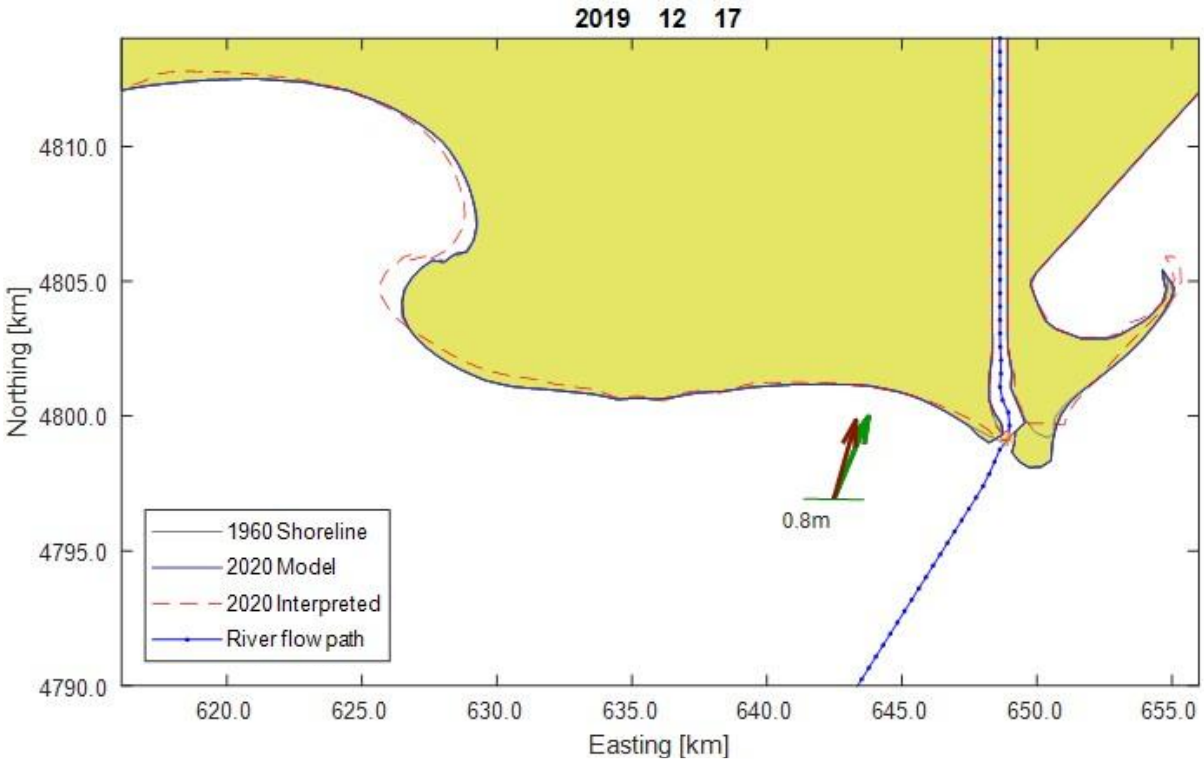

g.

Figure 52: Results of the simulations being run with the a: CERC, b: CERC2, c: CERC3, d: KAMP, e: Kamp adapted, f: MILH, and g: MILH adapted transport formulas.

6.4.4. Mean bed slope

The shoreline development in the simulation with a bed slope of 0.0045 (Figure 53 a) differs from the standard simulation. The simulation with the gentler slope shows more sediment being deposited at both banks of the river mouth. It also shows less accretion at the Beauduc spit while there is more accretion at the La Gracieuse spit. The bed slope of 0.0045 corresponds to the mean bed slope for the part of the shoreline of the Rhône delta that has the Bras de Fer and Pégoulier relict sediment lobes. It represents the gentlest part of the shoreline profile in the region of interest.

The shoreline development in the simulation with a bed slope of 0.042 (Figure 53 b) has a result that differs significantly compared to the standard simulation. There is less sediment being deposited at the river mouth while there is more accretion at both spits. Furthermore, there is significant erosion at the shores sheltered by the spits. The bed slope of 0.042 corresponds to the mean bed slope for the part of the shoreline of the Rhône delta that has the Beauduc and La Gracieuse spits. It represents the steepest part of the shoreline profile in the region of interest.

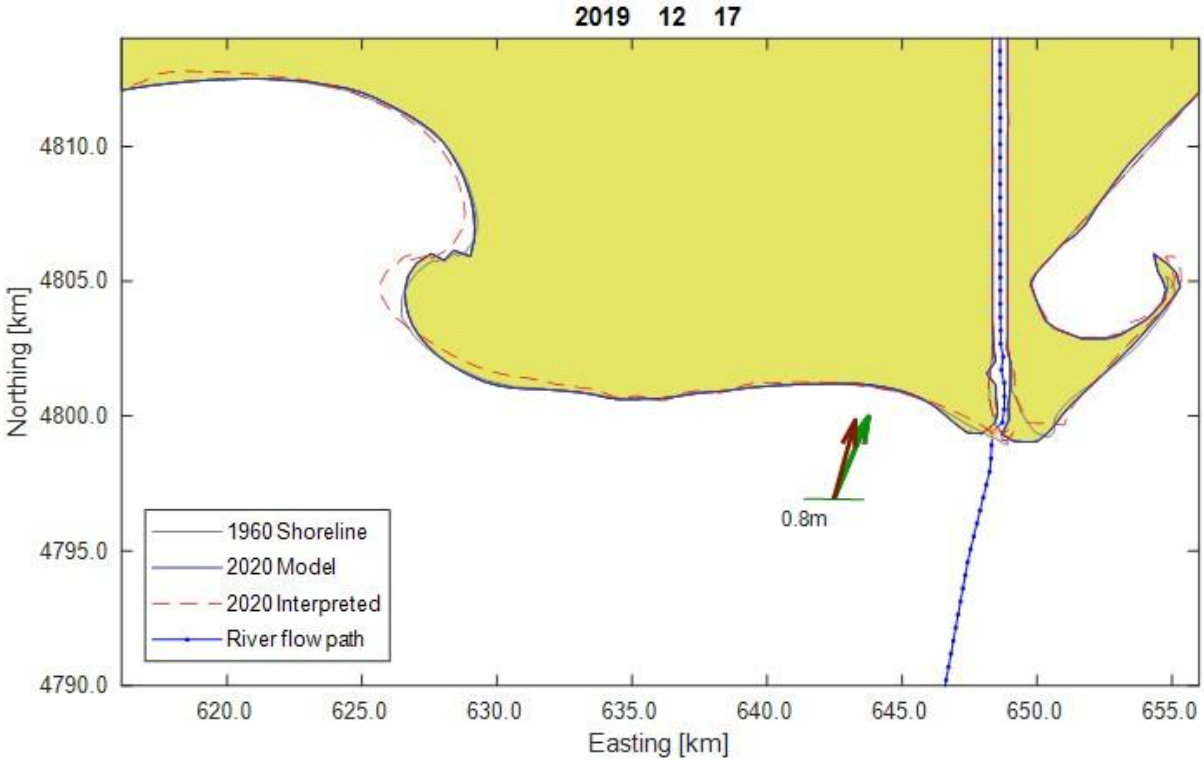

a.

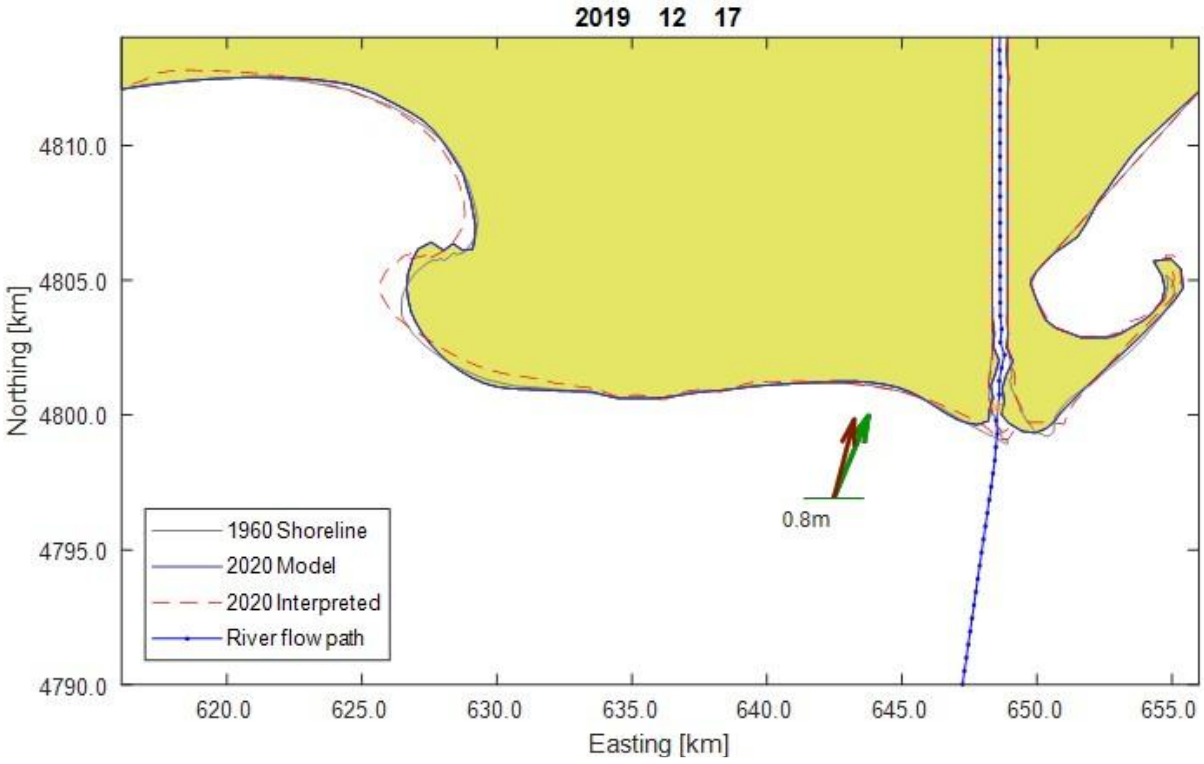

b.

Figure 53: Results of the simulations with a bed slope of a: 0.0045, and b: 0.042

6.4.5. Relative sea level rise

The shared socio-economic pathways developed by the IPCC (2023) illustrate a range of possible scenarios. The sea level rise predicted for the remainder of this century ranges from about 5.5 mm/yr for SSP1 to about 11 mm/yr for SSP5 (IPCC, 2023).

The shoreline development in the simulation with a relative sea level rise of 5.5 mm/yr (Figure 54 a) differs from the standard simulation by showing more erosion. This is mostly visible at both spits, at the beach of Beauduc, directly at the mouth of the Grand-Rhône, and along both banks of the channel of the Grand-Rhône. The shores of Faraman, Piémanson, and Napoléon remain mostly unaffected.

The shoreline development in the simulation with a relative sea level rise of 11 mm/yr (54 b) shows even more erosion compared to the SSP1 simulation. There is even more erosion where it was already visible. However, there is now also erosion at the Piémanson beach and the La Gracieuse spit has been disconnected from the shoreline and forms an island.

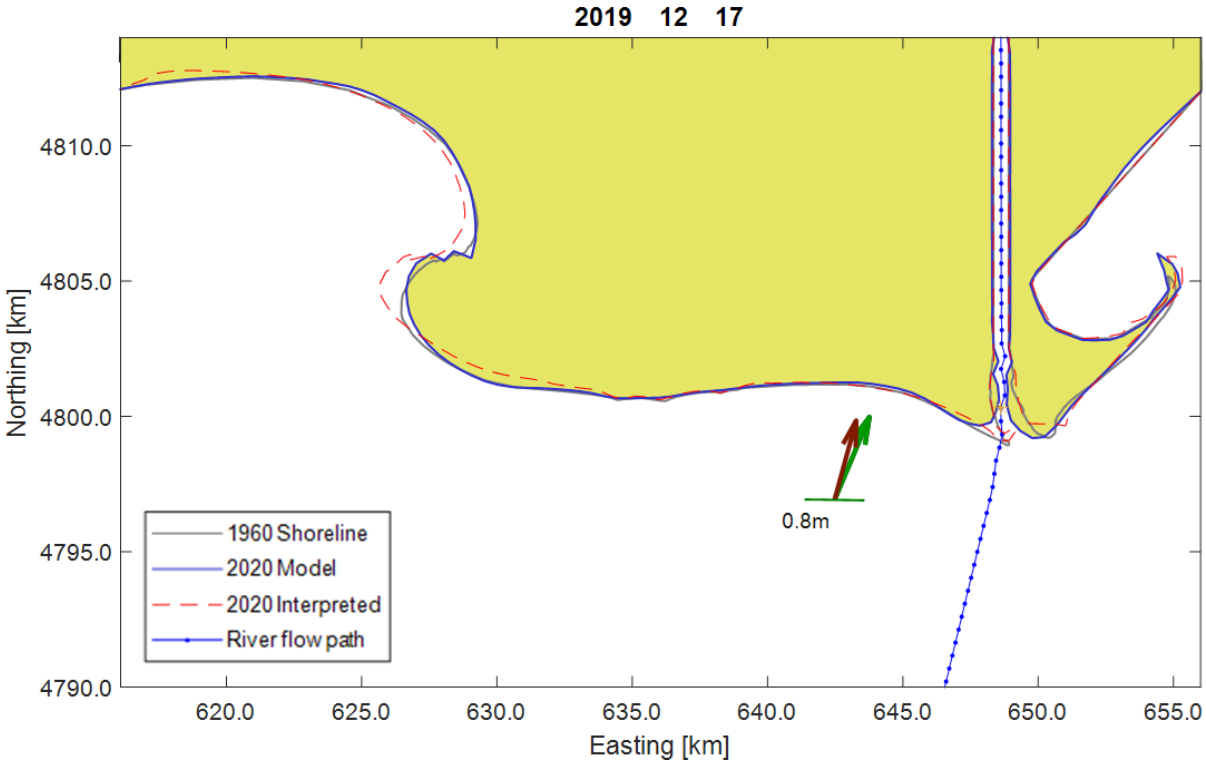

a.

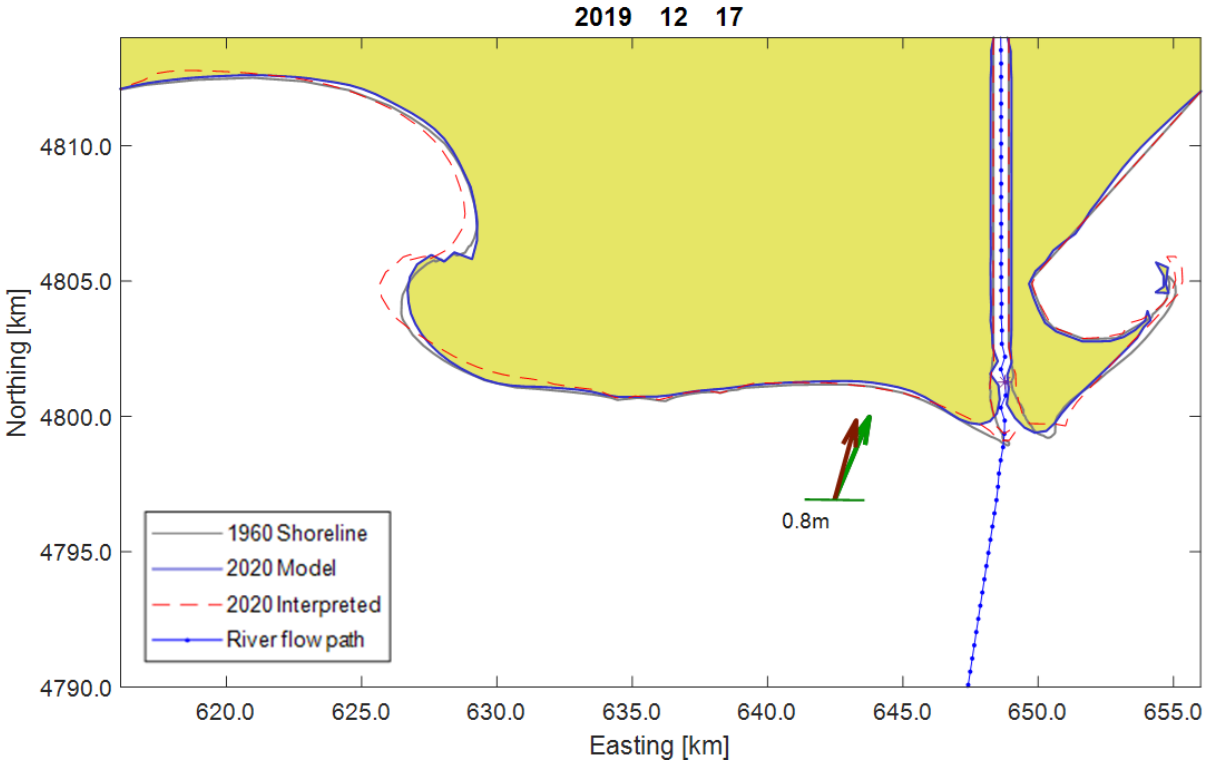

b.

Figure 54: Results of the simulations with a relative sea level rise of a: 5.5 mm/yr, and b: 11 mm/yr.

6.5. Discussion

The hindcast was set up to answer the question what the applicability of the ShorelineS model is to accurately simulate the development of a shoreline with a river mouth in a wave dominated delta and to attempt to validate the use of ShorelineS in such cases. The results of the hindcast will be discussed here.

6.5.1. Stability

The stability of the simulation is defined by the stability criterion (Eq. 10). This criterion shows that the stability depends on the time step and grid size, but also on the maximum transport rate. With the default time step of 0.05 yr and the default initial grid size of 500 m, a maximum transport rate of 12.5 Mm^3/yr still results in a stable simulation. The maximum transport rate during the simulation can be checked retroactively. The maximum transport rate in the standard simulation of the hindcast is 7.0 Mm^3/yr. Well within the range defined by the stability criterion. The maximum transport rate for the simulation with a timestep of 0.01 yr has a maximum transport rate of 15.1 Mm^3/yr. This is also within the range defined by the stability criterion since the range becomes bigger as the timestep becomes smaller. With the grid size at 500 m but with the default time step of 0.01 yr, the maximum transport rate within the range defined by the stability criterion is 62.5 Mm^3/yr.

The difference in simulation results between the standard simulation and the simulation with a timestep of 0.01 yr is surprising. Since both simulations are within the stability range, the results are expected to be the same. The fact that there is more accretion at the mouth while there is less accretion at the spits in the case with the lower timestep suggests that the longshore transport from

the mouth to the spits is either underestimated in the simulation with a timestep of 0.01 yr or overestimated in the standard simulation. What causes this is unknown.

6.5.2. Shoreline profile

A similar pattern with regards to the shoreline profile can be seen in the hindcast as is seen in the synthetic case. The steeper the profile gets, the less the river mouth progrades. Instead, the longshore transport moves the sediment from the mouth to the spits. A steeper profile also leads to erosion at the beach of Beauduc and at the harbour in the gulf of Fos. Of course, no erosion would take place at the harbour since it is a hard structure that can withstand the wave energy. However, ShorelineS does not take this into account. The extra strain on the harbour that this simulation shows can still be a useful result when accounting for harbour maintenance.

The spits represent the steepest part of the shoreline profile while the relict sediment lobes represent the gentlest part of the shoreline profile. Assuming that the longshore transport at the respective part of the shoreline is simulated accurately, this means that the longshore transport in the standard simulation is underestimated at the spits while the longshore transport at the relict sediment lobes is overestimated.

6.5.3. Wave interaction

No variations in wave climate were tested as the wave climate provided by ERA5 is assumed to be accurate. A pattern that can be discerned from the results of the hindcast simulations is that the shoreline gets rounded down much more than it should. This is evident especially near the mouth of the Grand-Rhône. The interpreted shoreline for 2020 is still quite pointy but the model rounds this point down right from the start of the simulation. This can be seen in the cross-shore distance plot and is likely the cause for the initial drop in the Brier skill score.

The difference between the positions of the simulated and interpreted shorelines near the mouth of the Grand-Rhône could be because in the simulations the waves interact with a shoreline with a constant profile. In the case of the mouth of the Rhône, where the difference is most notable, this could be explained by the existence of the delta plateau. The existence of this plateau is ignored in the simulations. Another possible explanation is that the rounding down of pointy coastal features is due to the discretisation of the shoreline.

6.5.4. Climate change

The results of the simulations with relative sea levels corresponding to SSP1 and SSP5 are not necessarily representative of the conditions in the Gulf of Lion as the relative sea level rise in the SSP1 and SSP5 scenarios is a prediction for a global mean sea level rise. The visible erosion in the two results of the relative sea level rise simulations is also not realistic. This erosion could happen at the natural beaches in the region of interest but not at the parts of the coast that are artificially kept in place, such as the banks of the channel of the Grand-Rhône. The erosion and eventual disconnecting of the La Gracieuse spit is an interesting development. Since the development of this spit is almost completely natural, an increase in relative sea level rise as illustrated in SSP5 could actually cause this result.

It should be noted that despite the constant profile along the shoreline that is used in the simulations, the transgression due to the relative rise in sea level is not constant along the shoreline. This would be the expected result with the passive inundation method. The fact that this is not the case further illustrates the importance of the shoreline development processes that the passive inundation method does not take into account.

6.5.5. Bulk longshore transport formula

The simulation with the CERC formula is rather similar to the standard simulation, despite the big differences between the two formulas. This same similarity is seen in the results for the synthetic case. The VR14 formula performs best of all the implemented bulk longshore transport formulas in ShorelineS since the standard simulation, which uses the VR14 formula, is the closest result to the interpreted shorelines. Considering this, it is worth noting that the simplest formula implemented in ShorelineS, the CERC formula, has so far shown better performance than expected.

Again, the simulations with the CERC2 and CERC3 formulas are similar. The CERC2 simulation may have crashed, but it is clear from the intermediate state of the shoreline before the crash that the simulation was heading in the same direction as the CERC3 simulation. The results of these two simulations being similar is not as surprising since the CERC2 and CERC3 formulas are themselves similar, with CERC2 being an adaptation of CERC3 that accounts for refraction and shoaling. The difference between the two formulas must have been what caused the difference in results, which in this case means the filling in of the channel. This causes the simulation to crash since the nourishment is still active but is now partly made on the coast. This is not possible in ShorelineS.

The results of the simulations with the original and adapted KAMP and MILH formulas are surprising. First of all, it is strange that the starting shoreline that represents the shoreline of the Rhône delta in 1960 has undergone no visible changes apart from at the mouth and at the La Gracieuse spit. This is likely incorrect model behaviour, although it is not known why this happens.

It is further unexpected that the use of the adapted version of the formulas results in slightly more progradation when compared to the original version of the formulas, since this is the inverse of what happened in the synthetic case.

6.5.6. Summation of findings

Overall, what can be discerned from the results from the hindcast is that no matter what bulk longshore transport formula is used, the progradation at the mouth of the Grand-Rhône is consistently overestimated by ShorelineS. The sediment deposited by the Rhône at the mouth is not being transported alongshore at a rate that results in the amount of progradation seen from the interpreted shorelines. There are two possible explanations for this observation.

The first explanation is that the amount of sediment deposited by the river is an accurate representation of the in-situ conditions. At the same time the longshore transport that should distribute this sediment along the shoreline is underestimated by the bulk longshore transport formulas implemented in ShorelineS. This results in more progradation at the mouth. The second explanation is that the amount of sediment deposited by the river is over evaluated and the longshore transport is accurately estimated, but incapable of handling such a big sediment deposition. This also results in more progradation and thereby a deviation from the interpreted shorelines.

Two other observations that can be made are that no matter what bulk longshore transport formula is used, the accretion at the Beauduc spit and the erosion at the shore of Faraman to the east of Grau de la Dent are consistently underestimated by ShorelineS. Of course, these observations are related to each other since the eroded sediment from the shore of Faraman ends up on the Beauduc spit, according to the littoral drift cell pattern. Nevertheless, the amount of sediment eroded from the shore of Faraman is not enough to provide all the sediment for the accretion at the spit of Beauduc that is seen from the interpreted shorelines.

The lack of erosion on the shore of Faraman can be explained by the existence of groynes on this shore. These groynes could have blocked the longshore transport which resulted in downdrift erosion (Sabatier et al, 2009). Since the model setup does not take coastal protection structures into account, this would be a logical explanation for the discrepancy in shoreline development between the simulation results and the interpreted shorelines.

The lack of accretion on the Beauduc spit cannot only be explained by the lack of erosion on the shore of Faraman. The sediment deficit could further be explained in two ways. The missing sediment could be deposited by the Rhône at its mouth, but without sufficient longshore transport to transport it towards the Beauduc spit. Or the missing sediment could be explained by the existence of the relict sediment lobe present at Grau de la Dent.

Sabatier et al (2006) conducted research into the bathymetry in the region of interest. They analysed bathymetric data from four time intervals in order to determine the long-term bathymetric changes of the Rhône delta. To do so they computed digital terrain modelling for all four periods. They found that the relict sediment lobes are reworked by the waves and that the sediment from the lobes contributes to the growth of the spits. This means that the relict sediment lobes can function as time limited sediment sources for the longshore transport to the Beauduc spit.

Considering that the development of the La Gracieuse spit in the simulations is close to the development seen from the interpreted shorelines, it seems likely that the longshore transport from the mouth of the Grand-Rhône to the La Gracieuse spit is accurately represented. This would mean that the longshore transport towards the Beauduc spit is also accurately represented and that the overestimation of progradation at the mouth is likely due to an overestimation of the sediment discharge. Such an overestimation could be caused by underestimating the limiting effect of dam construction on the suspended load and bedload of the Rhône.

With the assumption that the sediment deposited by the Rhône is overestimated, the lack of accretion at the Beauduc spit when compared to the interpreted shorelines is likely explained by the inability of ShorelineS to account for sediment sources in the form of relict sediment lobes, in this case the relict sediment lobe of the old Bras de Fer mouth.

The reason ShorelineS cannot account for the relict sediment lobes is because of the assumption that the shoreline profile is constant along the shoreline. The existence of the relict sediment lobes means that the bathymetry is varied and that the profile cannot be constant along the shoreline. Since the relict sediment lobes are the result of river related natural processes, this limits the applicability of ShorelineS in cases where the river has formed these sediment lobes.

The applicability of ShorelineS under conditions where the constant profile along the shoreline is a reasonable assumption has already been proven, for instance in the case of the ‘Sand engine’ in the Netherlands. This case was used to validate the ShorelineS model for shorelines without a river mouth (Roelvink et al, 2020).

Despite the differences between the standard simulation and the interpreted shoreline, the simulation of the shoreline of the Rhône delta is stable and has a good skill score. Considering that ShorelineS was able to simulate six decades worth of shoreline development in mere minutes while also resulting in a good approximation of the interpreted shoreline, there is very likely applicability for the ShorelineS model where quick evaluations of shoreline development are required.

The hindcast further showed that the more complex shoreline and more complex input parameters that are assumed to be representative of the Rhône delta can have unforeseen effects on the

simulation. This is seen from the unexpected model behaviour in the simulation with the smaller timestep as well as in the simulations with the original and adapted KAMP and MILH formulas. Since the explanation for this unexpected model behaviour was not found, a negative impact on the results of this study cannot be ruled out.

Unexpected model behaviour that does have an explanation showed another limitation of ShorelineS. When a river channel gets filled in with sediment, the simulation immediately crashes. This is because the nourishment, that represents the sediment discharge from the river, is located along the flow path of the river. When the flow path overlaps with the land, the nourishment needs to be placed on the land. This results in an error. This limits the applicability of ShorelineS in environments where a channel could reasonably get filled in with sediment.

Both the synthetic case and the hindcast showed that a relative rise in sea level will not automatically lead to a cross-shore shift of the shoreline as it would with passive inundation. This is despite the fact that ShorelineS assumes a constant shoreline profile.

Both the synthetic case and the hindcast also showed a surprising performance from the different implemented bulk longshore transport formulas. The van Rijn (2014) formula performed best, which is according to expectations. However, the simplified CERC formula also performed surprisingly well, considering how limited the formula is and that it was really only meant to illustrate the principles of the model behaviour. Theoretically, it should not be suitable for the complex shoreline of the Rhône delta. This is because it is not reasonable to assume that the wave conditions at the point of breaking are constant along the shoreline, which is a prerequisite for using the simplified CERC formula.

7. Conclusions and recommendations

7.1. Conclusions

The main research question in this study is: What is the applicability of the ShorelineS shoreline model to accurately simulate the development of a shoreline with a river mouth?

To help answer this question the following sub questions were asked:

- Can the model successfully simulate shoreline development of a shoreline with a river mouth in a simplified environment?
- What is the applicability of the ShorelineS model to accurately simulate the development of a shoreline with a river mouth in a wave dominated delta?

To answer the first sub question a synthetic case was set up to analyse the model behaviour with regards to a shoreline with a river mouth. To answer the second sub question a hindcast was set up to analyse the shoreline development of a shoreline with a river mouth in the more realistic setting of a wave dominated delta and to attempt to validate the use of ShorelineS in such cases.

ShorelineS handles simulating a river mouth through the simplified method of algorithms that keep a mouth open at a specified width depending on the discharge of the river. Combined with algorithms that redistribute sediment linked to the discharge of the river, implemented in the form of nourishments on the flow path of the river.

The results of the synthetic case show that this method is successful for simulating a river mouth with a constant sediment discharge in a simplified environment. The results show the expected model behaviour. The progradation of the river mouth lessens as the slope angle, the depth of closure, the significant wave height, the peak wave period and the relative sea level rise increase. This method also seems to work well in tandem with wave driven longshore sediment transport. The results are mostly in line with expectations, and the simulations are stable as long as they remain within the stability criterion. The results even remain stable under wave angles of incidence beyond the critical 45° angle of incidence that would lead to instability if a central scheme was used. This is the case as long as the channel does not get filled in with sediment because the implementation of the continuous sediment discharge in the form of a nourishment in combination with a filled in river channel results in unwanted model behaviour.

When looking at a more complex coastal form like the shoreline between Saintes-Maries-de-la-Mer and the La Gracieuse spit, the region of interest for the hindcast, the limitations of ShorelineS become noticeable. All simulations fail to accurately simulate the erosion to the east of Grau de la Dent at the shore of Faraman as well as the accretion at the Beauduc spit, and the progradation at the mouth of the Grand-Rhône. These observations can be explained by the overestimation of the sediment discharged by the Rhône and the inability of ShorelineS to account for the existence of the relict sediment lobes and their time limited sediment supply because of the constant bed slope assumed by ShorelineS.

The constant bed slope is one of the assumptions made by ShorelineS that makes it a less computationally heavy model compared to shoreline development models that account for bathymetry. This significantly cuts down on model runtime, resulting in simulations that take mere minutes to run instead of days. This is the big appeal that ShorelineS has compared to more detailed two-dimensional horizontal process-based models.

Unfortunately, the assumption of a constant bed slope is also the biggest weakness of ShorelineS since these relict sediment lobes are the direct result of the natural development of a delta, through

progradation and avulsion. ShorelineS was already incapable of simulating natural delta progression such as avulsion, a river getting filled in, or the formation of mouth bars. But the assumption of a constant profile slope further limits its applicability to simulate shoreline development of shorelines in natural conditions, such as in a wave dominated delta.

Nevertheless, the simulations made by ShorelineS are quite good. This is evidenced by the Brier skill score of -0.44 for the standard simulation in the hindcast. Aside from the missed sediment influx from the relict sediment lobes, the shoreline development of the Rhône delta by ShorelineS was successful. Despite a much more chaotic environment with a wave climate time series and a much more complicated shoreline, the simulations were nearly all stable and especially the simulations run with the CERC and van Rijn bulk transport formulas were accurate apart from the missed sediment influx.

Therefore, there is certainly applicability for ShorelineS to simulate the shoreline development of a shoreline with a river mouth. When the shoreline and channel are locked in place through the application of coastal engineering works ShorelineS will give much more satisfactory results. The applicability of ShorelineS in data limited environments or on a global scale is also an interesting option. The improvement of several magnitudes in cost and efficiency compared to more heavy-duty models makes ShorelineS uniquely suited for these situations. However, when a shoreline with a river mouth is considered, it will be a challenge to get data on river discharge and local bathymetry. In the end, the time and cost efficiency of ShorelineS will result in more applicability when the demand for accuracy of the simulation is lower.

7.2. Recommendations

The following recommendations form opportunities for future development of ShorelineS and are based on the conclusions and limitations of this study.

The limitations of ShorelineS with regard to the bathymetry could be remedied by coupling ShorelineS to relatively simple two-dimensional horizontal process-based models. These are more computationally heavy models that consider the bathymetry. This way, the bathymetry could be taken into account. This could make it possible to successfully simulate the development of deltas, despite the variable bed slope. If possible, the combination of these models could combine the best of both worlds. Removing the limitation from ShorelineS of not accounting for bathymetry while not sacrificing all the efficiency with which ShorelineS is able to simulate shoreline development.

Of all the implemented bulk longshore transport formulas in ShorelineS, the VR14 formula has the best performance. It is also the formula that takes the most different parameters into account and therefore requires more input based on prior knowledge compared to the simpler longshore transport formulas. This limits its applicability in data limited environments. However, throughout the simulations in the synthetic case as well as the hindcast, the CERC formula has performed above expectations. Since this is a much simpler formula that requires less inputs based on prior knowledge it could more readily be applied in data limited environments. To what extent the performance of the CERC and VR14 models stay close to each other could therefore be a worthwhile research subject.

The unwanted model behaviour that is the result of an active nourishment in a filled in channel is another limitation of the model that could be remedied with future development of the ShorelineS model. The unexpected model behaviour for simulations with a lower timestep and for simulations with the original and adapted KAMP and MILH formulas can be looked into. Further improvements to the model could be the ability to have more input parameters be variable throughout the

simulation by allowing the possibility of a time series as input. This could for instance be implemented for the wave spreading, for the mean bed slope, and for the active profile height and the related depth of closure.

With respect to the shoreline development of the delta of the Rhône, further research could be conducted to the effect of the coastal engineering works present, or to the effect of climate change on the delta. Not only through a rise in relative sea level, but also through a change in wave parameters and a change in the frequency of flooding events caused by the more extreme weather that is the result of global warming.

References

Anderson, T. R., Fletcher, C. H., Barbee, M. M., Romine, B. M., Lemmo, S., & Delevaux, J. M. (2018). Modeling multiple sea level rise stresses reveals up to twice the land at risk compared to strictly passive flooding methods. *Scientific Reports*, *8*(1), 14484.

Ashton, A. D., & Murray, A. B. (2006). High-angle wave instability and emergent shoreline shapes: 1. Modeling of sand waves, flying spits, and capes. *Journal of Geophysical Research: Earth Surface*, *111*(F4).

Ashton, A., Murray, A. B., & Arnoult, O. (2001). Formation of coastline features by large-scale instabilities induced by high-angle waves. *Nature*, *414*(6861), 296-300.

Barbariol, F., Davison, S., Falcieri, F. M., Ferretti, R., Ricchi, A., Sclavo, M., & Benetazzo, A. (2021). Wind waves in the Mediterranean Sea: An ERA5 reanalysis wind-based climatology. *Frontiers in Marine Science*, *8*, 760614.

Bell, B., Hersbach, H., Simmons, A., Berrisford, P., Dahlgren, P., Horányi, A., ... & Thépaut, J. N. (2021). The ERA5 global reanalysis: Preliminary extension to 1950. *Quarterly Journal of the Royal Meteorological Society*, *147*(741), 4186-4227.

Boudet, L., Sabatier, F., & Radakovitch, O. (2017). Modelling of sediment transport pattern in the mouth of the Rhone delta: Role of storm and flood events. *Estuarine, Coastal and Shelf Science*, *198*, 568-582.

Brier, G. W. (1950). Verification of Forecasts Expressed in Terms of Probability„Monthly Weather Review", 78 (1).

Bruun, P. (1962). Sea-level rise as a cause of shore erosion. *Journal of the Waterways and Harbors division*, *88*(1), 117-130.

Ciscar, J.C., Ibarreta, D., Soria, *et al.* Climate impacts in Europe: Final report of the JRC PESETA III project, EUR 29427 EN, Publications Office of the European Union, Luxembourg, 2018, ISBN 978-92-79-97218-8, doi:10.2760/93257, JRC112769.

Dronkers, J. (2025) Shoreface profile. Retrieved 17 May 2025: https://www.coastalwiki.org/wiki/Shoreface_profile

ECMWF. (2018) ERA5 data documentation and parameters therein. Retrieved 16 October 2024: https://confluence.ecmwf.int/display/CKB/ERA5%3A+data+documentation#ERA5:datadocumentation-Table8

Estournel, C., Mikolajczak, G., Ulses, C., Bourrin, F., Canals, M., Charmasson, S., ... & Verney, R. (2023). Sediment dynamics in the Gulf of Lion (NW Mediterranean Sea) during two autumn–winter periods with contrasting meteorological conditions. *Progress in Oceanography*, *210*, 102942.

Fouchier, F. (2015). A new purchase from the Conservatoire du Littoral at Salins du Midi. Retrieved 23 September 2025: https://www.zones-humides.org/un-nouvel-achat-du-conservatoire-du-littoral-aux-salins-du-midi

Hasselmann, K., Barnett, T. P., Bouws, E., Carlson, H., Cartwright, D. E., Enke, K., ... & Walden, H. (1973). Measurements of wind-wave growth and swell decay during the Joint North Sea Wave Project (JONSWAP). *Ergaenzungsheft zur Deutschen Hydrographischen Zeitschrift, Reihe A*.

Hersbach, H., Bell, B., Berrisford, P., Biavati, G., Horányi, A., Muñoz Sabater, J., Nicolas, J., Peubey, C., Radu, R., Rozum, I., Schepers, D., Simmons, A., Soci, C., Dee, D., Thépaut, J-N. (2018): ERA5 hourly data on single levels from 1940 to present. Copernicus Climate Change Service (C3S) Climate Data Store (CDS), DOI: 10.24381/cds.adbb2d47, (Accessed on 16-OCT-2024)

Houston, J. R. (1995). Beach-fill volume required to produce specified dry beach width, Coastal Engineering Technical Note 11-32.

IPCC, 2023: Climate Change 2023: Synthesis Report. Contribution of Working Groups I, II and III to the Sixth Assessment Report of the Intergovernmental Panel on Climate Change [Core Writing Team, H. Lee and J. Romero (eds.)]. IPCC, Geneva, Switzerland, 184 pp., doi: 10.59327/IPCC/AR6-9789291691647.

Kamphuis, J. W. (1991). Alongshore sediment transport rate. *Journal of Waterway, Port, Coastal, and Ocean Engineering*, *117*(6), 624-640.

Langlais, C., Barnier, B., Molines, J. M., Fraunié, P., Jacob, D., & Kotlarski, S. (2009). Evaluation of a dynamically downscaled atmospheric reanalyse in the prospect of forcing long term simulations of the ocean circulation in the Gulf of Lions. *Ocean Modelling*, *30*(4), 270-286.

de Madron, X. D., Wiberg, P. L., & Puig, P. (2008). Sediment dynamics in the Gulf of Lions: The impact of extreme events. *Continental Shelf Research*, *28*(15), 1867-1876.

Maillet, G. M., Vella, C., Berné, S., Friend, P. L., Amos, C. L., Fleury, T. J., & Normand, A. (2006). Morphological changes and sedimentary processes induced by the December 2003 flood event at the present mouth of the Grand Rhône River (southern France). *Marine Geology*, *234*(1-4), 159-177.

Makaske, B., & Augustinus, P. G. (1998). Morphologic changes of a micro-tidal, low wave energy beach face during a spring-neap tide cycle, Rhone-Delta, France. *Journal of Coastal Research*, 632-645.

Masselink, G. (1992). Longshore Variation of Grain Size Distribution along the Coast of the Rhone Delta, Southern France: A Test of the" McLaren Model". *Journal of Coastal Research*, 286-291.

Meehl, G. A., Stocker, T. F., Collins, W. D., Friedlingstein, P., Gaye, A. T., Gregory, J. M., ... & Zhao, Z. C. (2007). Global climate projections. Chapter 10.

Mil-Homens, J., Ranasinghe, R., de Vries, J. V. T., & Stive, M. J. F. (2013). Re-evaluation and improvement of three commonly used bulk longshore sediment transport formulas. *Coastal Engineering*, *75*, 29-39.

Milliman, J. D., & Syvitski, J. P. (1992). Geomorphic/tectonic control of sediment discharge to the ocean: the importance of small mountainous rivers. *The journal of Geology*, *100*(5), 525-544.

Millot, C. (1990). The gulf of Lions' hydrodynamics. *Continental shelf research*, *10*(9-11), 885-894.

Mudde, C. (2019). Development and verification of ShorelineS on longshore sediment transport and spit formation: A case study of Lobito, Angola.

NORA. Tides and water levels: Frequency of tides - The lunar day. Retrieved 18 February 2025: https://oceanservice.noaa.gov/education/tutorial_tides/tides05_lunarday.html

Obermann, A., Bastin, S., Belamari, S., Conte, D., Gaertner, M. A., Li, L., & Ahrens, B. (2018). Mistral and Tramontane wind speed and wind direction patterns in regional climate simulations. *Climate Dynamics*, *51*, 1059-1076.

Piégay, H., Radakovitch, O., Arnaud, F., Belletti, B., Camenen, B., Cassel, M., ... & Clémens, A. (2022). L'Observatoire des Sédiments du Rhône. 12 années de recherche pour la connaissance et la gestion hydro-sédimentaire du fleuve. Bilans et perspectives scientifiques.

Pont, D., Simonnet, J. P., & Walter, A. V. (2002). Medium-term changes in suspended sediment delivery to the ocean: consequences of catchment heterogeneity and river management (Rhône River, France). *Estuarine, Coastal and Shelf Science*, *54*(1), 1-18.

Press, F., Siever, R., Grotzinger, J., & Jordan, T. H. (2004). *Understanding earth*. Macmillan.

Provansal, M., Dufour, S., Sabatier, F., Anthony, E. J., Raccasi, G., & Robresco, S. (2014). The geomorphic evolution and sediment balance of the lower Rhône River (southern France) over the last 130 years: Hydropower dams versus other control factors. *Geomorphology*, *219*, 27-41.

QGIS 3.22 documentation. OSGEO. Retrieved 3 September 2024: https://docs.qgis.org/3.22/en/docs/user_manual/working_with_raster/georeferencer.html

Reading, H. G. (Ed.). (2009). *Sedimentary environments: processes, facies and stratigraphy*. John Wiley & Sons.

van Rijn, L. C. (2014). A simple general expression for longshore transport of sand, gravel and shingle. *Coastal Engineering*, *90*, 23-39.

Roelvink, D., Huisman, B., Elghandour, A., Ghonim, M., & Reyns, J. (2020). Efficient modeling of complex sandy coastal evolution at monthly to century time scales. *Frontiers in Marine Science*, *7*, 535.

Rozynski, G. (2024). Closure depth. Retrieved 23 September 2025: https://www.coastalwiki.org/wiki/Closure_depth

Sabatier, F., & Anthony, E. (2015). The sand spits of the Rhone River delta: Formation, dynamics, sediment budgets and management. In *Sand and Gravel Spits* (pp. 259-274). Cham: Springer International Publishing.

Sabatier, F., Maillet, G., Provansal, M., Fleury, T. J., Suanez, S., & Vella, C. (2006). Sediment budget of the Rhône delta shoreface since the middle of the 19th century. *Marine Geology*, *234*(1-4), 143-157.

Sabatier, F., Samat, O., Ullmann, A., & Suanez, S. (2009). Connecting large-scale coastal behaviour with coastal management of the Rhone delta. *Geomorphology*, *107*(1-2), 79-89.

Sabatier, F., & Suanez, S. S. (2003). Evolution of the Rhône delta coast since the end of the 19th century. *Géomorphologie: relief, processus, environnement*, *9*(4), 283-300.

Seymour, R. J. (2005). Cross-shore sediment transport. *Encyclopedia of coastal science*, 352.

Suanez, S. S., Bruzzi, C., & Arnoux-Chiavassa, S. (1998). Données récentes sur l'évolution des fonds marins dans le secteur oriental du delta du Rhône (plage Napoléon et flèche de la Gracieuse). *Géomorphologie: relief, processus, environnement*, *4*(4), 291-311.

Suanez, S., & Provansal, M. (1996). Morphosedimentary behaviour of the deltaic fringe in comparison to the relative sea-level rise on the Rhone delta. *Quaternary Science Reviews*, *15*(8-9), 811-818.

Suanez, S. S., & Sabatier, F. (1999). Eléments de réflexion pour une gestion plus cohérente d'un système anthropisé: exemple du littoral du delta du Rhône. *Revue de géographie de Lyon*, *74*(1), 7-25.

Touzani, A., & Giresse, P. (2002). The Rhone River Prodelta. *Journal of Coastal Research*, *18*(1).

US Army Corps of Engineers. (1984). *Shore protection manual*. Department of the Army, Waterways Experiment Station, Corps of Engineers, Coastal Engineering Research Center.

Appendices

Appendix A

Volume calculations for sediment budget of Grand Rhône.

Besides using the bedload and suspended sediment transport of the Grand-Rhône, another way of determining the sediment budget of the Grand-Rhône is with the use of volume calculations. This is done by analysing the amount of sediment that is actively added to or subtracted from the shoreline between two points in time. This approach requires the assumption that the difference in sediment volume across the shoreline can be attributed solely to the sediment discharged by the Rhône. For the region of interest, this assumption is not realistic which is why the sediment budget was based on the discharge of the Rhône.

Nevertheless, the volume calculation is still carried out to have a better understanding of the sediment budget for the entire region. This is done by calculating the total surface area of the two shapes formed by the shoreline, the banks of the channel and two added corner points (Figure A.1). The sediment volume can then be determined with the previously determined slope of the shoreline profile, the active profile height, and the calculated surface area.

Since there are only 8 shoreline datapoints in the time period covered by the simulation, 1960 to 2020, the result is not very reliable. These 8 datapoints are represented by the interpreted shorelines from 1960, 1985, 2003, 2008, 2011, 2014, 2017, and 2021. The possible error introduced to the extraction of the shorelines propagates further into the sediment volume calculations. With a slope of 0.0066, the tidal range of about 20 centimetres could cause a deviation in the shoreline of 30 metres. Any further deviation from the mean water level at the time of the image that the interpreted shorelines are based on could result in an even bigger error.

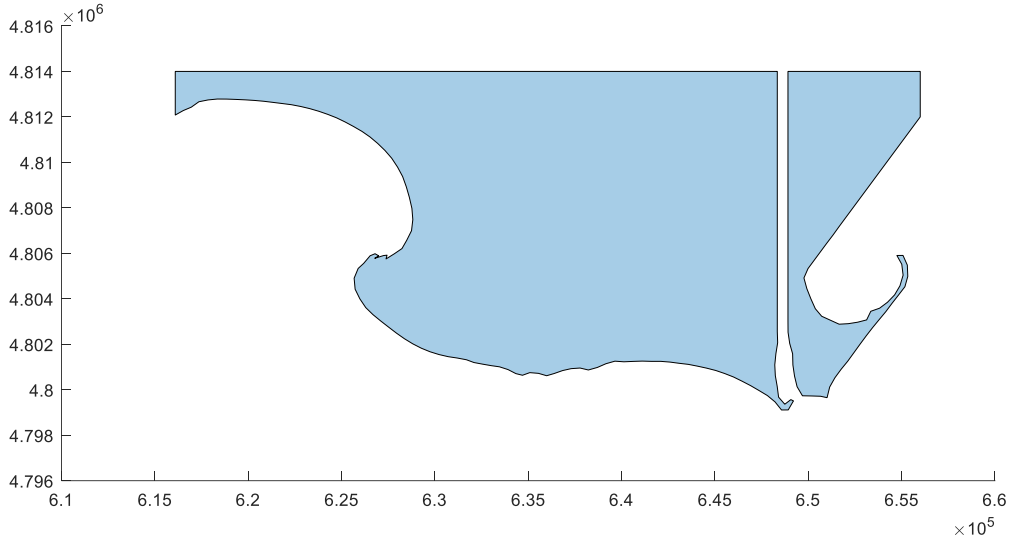

Figure A.1: Illustration of the shape defined by the shoreline of the Rhône, the Rhône channel, and the two corner points in the northwest and northeast.

Looking at the trend in total volume over the span of the simulated time period (Figure A.2), two things jump out. First, the overall trend seems to be downward, pointing to an overall erosional regime in the region of interest. Secondly, there is a major peak in 1985. This is unusual since no major flood happened around this time. This peak could be an outlier.

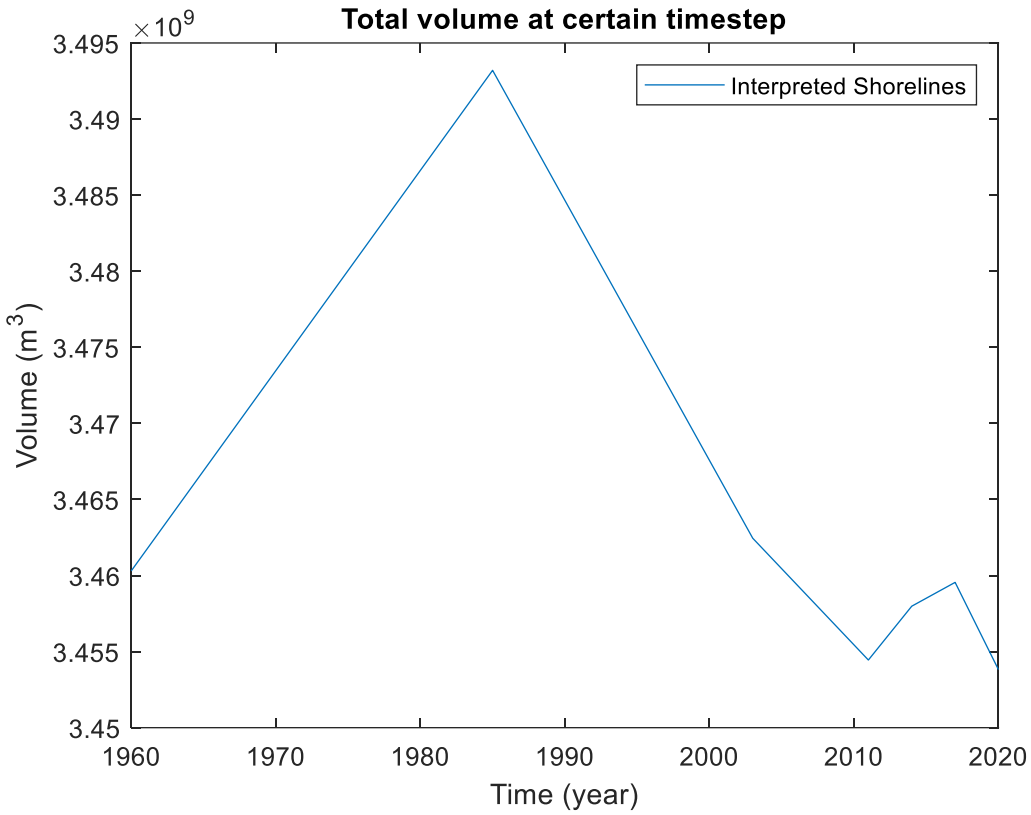

Figure A.2: Total surface area of the area calculations performed on the interpreted shorelines.

Appendix B

Results from the synthetic case with no perceivable difference to the standard simulation.

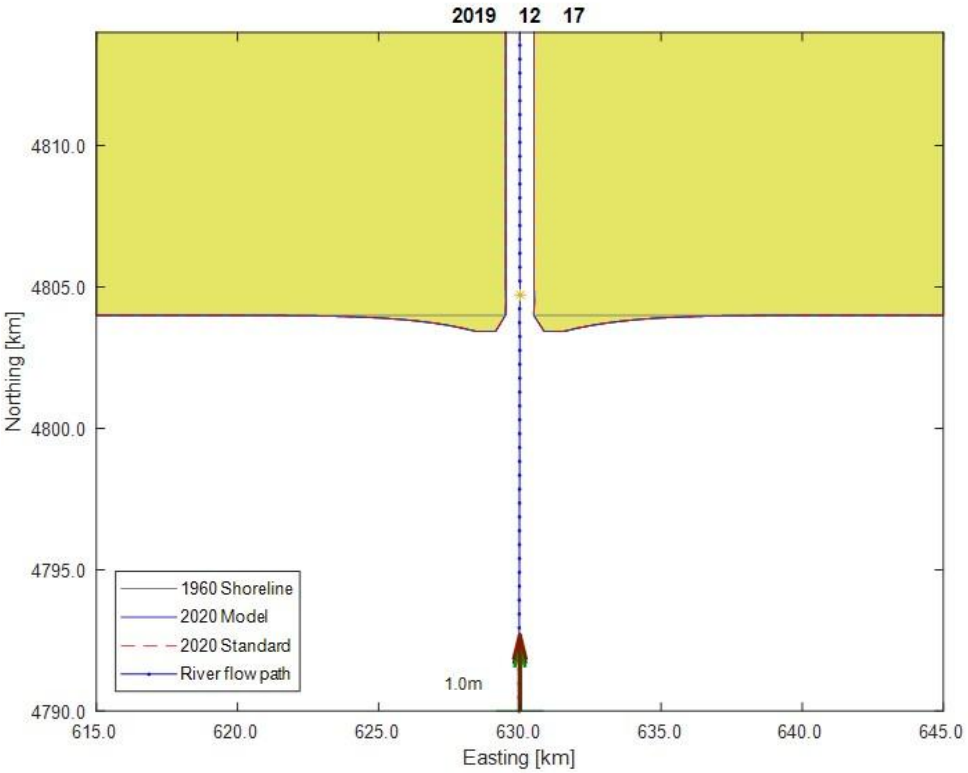

a.

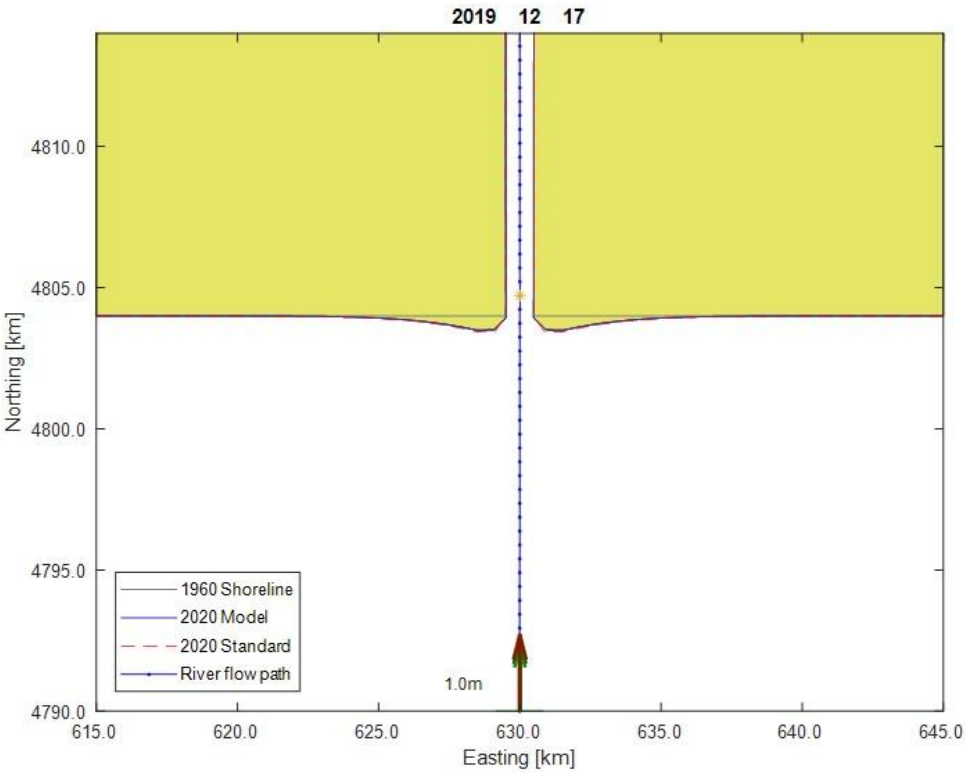

b.

Figure B.1: Results of the simulations of the synthetic case with a timestep of a: 0.01 and b: 0.2.

Timestep

With a timestep of 0.01 yr the result of the simulation (Figure B.1a) is the exact same as the result of the standard simulation. When the timestep is instead increased to 0.2 the result is slightly different (Figure B.1b). The buildup of sediment at the river mouth is slightly less compared to the result of the standard simulation. This is unexpected behaviour when only the timestep is changed. The fact that there is only a difference for the bigger timestep points to erroneous handling of the nourishment or erroneous updating of the shoreline at such a large timestep. This is positive because it means there is no unintended factoring of the timestep taking place in the handling of the nourishment or the updating of the shoreline.

Depth of closure

The result of the simulation with a depth of closure at a depth of 4 m (Figure B.2 a) differs from the result of the standard simulation with a depth of closure at a depth of 8 m, not only by having a bigger buildup of sediment at the river mouth, but the sediment is also spread out further along the shoreline. At the same time, the mouth does not prograde further compared to the result of the standard simulation. The result of the simulation with a depth of closure at a depth of 12 m (Figure B.2 b) differs from the result of the standard simulation by having a smaller buildup of sediment at the river mouth. This shows a relation where the buildup of sediment increases with a shallower depth of closure.

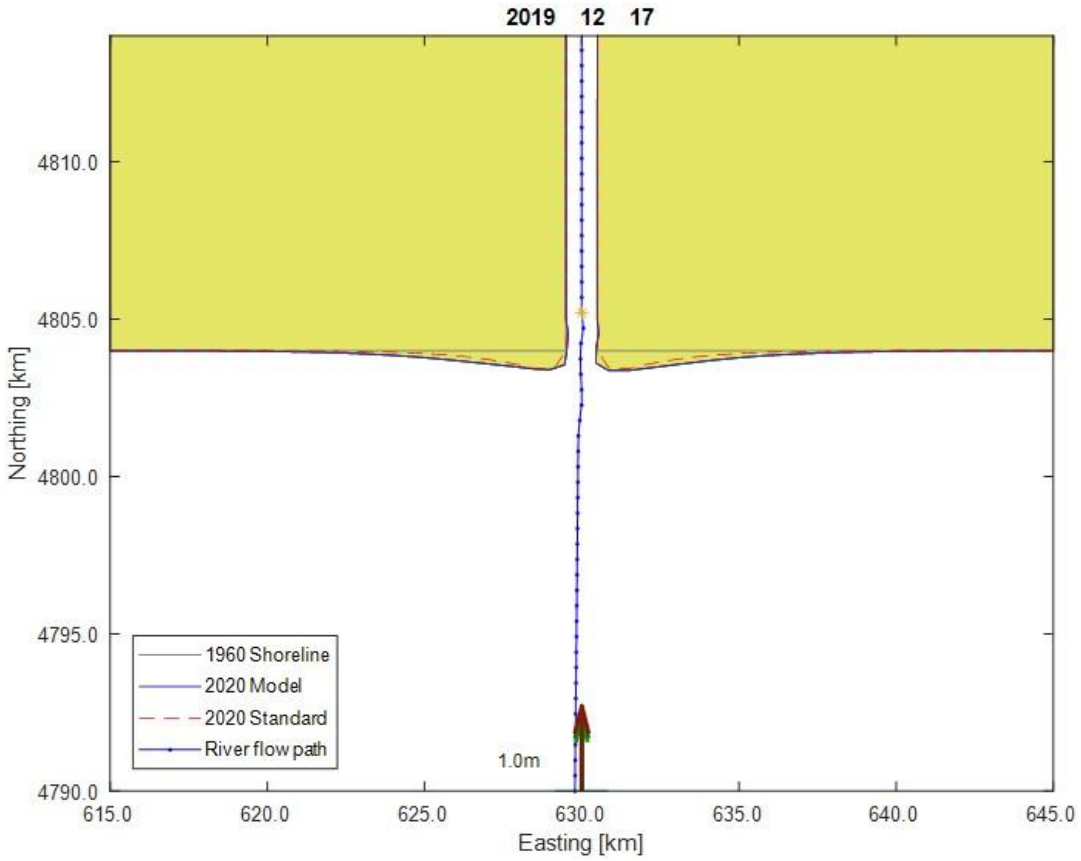

a.

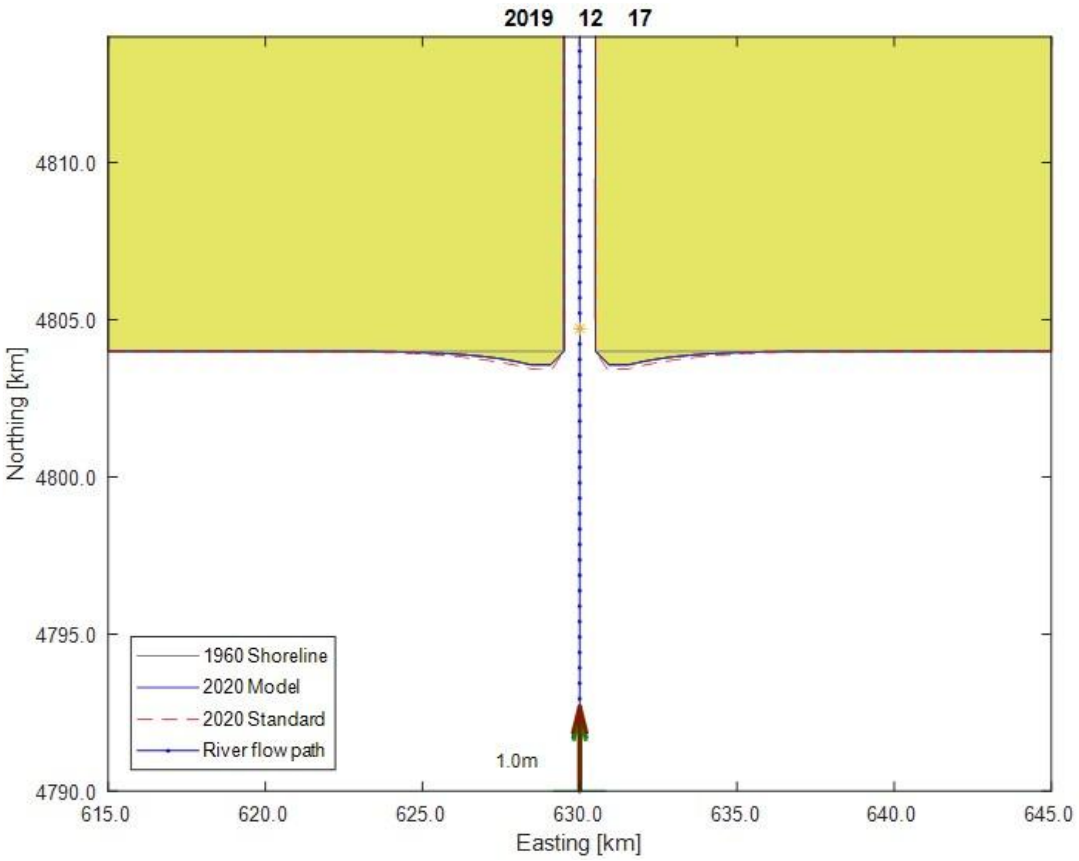

b.

Figure B.2: Results of the simulations of the synthetic case with a depth of closure at a depth of a: 4 m and b: 12 m.

Wave height

For the analysis of the effect of $H_{s,0}$ on the simulations both a simulation with a lower and higher $H_{s,0}$ were carried out. A constant $H_{s,0}$ of 0.5 m and a constant $H_{s,0}$ of 1.3 m were used in these simulations.

The result of the simulation with a constant $H_{s,0}$ of 0.5 m (Figure B.3 a) shows a river mouth that progrades further compared to the result of the standard simulation. Although the amount of sediment buildup is similar, the lower waves have spread the sediment out much less. On the other hand, the result of the simulation with a constant $H_{s,0}$ of 1.3 m (Figure B.3 b) shows that higher waves are capable of spreading the sediment near the river mouth across the shoreline and even into the river channel where the wave force competes with the adaptation factor of the channel that resembles the discharge of the river.

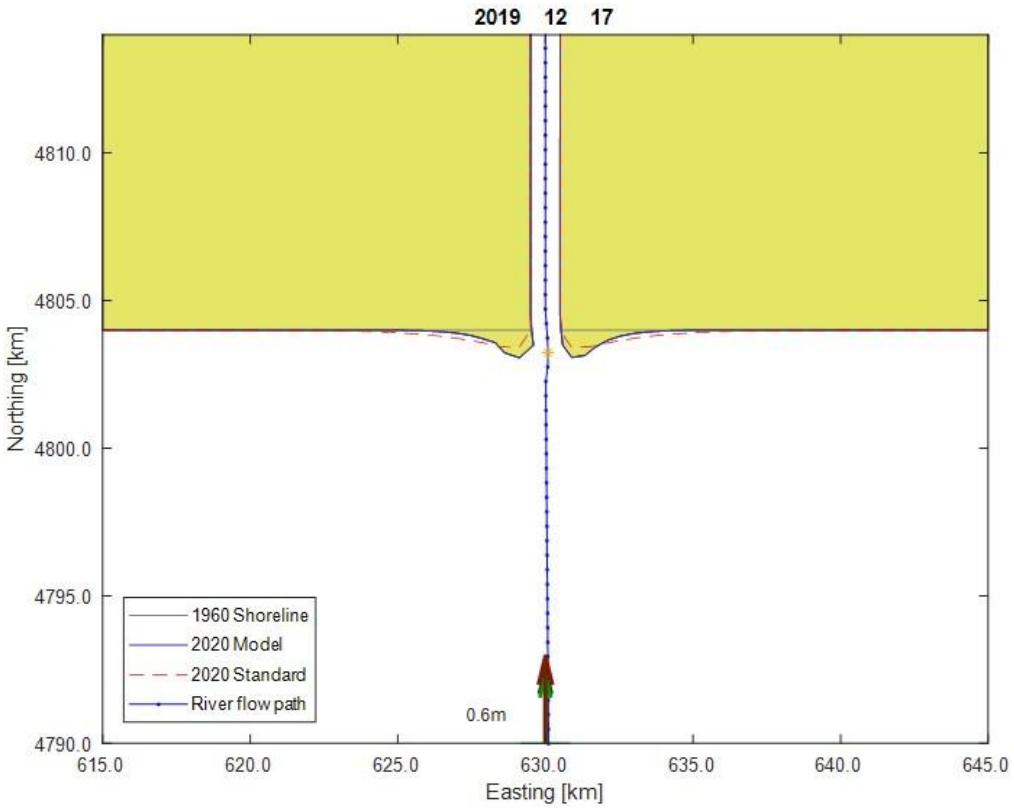

a.

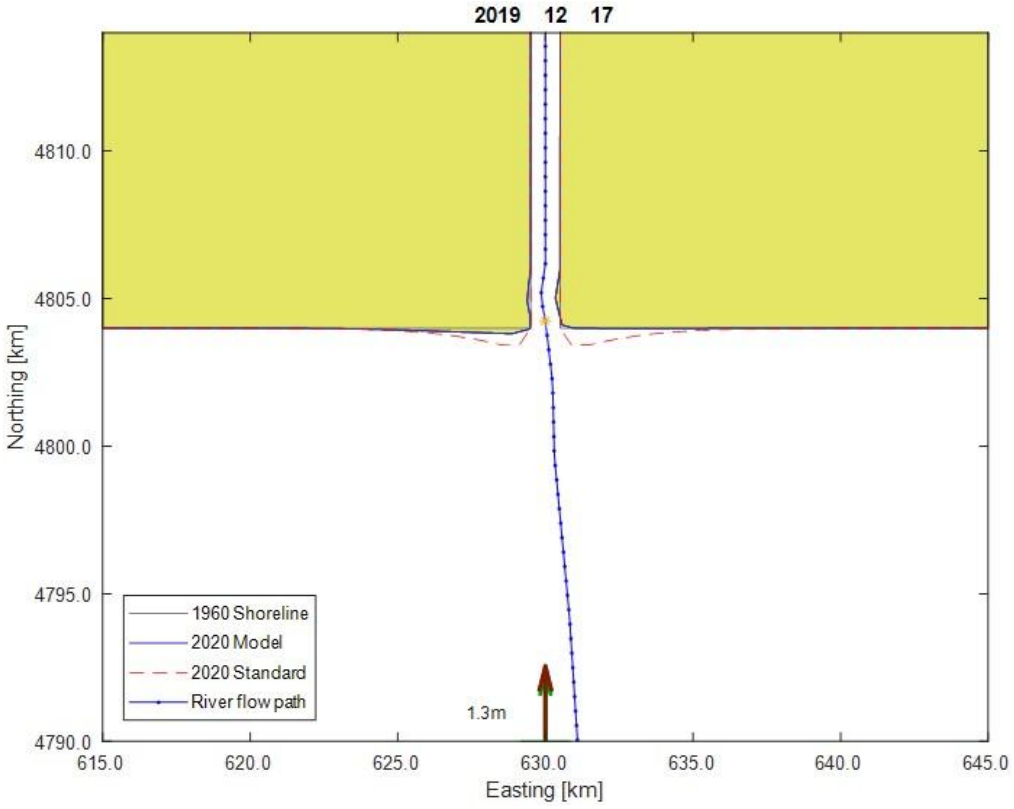

b.

Figure B.3: Results of the simulations of the synthetic case with a significant wave height of a: 0.5 m and b: 1.3 m.

Wave period

There is little difference in simulation results between the 3 s T_p and the 5 s T_p used in the standard simulation. The result of the simulation with the 3 s T_p (Figure B.4 a) has a slightly bigger buildup of sediment at the river mouth, implying that the wave driven longshore transport of sediment away from the mouth has been less impactful. The result of the simulation with the 7 s T_p (Figure B.4 b) has less buildup of sediment at the mouth compared to the standard simulation, which shows this same relation between sediment buildup at the mouth and peak wave period. However, the difference in the amount of sediment is much bigger while the difference in peak wave period is the same.

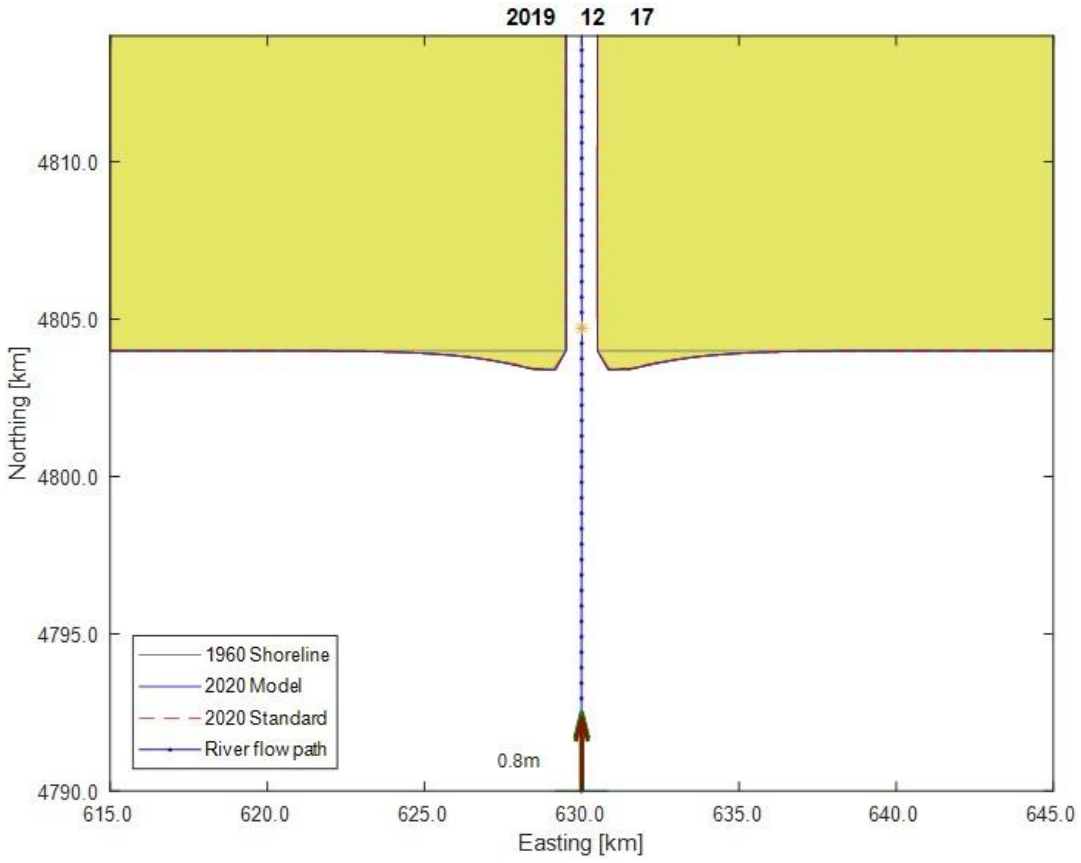

a.

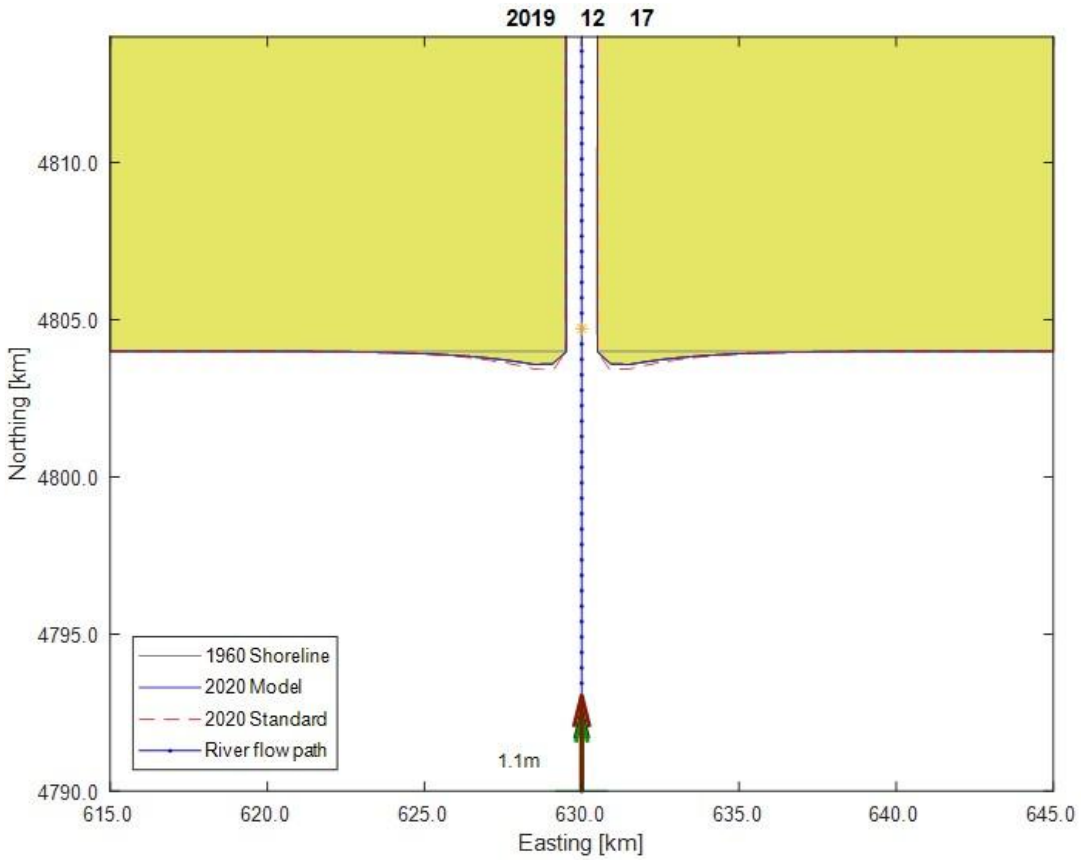

b.

Figure B.4: Results of the simulations of the synthetic case with a peak wave period of a: 3 s and b: 7 s.

Wave spread

The result of the simulation with a spread of 45° added to the constant wave direction of 180° (Figure B.5 a) shows that there is slightly less buildup of sediment at the river mouth compared to the result of the standard simulation. It also shows a slight deviation from the perfectly straight channel in the result of the standard simulation.

The result of the simulation with a spread of 90° added to the constant wave direction of 180° (Figure B.5 b) shows that there is a similar amount of buildup of sediment at the river mouth compared to the result of the standard simulation. It also shows the same deviation from the perfectly straight channel in the result of the standard simulation.

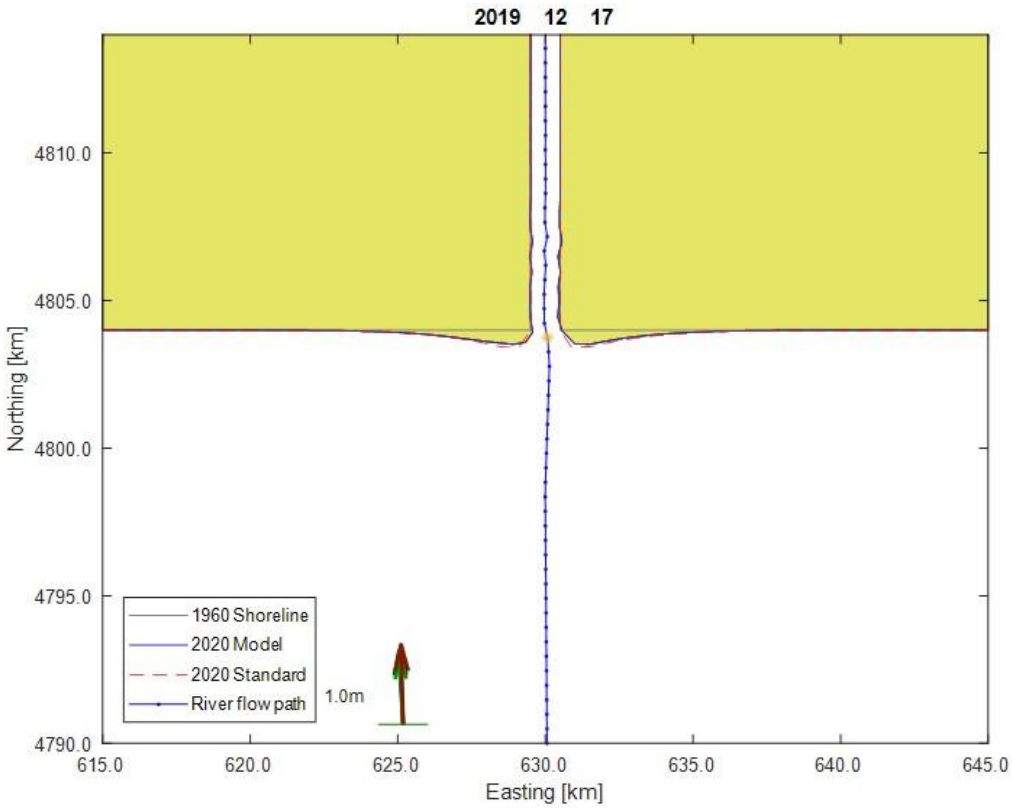

a.

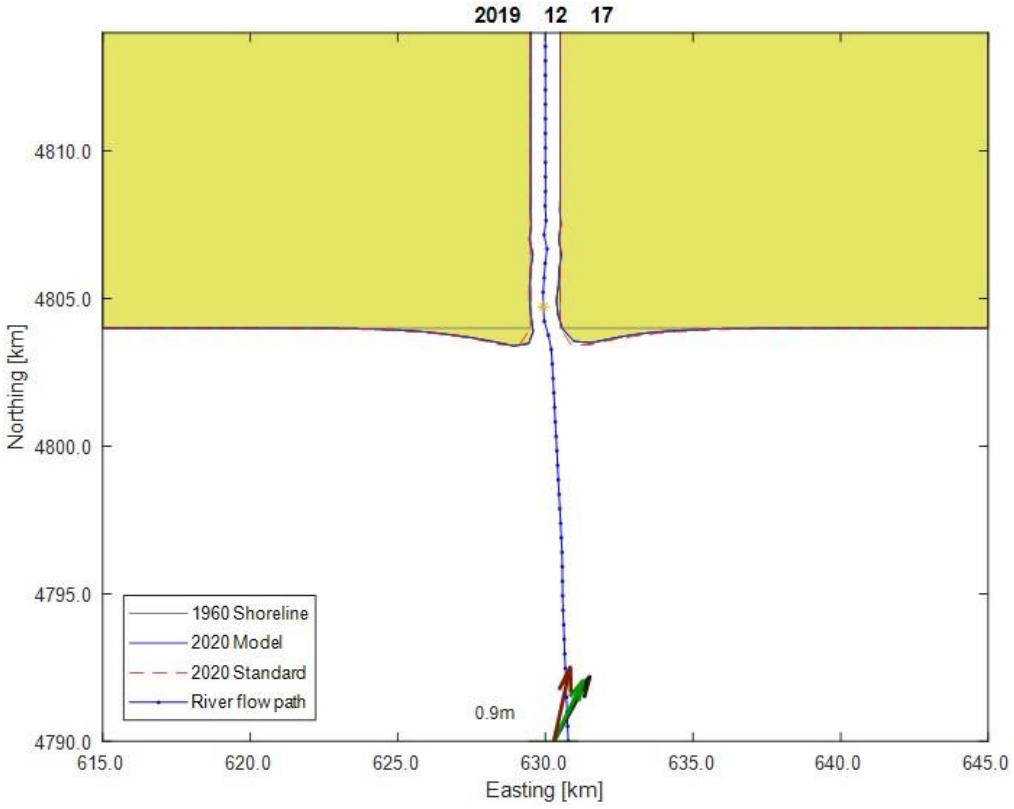

b.

Figure B.5: Results of the simulations of the synthetic case with a uniform spread of a: 45° and b: 90° added to the constant wave direction of 180°.

Appendix C

Detailed description of the post processing model comparison tool.

The comparison between the reference shoreline and the model shoreline is made based on the difference in cross-shore distance with respect to the initial situation at the start of the simulation. That is to say that the increase and decrease in cross-shore distance between the starting position of the shoreline and the shoreline positions throughout the simulation are determined for both the modelled and the reference shoreline. These distances can then be plotted and compared. This gives a way of quantifying the result of the model.

First, for every point on the reference shoreline, the distance between that point, Pr, and the nearest point on the modelled shoreline is determined. This is done by creating a line between two points, P1 and P2 (Figure C.1). The line P1-P2 crosses Pr, and the points P1 and P2 are separated from Pr by a predetermined fraction of the average distance between the points on the reference shoreline on either side of Pr (In this study the fraction used is always 1). Next, a projected point P' is determined as the point on the line P1-P2 where the normal to the line P1-P2 intersects with point Pm. The fraction of the distance of point P' along the line P1-P2 is used to determine on what side of the line normal to the reference coast the projected point lies. This is done for all points on the modelled shoreline.

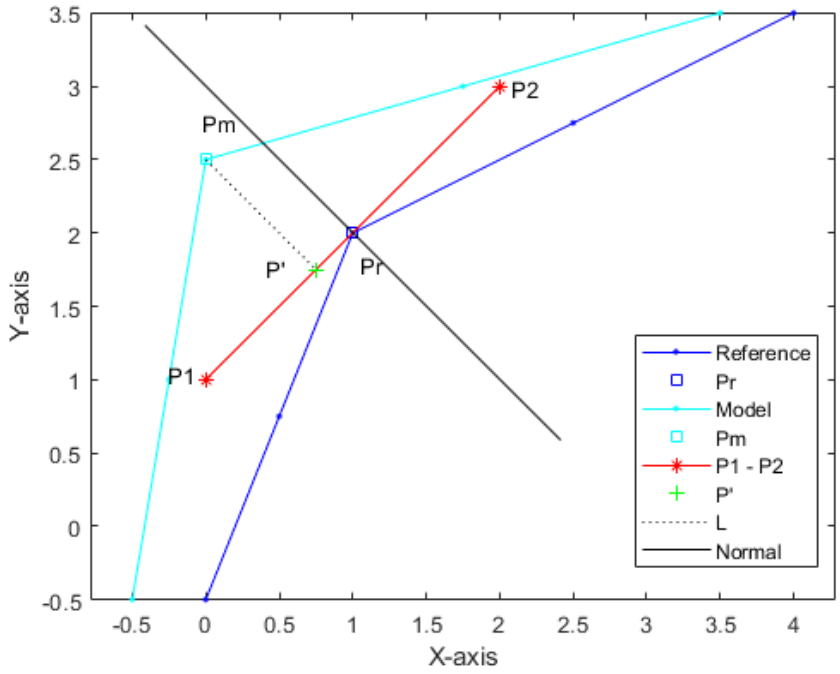

Figure C.1: Approximation of distances between reference shoreline and modelled shoreline.

Next, the crossing points of the modelled shoreline with the line normal to the reference shoreline are determined by considering all instances where one model point lies on one side of the normal line and the next model point lies on the other side (Figure C.2). All the crossing points can then be filtered by applying a critical cross-shore distance. The resulting pairings of points on both sides of the normal line are then used to determine the crossing points of the normal line with the segment of shoreline between the pairs of points. From these crossing points the closest point is chosen and the distance between it and the point Pr is considered as the distance between the modelled shoreline and the reference shoreline in this particular point. This is then repeated for all points on the reference shoreline.

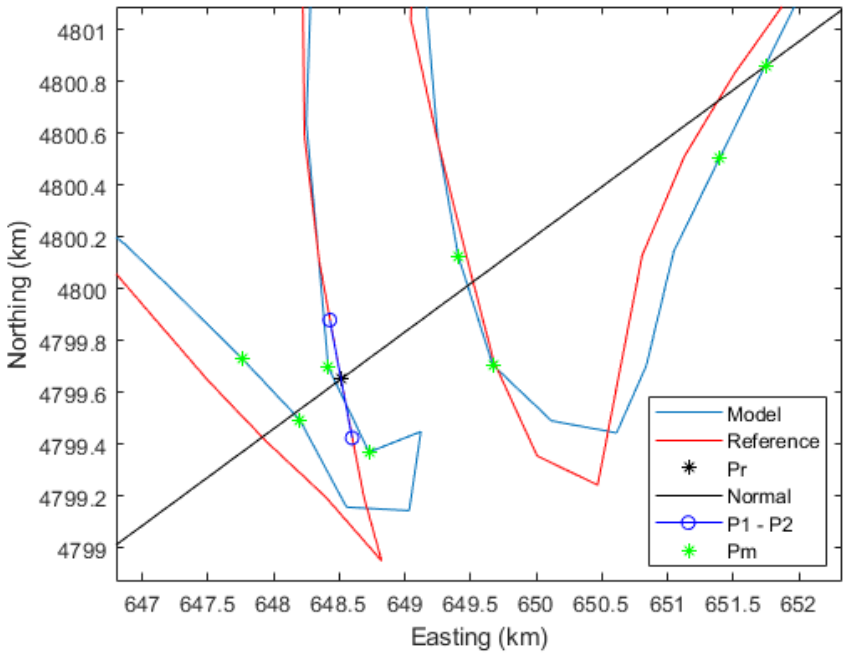

Figure C.2: Example of determination of crossing points of the modelled shoreline with the line normal to the reference shoreline.

The method used to calculate the distances between shorelines is reliable for shorelines that have a low degree of variability and do not include any coastal formations with a sharp angle, such as can be expected with certain spits. This is because higher variability and sharp angles in the shoreline are prone to misinterpretation under this method. This is illustrated in Figure C.3, where the shoreline that would be expected to be taken as comparison is not considered because it does not have a line segment that is crossed by the perpendicular line. Instead, the closest crossing on the other part of the shoreline will be considered and as a result the calculated distance between the two shorelines in this particular point will be incorrect.

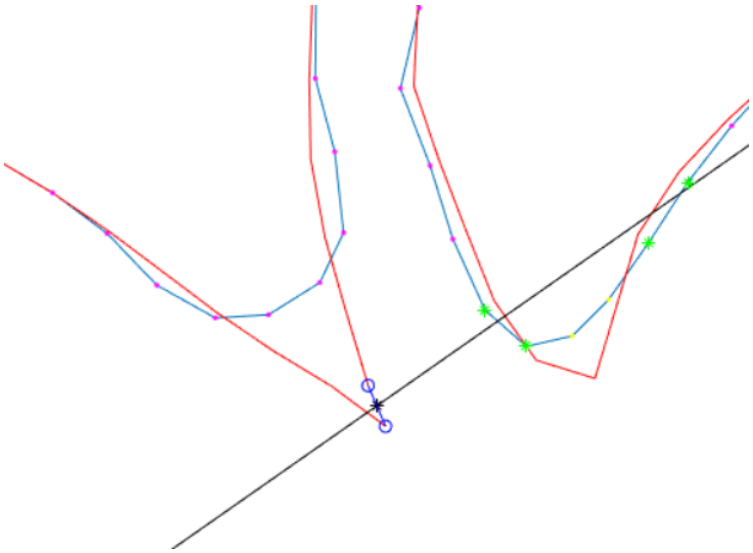

Figure C.3: Illustration of how the distance between shorelines can be misinterpreted for more complicated shorelines.

Appendix D

Asymmetry due to rounding errors in discretisation of shoreline.

Some of the simulations result in asymmetrical shoreline development even though all the inputs (except for the simulations with spread added) are completely without randomness and all the input is perfectly perpendicular to the shoreline. This behaviour can be explained by a very slight divergence from the desired shoreline, as defined by the two sets of 3 corner points. This divergence is the result of very slight rounding errors in the discretisation of the shoreline (Figure D).

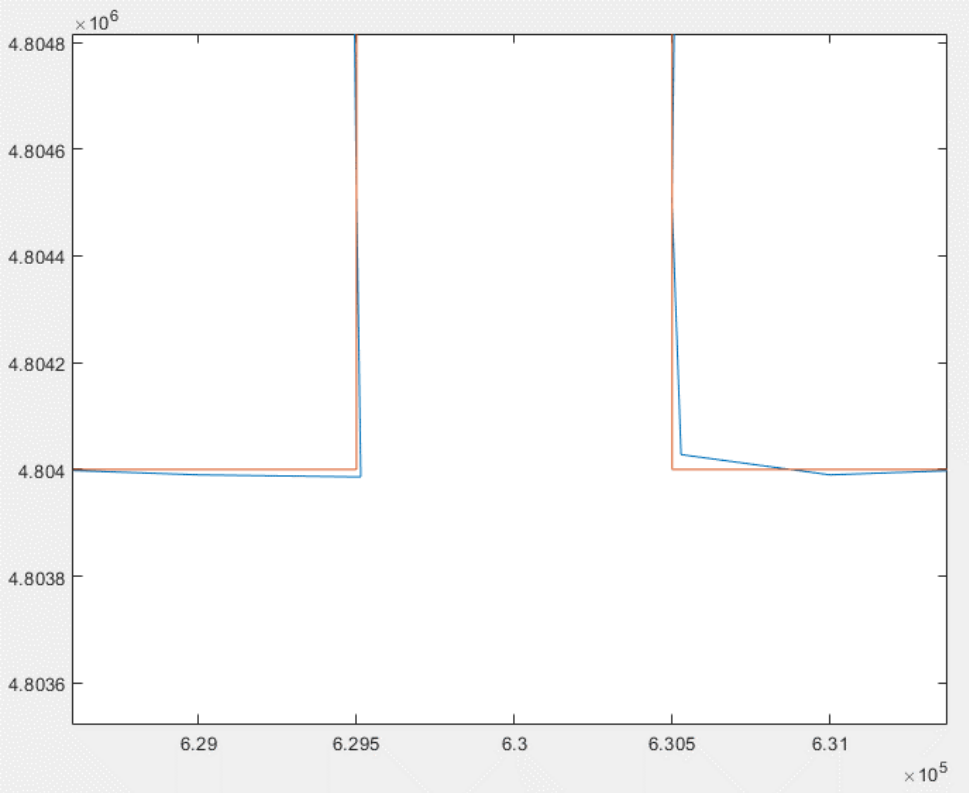

Figure D: Slight offset in shoreline positions near the river mouth after discretisation of the initial shoreline.

Appendix E

Changelog. This part of the appendix contains adaptations made to the ShorelineS model and its subscripts:

- prepare_waveconditions.m

  Adaptation to correctly import xy coordinates of wave conditions.

```
                try
%                   WVC(kk).x = WAVE.WVCfile{kk,2};
%                   WVC(kk).y = WAVE.WVCfile{kk,3};
                  WVC(kk).x = WAVE.WVCfile{2,kk};                % adaptation to get correct xy coordinates of WVC file
                  WVC(kk).y = WAVE.WVCfile{3,kk};
                catch
```

- fitCoastlineOnReferenceline.m

  Adaptation to account for exactly overlapping shorelines (for instance for same starting ldb file).

```
            if isempty(idneg) && isempty(idpos)                % Adaptation to account for situations where line normal to coast
            else                                               % only crosses model coastline in the reference point
```

  Adaptation for always choosing closest shoreline segment in comparison.

```
%         Yl     = Ylall(1,:);
        Yl     = min(abs(Ylall));                              % Adaptation made to not allow Yl to be a bigger result
```

- transport.m

  Adaptation to use Hs_breaking instead of Hs_offshore in KAMP and VR14 transport formulas.

```

    %% Transport : Kamphuis
    elseif strcmpi(TRANSP.trform,'KAMP')
        QSkampmass=TRANSP.qscal .* 2.33 .* WAVE.TP.^1.5 .* TRANSP.tanbeta.^0.75 .* TRANSP.d50.^-0.25 .* WAVE.HSbr.^2 .* (abs(sind(2.*WAVE.dPHIbr)).^0.6.*sig
        QS = 365*24*60*60*(QSkampmass ./(TRANSP.rhos-TRANSP.rhow)) ./(1.0-TRANSP.porosity);
        if  STRUC.diffraction==1            % use HS and dPHI, and second-order component
            QSkampmass=TRANSP.qscal .* 2.33 .* WAVE.TP.^1.5 .* TRANSP.tanbeta.^0.75 .* TRANSP.d50.^-0.25 .* WAVE.HSbr.^2 .* ( abs(sind(2*WAVE.dPHIbr)).^0.6.
            QS = TRANSP.qscal .* 365*24*60*60*(QSkampmass /(TRANSP.rhos-TRANSP.rhow)) /(1.0-TRANSP.porosity);
        end
        QS(abs(WAVE.dPHIbr)>90)=0;      % Set transport to 0 when angle exceeds 180 degrees

    %% Transport : Mil-Homens (2013)
    elseif strcmpi(TRANSP.trform,'MILH')
        QSmilhmass=TRANSP.qscal .* 0.15.* WAVE.TP.^0.89 .* TRANSP.tanbeta.^0.86 .* TRANSP.d50.^-0.69 .* WAVE.HSbr.^2.75 .* (abs(sind(2.*WAVE.dPHIbr)).^0.5.*
        QS = 365*24*60*60*(QSmilhmass ./(TRANSP.rhos-TRANSP.rhow)) ./(1.0-TRANSP.porosity);
        QS(abs(WAVE.dPHIbr)>90)=0;     % Set transport to 0 when angle exceeds 180 degrees
```

- Diff_2Models.m

  Adapted pretty much the entire script for:

  - use with 2 separated shorelines (because of the river cutting it in 2).
  - flexibility in comparing with different starting timepoints for the reference shoreline.
  - Cosmetic changes to the BSS plot.

Appendix F

The wave data distributions agree with the distributions from the study by Boudet et al (2017) (Figure F). Both distributions show an absence of waves with a wave direction of about 50 degrees, and both show similar peaks at around 120 and 200 degrees. The notable difference is the height of waves with a direction between about 280 and 360 degrees. This can be explained by the fact that the data from Boudet et al (2017) comes from the mouth of the Rhône whereas the data used for this study comes from 16 kilometres offshore. This allows for northerly winds to increase the size of the waves further from the coast.

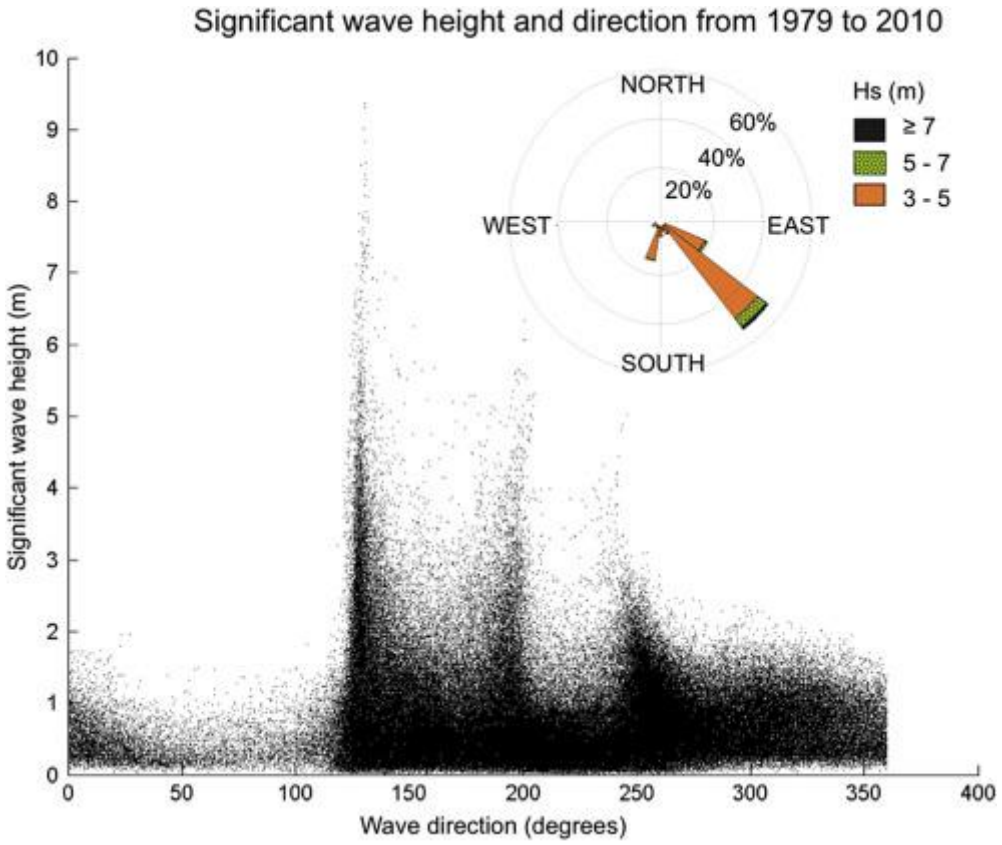

Figure F: Hourly significant wave height and wave direction with wave rose. Wave rose excludes waves with significant wave height below 3 metres (Boudet et al, 2017).

Appendix G

Different visualisation of the wave data pre and post filtering.

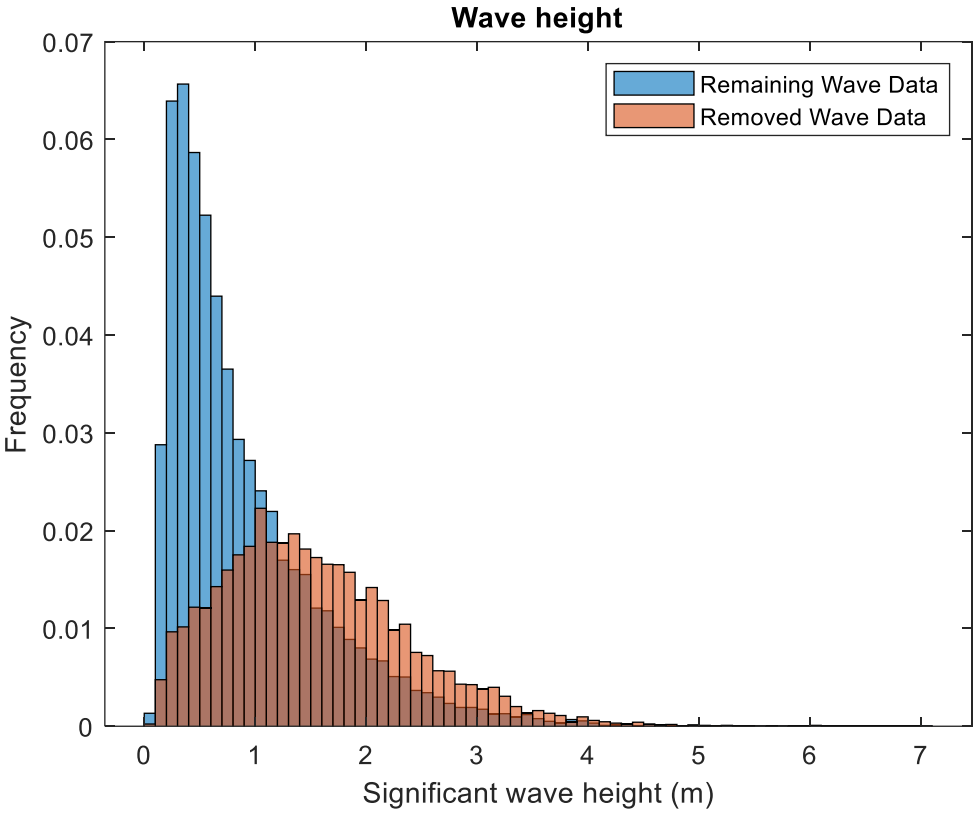

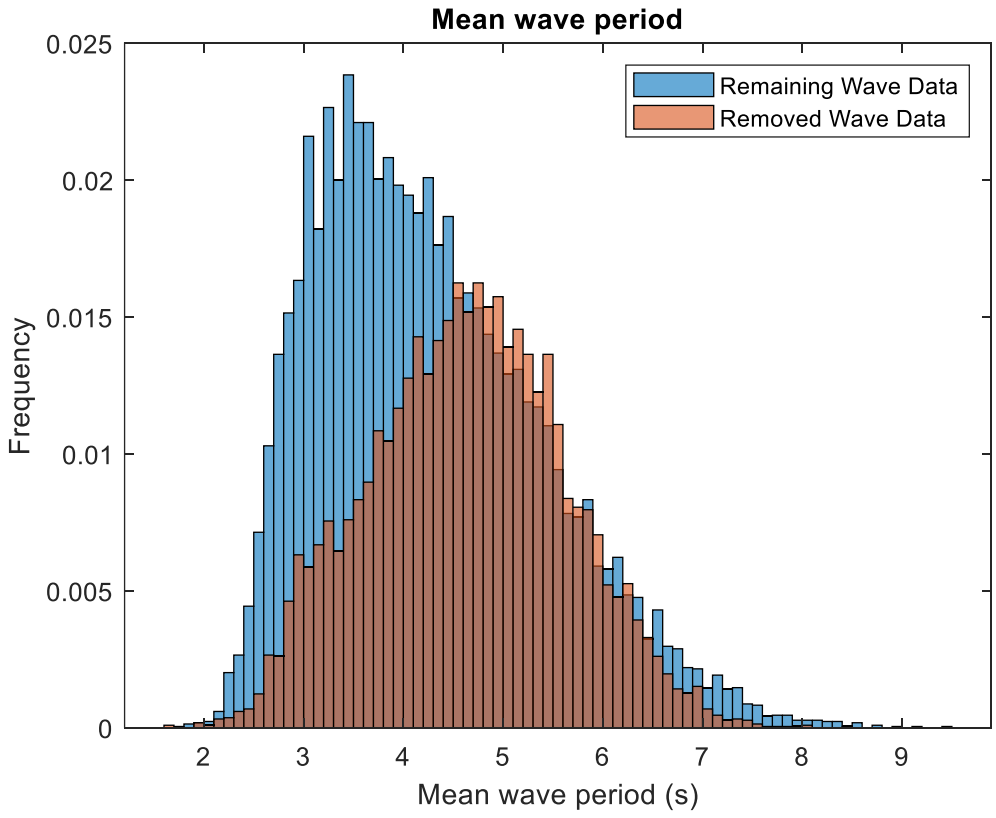

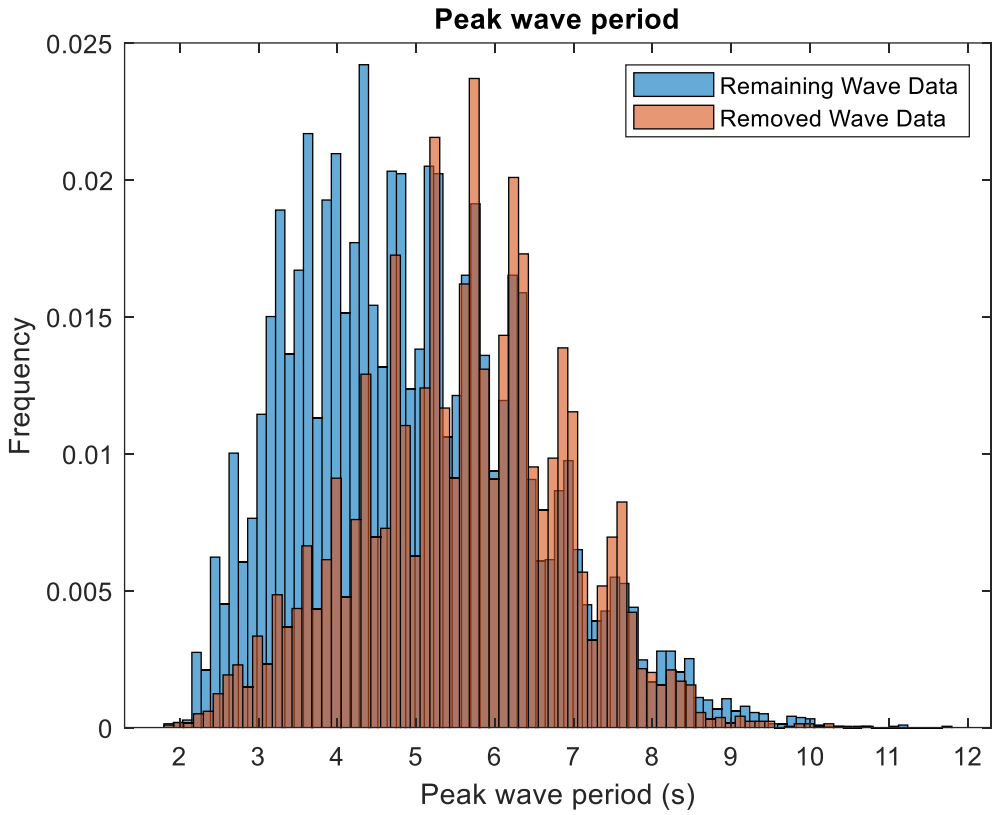
Peak wave period
Remaining Wave Data
Removed Wave Data
Frequency
0.025
0.02
0.015
0.01
0.005
0
2
3
4
5
6
7
8
9
10
11
12
Peak wave period (s)

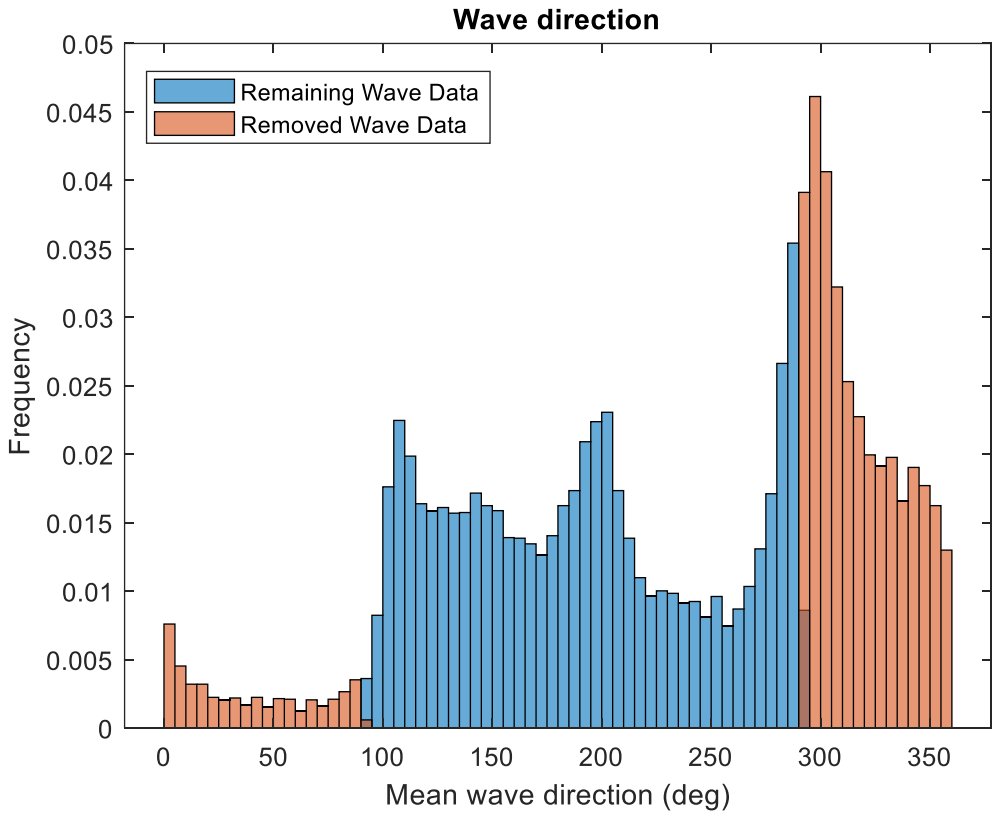
Wave direction
Remaining Wave Data
Removed Wave Data
Frequency
0.05
0.045
0.04
0.035
0.03
0.025
0.02
0.015
0.01
0.005
0
0
50
100
150
200
250
300
350
Mean wave direction (deg)

Appendix H

Aerial imagery with interpreted shorelines highlighted in red.

a.

b.

c.

d.

e.

f.

g.

Figure 23: Satellite (a) and aerial (b – g) imagery of the Rhône delta with the coast highlighted in red at different years.

a: 1985 (Google Earth), b: 2003, c: 2008, d: 2011, e: 2014, f: 2017, g: 2021 (Remonter le temps - IGN).

Acknowledgement:

Hersbach, H. et al., (2018) was downloaded from the Copernicus Climate Change Service (2023).

The results contain modified Copernicus Climate Change Service information 2020. Neither the European Commission nor ECMWF is responsible for any use that may be made of the Copernicus information or data it contains.